DEGRADABLE POLYCARBONATE NETWORKS DERIVED FROM QUINIC ACID AND DESIGNED FOR BIOMEDICAL APPLICATIONS

A Dissertation

by

LAUREN ASHLEY LINK

Submitted to the Office of Graduate and Professional Studies of
Texas A&M University
in partial fulfillment of the requirements for the degree of

DOCTOR OF PHILOSOPHY

Chair of Committee,	Karen L. Wooley
Committee Members,	Melissa A. Grunlan
	Duncan J. Maitland
	James D. Batteas
Head of Department,	Ibrahim Karaman

December 2015

Major Subject: Materials Science and Engineering

ABSTRACT

The pursuit of polymers with natural and renewable precursors is driven by two specific aims: (i) to develop sustainable and biodegradable plastics which decrease dependence on petroleum feedstocks and address problems associated with plastic waste and pollution, and (ii) to design novel biomaterials with built-in biocompatibility and the ability to degrade under physiological conditions to produce resorbable natural byproducts. Herein, a new family of nontoxic bio-based polycarbonate networks that exhibit a wide range of achievable thermomechanical properties and have the potential to breakdown hydrolytically into biologically-beneficial and environmentally-benign degradation products is described.

The natural product quinic acid, known for its antioxidant and growth-promoting properties, was selected as the monomeric building block, and hydrolytically labile carbonates were selected as the linkages. Solvent-free thiol-ene chemistry was utilized in the copolymerization of *tris*(alloc) quinic acid and a variety of multifunctional thiol monomers to obtain poly(thioether-*co*-carbonate) networks. Natural multifunctional thiols derived from lipoic acid, a metabolic antioxidant, were explored to further increase the overall natural content of the material. A wide range of tunable thermomechanical properties including glass transition temperatures from −18 to 65 °C and mechanical characteristics from a rubbery elastomer to a rigid plastic was achieved by careful selection of thiol monomers. Special attention was paid to the characterization of structure-thermomechanical property relationships and how these

relationships change under physiological conditions. The short-term mechanical changes triggered by solvent plasticization in a physiologically-relevant environment (PBS, pH 7.4, 37 °C) were observed by submersion dynamic mechanical analysis. The long-term degradation kinetics, including swelling and mass loss, were monitored, and the results showed a range of degradation times from 5 to ~35 weeks based on the crosslink density and hydrophilicity of the polymer network. *In vitro* cytotoxicity and cell attachment studies were performed, and X-ray imaging contrast properties were observed to investigate the feasibility of the poly(thioether-*co*-carbonate) networks to serve as platform materials in biomedical applications, specifically as orthopedic implant devices. Overall, by using simple fabrication techniques and reliable chemistry, the poly(thioether-*co*-carbonate) networks developed in this work represent a versatile and nontoxic family of materials which may be used for to a wide variety of applications.

ACKNOWLEDGEMENTS

I would like to express my deepest gratitude to my advisor, Prof. Karen L. Wooley, for her encouragement, enthusiasm, and guidance. I have been exceptionally fortunate to know her and be a part of her research group, where I have grown as a person, a scientist, and a professional. Beyond the scientific aspects, the skills and experience I have acquired will help me to be successful in all aspects of my career and life after graduate school.

I would also like to thank my committee members, Prof. Melissa A. Grunlan, Prof. Duncan J. Maitland, and Prof. James D. Batteas for their guidance and support throughout the course of this research. I am grateful to my friends and colleagues and the department faculty and staff for making my time at Texas A&M University a great experience. From the materials science and engineering department and the Society of Plastics Engineers I would like to thank Jan R. Gerston, Prof. H. J. Sue, Isabel C. Cantu, Prof. Jodie L. Lutkenhaus, and Prof. Nicole S. Zacharia. I would like to thank the entire Wooley group for their day-to-day help, camaraderie, and intellectual conversations. I especially have to thank Alexander Lonnecker and Keith Hearon because I could not have completed this dissertation without their inspiration and guidance. I also want to extend my gratitude to Jeffery E. Raymond, Soon Mi Lim, Sarosh Khan, Marco D. Giles, Justin A. Smolen, Cameron A. Maher, and Brooke A. Versaw for their contributions to this work, and Amandine Noel, Simcha E. Felder, Samantha L.

Kristufek, Jennifer S. Zigmond, and Tiffany P. Gustufson for their collaboration and insightful conversation.

Most importantly, I wish to thank my family: my mother, Catherine G. Link, my father, Ted C. Link, Isabel J. Link, and my brother, T.J. Link for their constant praise and support. I would like to thank my closest friends Kayla M. Hartzog, Kristina N. Adams, and Chelsea L. Hansen, my childhood best friend, Kristina M. Moran, as well as my best friend and the love of my life, James R. Spofford, for providing me with emotional support, entertainment, and laughter throughout my time in school.

I acknowledge financial support from the National Science Foundation (Grant CHE-1410272) and the Welch Foundation W. T. Doherty-Welch Chair in Chemistry (A-0001). I also acknowledge contributions from the Laboratory for Biological Mass Spectrometry and the Laboratory for Synthetic-Biologic Interactions at Texas A&M University.

NOMENCLATURE

1,2-EDT	1,2-ethanedithiol
1,6-HDT	1,6-hexanedithiol
2,3-BDT	2,3-butanedithiol
AFM	Atomic force microscopy
DCM	Dichloromethane
DHLAc	Dihydrolipoic acid
DHLAm	Dihydrolipoamide
DI	Deionized
DMA	Dynamic mechanical analysis
DMF	*N*,*N*-dimethylformamide
DMPA	2,2-dimethoxy-2-phenylacetophenone
DSC	Differential scanning calorimetry
ESI-MS	Electrospray ionization mass spectrometry
FTIR	Fourier transform infrared spectroscopy
LAc	Lipoic acid
LAm	Lipoamide
NMR	Nuclear magnetic resonance
QA	Quinic acid
PBS	Phosphate buffered saline
PETMP	Pentaerythritol *tetrakis*(3-mercaptopropionate)

PGA	Poly(glycolic acid)
PLA	Poly(lactic acid)
TAQA	*Tris*(alloc) quinic acid
TATATO	Triallyl-1,3,5-triazine-2,4,6-trione
TEGBMP	Tetraethylene glycol *bis*(3-mercaptopropionate)
TGA	Thermogravimetric analysis
THF	Tetrahydrofuran
TMEDA	*N*,*N*,*N'*,*N'*-tetramethylethylenediamine
TMPTMP	Trimethylolpropane *tris*(3-mercaptopropionate)

TABLE OF CONTENTS

Page

LIST OF FIGURES

FIGURE Page

FIGURE Page

LIST OF TABLES

CHAPTER I

INTRODUCTION

Commodity plastics, many of which are intended to be disposable (*e.g.* packaging, food containers, and plastic bottles), take up more space in landfills than any other non-degradable material and cover an estimated 35% of the world's ocean surfaces, causing devastating effects to global seabird populations.[1-3] The main problem is the polymers that make up these plastics take thousands of years to fully degrade, but plastic objects are broken down by solar radiation overtime into smaller and smaller pieces, which are easily ingested by seabirds, fish, and other marine animals.[4] Plastic microparticles have been found in marine algae and plankton, which means they are entering the marine food chain even at the lowest levels.[5] Additionally, plastics are manufactured from petroleum-derived starting materials using energy from fossil fuels and may contain phthalates and bisphenol A, implicated as endocrine disruptors with harmful health effects.[6-7] The pursuit of sustainable commodity plastics with more "after-life" options, including degradability or more cost-effective and efficient recycling options, has led to the development of polymers derived from non-petroleum-based natural products.[8-9] Polymers derived from compounds naturally found in plants and animals and that are capable of reverting back into those biological products upon degradation are not only more environmentally-friendly, but also safer for wildlife and humans.

In addition to forming more sustainable and eco-friendly plastics, bio-based polymers may have the ability to form biocompatible plastics with resorbable degradation products. By building polymers from precursors which are naturally produced or broken down in the human body and hydrolytically labile linkages, it may be possible to develop degradable biomaterials with biologically-beneficial by-products. Degradable polymers are used as platform materials in tissue engineering, regenerative medicine, gene therapy, controlled drug delivery, bionanotechnology, and other advanced fields, where, in general, they serve as temporary support during tissue repair and/or transport vessel for the delivery of therapeutic or biologic agents.[10] For example, in bone tissue engineering degradable polymers have been developed as an alternative to conventional metal biomaterials for fracture repair.[11] Because metals and alloys used in orthopedic applications have modulus values (E = 100 GPa) that are five (or more) times greater than the modulus values of bone (cortical bone, E = 17-24 GPa, cancellous bone, E = 0.1-4.5 GPa), metal implants shield the conditioning stresses required for healthy bone growth, may cause damage to surrounding tissue, and loosen over time.[12] They are also permanent unless a secondary surgery is performed. Ideally, the design criteria for bioresorbable polymers for orthopedic devices include, but are not limited to, moduli and ultimate strength values similar to those of bone and a high degree of compatibility with surrounding tissue form initial implantation and throughout degradation.[13] Furthermore, besides providing the physical and biological cues mimicking those found in the native tissue environment, all these features must be combined into a device

design that degrades at rates matching those of tissue formation, until the injured tissue is completely restored with healthy functional tissue.

Synthetic strategies for the development of degradable polymers for biomedical applications have focused largely on the use of naturally-occurring acids or carbohydrates as monomers, polymerized to form hydrolytically labile linkages, *i.e.* ester, anhydride, or carbonate bonds. Numerous degradable polymer systems, which use hydrolytically-labile ester linkages as sites for polymer degradation have been developed from natural products, including polyesters from citric acid,[14] poly(ester-*co*-urethane)s from sugar-derivatives,[15] poly(ester-*co*-amide)s from succinic acid,[16] and poly(ester-*co*-urea)s from amino acids.[17] To this day the most widely accepted degradable polymers are polyesters of lactic acid, glycolic acid, and caprolactone, and devices composed of these polymers, including fracture fixation devices, spinal fixation devices, and abdominal wall repair devices, are FDA-approved and commercially available.[18-19] Poly(lactic acid) (PLA), poly(glycolic acid) (PGA), and their copolymers can be produced with high molecular weights by ring-opening polymerization of lactide and glycolide. However, these semicrystalline thermoplastic linear polymers and polyesters, in general, have received considerable scrutiny due to their acidic degradation products which can decrease the pH of the surrounding medium. In the case of PLA and PGA, there is a very high weight fraction of ester linkages within each polymer, which results in a high acidic concentration after degradation. Additionally, degradation proceeds by bulk erosion, as opposed to surface erosion, where hydrolysis is slow, allowing for water uptake to occur. Swelling increases the breakdown of ester groups within the material

causing a decrease in the pH within the bulk of the material auto-catalyzing degradation and eventually may result in failure of the material at the surface and the burst-release of concentrated acidic byproducts. In small implant devices this may not be a big concern, but as the physical size of the bulk material increases it becomes more difficult to predict degradation kinetics and there is a higher chance for adverse side effects including inflammation and pain as a result of acidic degradation products. Polyesters degrade on the order of months to years depending on the degree of crystallinity (semicrystalline polymers degrade slower) and physical size of the implant (larger/thicker implants degrade faster). The size-dependent degradation rate of amorphous poly(DL-lactic acid) was demonstrated by comparing the degradation of a thin film (0.3 mm thick) to the degradation of a disc (2 mm thick), and it was observed that the disc degraded heterogeneously (by bulk erosion) much faster than the thin film.[20] Polyanhydrides, the second most-recognized degradable polymers after polyesters, degrade *via* surface erosion, where hydrolysis occurs quickly and thus, the outer layers of the material are the first to exhibit mass loss.[21] By comparison, polyanhydrides are less stable toward hydrolytic degradation relative to polyesters and degradation rates are limited to hours to days, which for mechanically-strenuous implant device applications, such as some orthopedic applications, is much too fast.

Polycarbonates, on the other hand, found in engineering materials where high toughness, optical clarity, and solvent resistance are desired, are more stable toward hydrolytic degradation than amorphous polyesters.[22] When aliphatic carbonates undergo hydrolytic degradation, they are converted to alcohols and carbon dioxide, which may

decrease the risk of undesirable side effects and slow the rate of erosion, compared to the degradation products of polyesters.[23-25] Their low toxicity and versatility (ease of incorporating different functionalities) make them ideal biomaterial candidates, yet efforts to develop degradable polycarbonates for biomedical applications have been limited until very recently.[26] Hendrick and Yang *et al.* have developed antimicrobial aliphatic polycarbonate hydrogels with broad-spectrum antimicrobial activity and fast degradation rates (4 to 6 days).[27-28] Recently, hydrophilic polycarbonates have also received attention as degradable alternatives to poly(ethylene glycol) hydrogels.[29-30]

By utilizing the mechanical and degradation properties of polycarbonates, improvements in the limitations of conventional polyester and polyanhydride systems may be possible. In the Wooley research group, degradable polycarbonates are being developed from sugars (*i.e.* glucose and mannose),[31-32] polyphenolic compounds (*i.e.* quercetin), neolignins (*i.e.* honokiol), and other polyhydroxyl natural products (*i.e.* ferulic acid and quinic acid)[33-34]. In the case of polycarbonates built from natural products, it is possible to design materials that produce bioactive products upon degradation. One specific natural building block is quinic acid (QA), a polyhydroxyl compound found freely and in the form of esters with cinnamic acids, known as chlorogenic acids, in many agricultural products such as tree barks, tobacco, teas, coffee, and many fruits and vegetables.[35] Free QA occurs naturally in green coffee beans, and upon roasting, hydrolysis of chlorogenic acids produces additional QA, making QA one of the dominant acids present in roasted coffee.[36] Quinic acid can be isolated from natural sources or produced from glucose through environmentally-friendly and cost-

effective methods.[37] Quinic acid is metabolized by intestinal microflora to afford tryptophan and nicotinamide and promotes antioxidant activity and growth.[38-40] The combination of polyhydroxyl compounds and carbonate linkages is special because if the carbonate linkages are placed intermolecularly between two hydrolxyl groups, then upon hydrolysis the two hydroxyl groups would be reproduced and carbon dioxide released leaving the pure polyhydroxyl starting material. Thus, a polycarbonate built from QA has the potential to degrade and regenerate QA (with its beneficial bioactivity intact) under physiological conditions. Previously, the synthesis of linear poly(QA carbonate)s was investigated by copolymerization of *tert*-butyldimethylsilyloxy-protected 1,4- and 1,5-diol monomers of quinic acid and phosgene.[33] Although the polymers exhibited high glass transition temperatures (209 °C for poly(1,4-QA carbonate) and 229 °C for poly(1,5-QA carbonate)), they possessed only poor mechanical strengths, which likely resulted from limited molecular weights (7.5 kDa for poly(1,4-QA carbonate) and 7.7 kDa for poly(1,5-QA carbonate)) and incomplete deprotection (59 % removal for poly(1,4-QA carbonate) and 73% removal for poly(1,5-QA carbonate)) being achieved. Additionally, although widely employed in industrial settings due to its efficiency, the use of phosgene, a highly toxic chemical synthesized from CO and Cl_2 using an energy intensive process, is not ideal for the development of "green" plastics.

To design mechanically-robust polycarbonates, three-dimensional thermosets, crosslinked by energy efficient photo-initiated thiol-ene chemistry and derived from QA, are described here. Thermosets, as opposed to thermoplastics, are covalently crosslinked networks formed by curing under heat or irradiation. The crosslinking limits mobility

and flexibility of polymer chains and gives thermosets increased thermal and mechanical properties and solvent resistance compared to equivalent thermoplastics. The structure can be considered a giant macromolecule made up of repeat units or monomers which are covalently crosslinked by heat and/or light. The simplest form that the monomers take is A_2+B_3 (or just $A_{3)}$, where A and B are monomers, oligomers, or polymers, and the subscripts describe the functionality of each. There must exist a molecule with functionality greater than or equal to three in order to form crosslinks. If at least three of the functional groups react, then it is called a branching point. If the length of each chain beginning at the branching point extends to the boundaries of the system, (*i.e.* reaches infinity), then it is called a crosslink or crosslink point. Upon curing copolymerization occurs and chains grow by branching to form a network. As the network grows, the viscosity of the material increases as does the molecular weight, and the total number of molecules decreases. Theoretically, when network formation is complete one molecule of infinite molecular weight is left. The point at which the weight average molecular weight begins to diverge to infinity is called the gel point.[41] At the gel point the viscosity diverges to infinity and the thermoset loses its ability to flow. Mathematically the gel point can be described as the limit of the functional group conversion, p, as the degree of polymerization, $\overline{X}_n$, diverges to infinity:

$$p_{gel} = \lim_{\overline{X}_n \to \infty} p$$

The Carothers equation (shown below) relates the extent of reaction (functional group conversion) and the degree of polymerization to the average functionality of the system, f_{avg}.

$$p = \frac{2}{f_{avg}} - \frac{2}{\overline{X}_n f_{avg}}$$

Combining the two equations, the critical extent of reaction, p_c, at the gel point is

$$p = \frac{2}{f_{avg}}$$

given that there is a stoichiometric balance of functional groups. Therefore in an A_2+B_3 system (where there are 3 equivalents of A_2 and 2 equivalents of B_3 to achieve a stoichiometric balance) the average functionality is 2.4 and the extent of conversion needed to reach the gel point is 0.83, meaning that at the gel point 83% of functional groups have reacted. Beyond the gel point and as reactions proceed, the crosslink density continues to grow along with the material's glass transition temperature and mechanical properties, but it becomes impossible to process and is no longer workable.

Thermosets are generally amorphous because the presence of crosslinks makes it difficult to form any ordered regions in the material. An important thermal property of crosslinked networks is the glass transition temperature, T_g. Below the T_g the material performs as a glassy solid, and above the T_g it becomes rubbery. Depending on the desired temperature at which the material will be used and whether it will be used in its rubbery or glassy state, the T_g of the material should coincide accordingly. Thermosets that have a T_g below room temperature or in other words, are rubbery at room temperature are called elastomers.

In biomedical applications, thermosets are attractive because the three-dimensional, crosslinked structure more closely matches that of natural tissue, specifically extracellular materials, which provide direction for cell organization,

structural integrity, and mechanical support to complex tissues, compared to the structure of thermoplastics.[42] Polymer networks exhibit more favorable material kinetics (swelling, degradation, breakdown of properties) upon tissue integration, and overcome many of the processing limitations possessed by degradable polyesters, including the use of harsh solvents and conditions and the dependence of properties on the physical size of the implant device.[20, 43] Photo-polymerizable networks are especially attractive for their ability to form *in situ* and fill complex geometries.

One reliable and powerful tool for photo-crosslinking is thiol-ene chemistry, which is widely accepted academically and industrially in many different fields due, mainly to the pioneering work of Hoyle *et al.* and carried on by Bowman and coworkers.[44-47] Thiol-ene chemistry is highly efficient, easily accessible, tolerant of many functional groups, and has been employed in various tissue engineering applications.[48-50] The thiol-ene polymerization mechanism consists of the addition of a thiyl radical across an alkene, followed by chain transfer to a thiol, thus regenerating the thiyl radical. This step-growth, free radical polymerization proceeds under mild conditions to high conversions even in the presence of water or oxygen and produces crosslinked networks, which are significantly more uniform and contain less residual stresses post cure compared to acrylate networks.[51-52] The homogeneity of the networks produced by thiol-ene crosslinking has made it an attractive technique in applications where highly uniform network structures are criterial such as soft lithography, gas barriers, and transport materials.[52-53]

In this dissertation, the relatively low energy requirements and rapid speed of photo-initiated thiol-ene crosslinking was utilized to synthesize polymers containing carbonate linkages without the use of harsh reagents or conditions. A QA lactone was modified to produce the *tris*(alloc) quinic acid (TAQA) alkenyl monomer, and three-dimensional poly(thioether-*co*-carbonate) networks were achieved by copolymerization with multifunctional thiols upon UV exposure. The bicyclic monomer, TAQA, is of interest because of its rigidity and the potential for two-stage degradation, where hydrolysis of the lactone may trigger carbonate backbone degradation.

Initial demonstration of crosslinked network formation is extended to fully investigate structure-property relationships by varying the multifunctional thiol composition and stoichiometry, including mixtures of thiol monomers. Each variation in chemical composition and architecture is designed to exploit the range of achievable thermomechanical properties and potential target applications. Aside from the significant benefits of synthesizing and characterizing UV-curable poly(thioether-*co*-carbonate)s, the work herein also investigates several critical areas that need to be understood before these materials can be seriously considered for biomedical applications. For example, a full life-time analysis of polymer degradation kinetics in physiologically-relevant conditions, changes in the thermomechanical properties from initial introduction into an aqueous environment and throughout degradation, and degradation product identification and cytotoxicity are important factors that influence the usability of these materials. Key efforts were directed toward *in situ* changes in mechanical properties due to solvent plasticization and temperature effects. This

dissertation is divided into four chapters based on desired properties and how the materials are meant to function in the target applications. The goal of the first project, described in Chapter II, was to develop rigid polycarbonate networks for mechanically-strenuous biomedical implant applications. The second project, described in Chapter III, focuses on the feasibility of the materials introduced in Chapter II for biomedical applications. Studies were performed to understand how the material would be affected by a physiological environment and how the tissue environment would be affected by the materials. The third project, described in Chapter IV, focused on materials designed to be rigid at room temperature and soften under physiological conditions, and special attention will be paid to evaluating their mechanically-adaptive nature and designing materials with one-dimensional mechanical gradients. Appendix A describes an ongoing project in which natural multifunctional thiols derived from lipoic acid are utilized to increase the overall natural content of the material.

CHAPTER II

PHOTO-CROSSLINKED POLY(THIOETHER-*CO*-CARBONATE) NETWORKS DERIVED FROM THE NATURAL PRODUCT QUINIC ACID*

2.1 Introduction

Polymers derived from natural resources have attracted increased attention not only for their ability to form commodity plastics, which decrease dependence on petroleum processes, but also for their ability to form biocompatible materials with resorbable degradation products.[54-56] Recently, polymers derived from naturally-occurring precursors, such as nucleotides,[57] carbohydrates,[32] ferulic acid,[34] and D-limonene[58-59] have been reported as prospective degradable biomaterials. Common polyesters, including poly(lactic acid) and poly(glycolic acid), have shown to be useful in various tissue engineering applications including some orthopedic applications.[19, 60] They possess modulus values similar to cancellous bone (0.1 – 4.5 GPa) but still low compared to cortical bone (17 – 24 GPa), and orthopedic devices made from these materials may require challenging and costly fabrication and sterilization techniques.[11, 61] Materials for implant device applications demand polymer functionality both at the macromolecular and molecular levels to satisfy material design requirements and enable a desired physiological response. In the case of bioresorbable polymers for orthopedic devices, the design criteria include moduli and ultimate strength values similar to those

*Reprinted with permission from Lauren A. Link, Alexander T. Lonnecker, Keith Hearon, Cameron A. Maher, Jeffery E. Raymond, and Karen L. Wooley, *ACS Appl. Mater. Interfaces* **2014**, *6*, 17370-17375, Copyright 2014 American Chemical Society.

of bone and a high degree of compatibility with surrounding tissue from initial implantation and throughout degradation.[13] In the case of polyesters, inflammation and pain may arise if acidic degradation products are not cleared quickly.[62]

By utilizing the mechanical and degradation properties of polycarbonates, improvements in the limitations of conventional systems may be possible. When aliphatic carbonates undergo hydrolytic degradation, they are converted to alcohols and carbon dioxide, which may decrease the risk of undesirable side effects and slow the rate of erosion, compared to the degradation products of polyesters.[23-25] Furthermore, in the case of polycarbonates built from natural products, it is possible to design materials that produce bioactive products upon degradation. One such natural building block is quinic acid (QA), a polyhydroxyl compound found freely and in the form of esters with cinnamic acids, known as chlorogenic acids, in many agricultural products such as tree barks, tobacco, teas, coffee, and many fruits and vegetables.[35] Free QA occurs naturally in green coffee beans, and upon roasting, hydrolysis of chlorogenic acids produces additional QA, making QA one of the dominant acids present in roasted coffee.[36] Quinic acid can be isolated from natural sources or produced from glucose through environmentally-friendly and cost effective methods.[37] Quinic acid is metabolized by intestinal microflora to afford tryptophan and nicotinamide and promotes antioxidant activity and growth.[38-40] Previously, the synthesis of poly(QA carbonate)s was investigated by copolymerization of tert-butyldimethylsilyloxy-protected 1,4- and 1,5-diol monomers of quinic acid and phosgene.[33] Although the polymers exhibited high glass transition temperatures (209 °C for poly(1,4-QA carbonate) and 229 °C for

poly(1,5-QA carbonate)), they possessed only poor mechanical strengths, which likely resulted from limited molecular weights and incomplete deprotection being achieved.

To introduce mechanically-robust bio-based polycarbonates, the synthesis and thermomechanical characterization of covalently crosslinked networks derived from QA are reported in this study. A QA lactone was modified to produce the *tris*(alloc) quinic acid (TAQA) alkenyl monomer shown in Figure 2.1. Three-dimensional networks were achieved by photo-catalyzed thiol-ene chemistry upon polymerization with the multifunctional thiols also illustrated in Figure 2.1. Thermomechanical properties of the poly(thioether-*co*-carbonate) networks were compared to networks containing the commercially-available monomer, triallyl-1,3,5-triazine-2,4,6-trione (TATATO). Thiol-ene chemistry[44, 52, 63] is highly efficient, easily accessible, proceeds under mild conditions, tolerant of many functional groups, and has been employed in various tissue engineering applications.[48-50] Several material design criteria drove the monomer selection. Because one end goal is synthesizing amorphous polymers for use in orthopedic applications, it is important that the materials perform as a glassy solid at physiological temperature with modulus close to that of bone. Thus, the optimal glass transition temperature (T_g) would be significantly above body temperature (37 °C). Many thiol-ene polymers undergo glass transitions below 37 °C because of the high flexibility of the thioether linkage, and increasing the T_g has traditionally been a significant synthetic challenge.[64] One method of increasing the T_g in network polymers is to increase crosslink density by increasing monomer functionality; however, increasing crosslink density to the extent necessary to raise the T_g above 37 °C in thiol-

ene polymers has often resulted in significantly decreased toughness, which is undesirable.[65-66] Therefore, an ideal material would have a T_g well above 37 °C and a low, but sufficient, crosslink density. In this study, the bicyclic structure of TAQA is predicted to increase the T_g by increasing network rigidity in comparison with the commercially-available triallyl monomer, TATATO. Concerning thiol monomer selection, the 1,2-ethanedithiol (1,2-EDT) monomer is predicted to form networks with high rigidity and toughness compared to other commercially-available polythiols because the 1,2-EDT-*co*-TAQA polymer has the greatest TAQA weight fraction while also having a moderate crosslink density because of the difunctionality of 1,2-EDT.

The two-step synthesis of the TAQA monomer (Figure 2.1, bottom) coupled with the solvent-free, binary copolymerization enabled the facile production of highly-uniform crosslinked networks. The first step of the monomer synthesis was well-established lactonization of QA under acidic conditions.[67] Quinic acid and acidic Amberlyst resin were suspended in benzene and *N*,*N*-dimethylformamide and heated to reflux with azeotropic removal of water to afford the bicyclic triol, QA lactone in 96% yield. To install the three alloc functional groups, allyl chloroformate was added drop-wise to QA lactone suspended in *N,N,N',N'*-tetramethylethylenediamine and dichloromethane, to give 74% yield of TAQA as a clear, viscous oil. The structure of TAQA was confirmed by FTIR and ESI-MS, as well as ^{1}H, ^{13}C, COSY, and HSQC NMR spectroscopies. Solvent-free crosslinking copolymerization by thiol-ene radical addition in the presence of 1 wt% 2,2-dimethoxy-2-phenylacetophenone (DMPA) photoinitiator was performed by mixing TAQA and multifunctional thiol monomers,

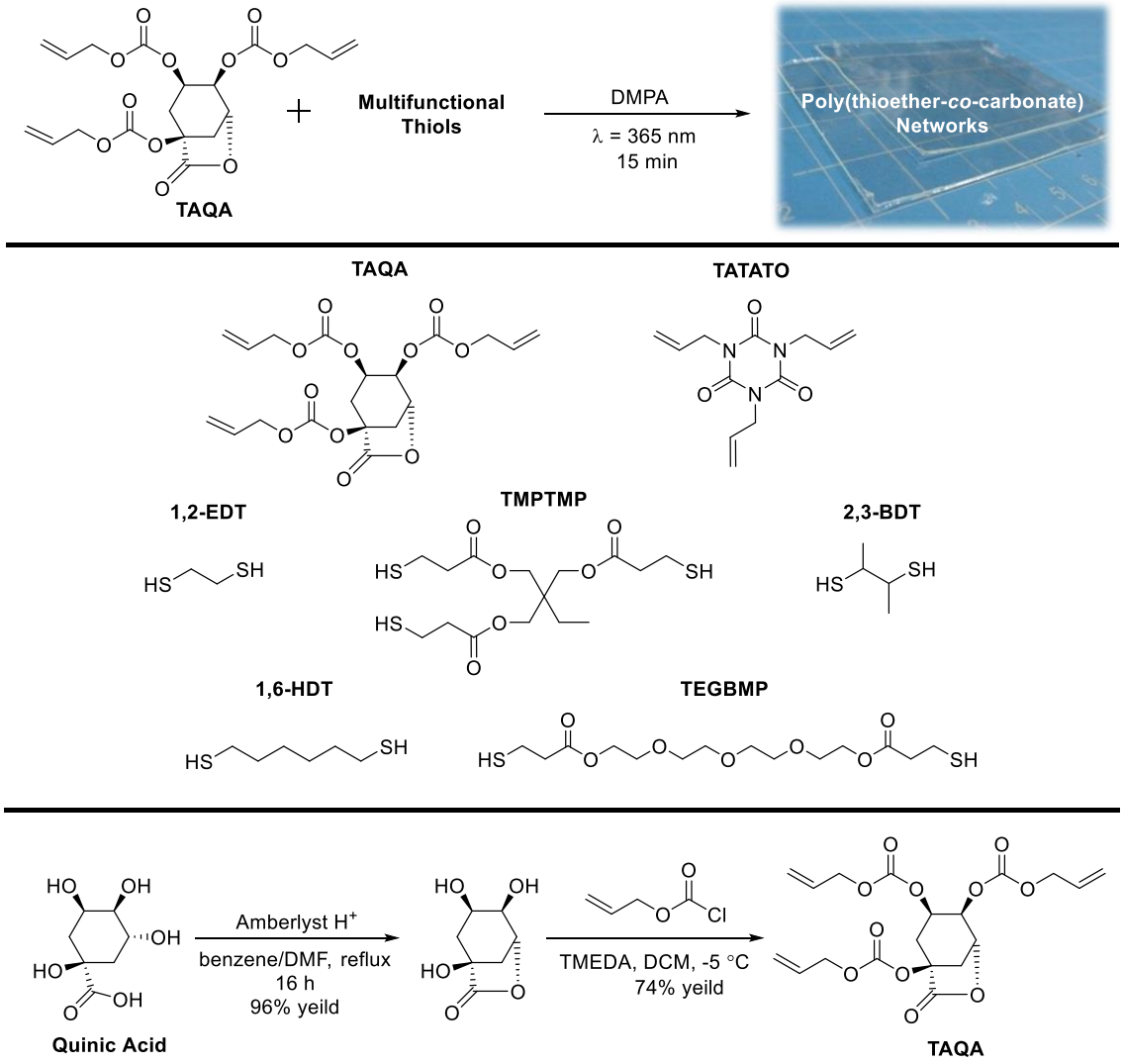

Figure 2.1. General scheme for photo-crosslinking of poly(thioether-*co*-carbonate) networks and photograph of cured films (top), monomer structures with abbreviations (middle), two-step synthesis of TAQA from quinic acid (bottom).

based on equal molar functional groups, mold casting, and exposing to UV light (λ = 365 nm) to produce films with uniform thickness (0.4 mm). This was followed by post-curing at 120 °C for at least 4 h to vulcanize residual thiol groups. The samples were characterized by FTIR spectroscopy to verify consumption of alkene (1650 cm^{-1}) and thiol (2570 cm^{-1}) groups upon network formation. A variety of multifunctional thiols was investigated including 1,2-EDT, 2,3-butanedithiol (2,3-BDT), 1,6-hexanedithiol (1,6-HDT), trimethylolpropane *tris*(3-mercaptopropionate) (TMPTMP), and tetraethylene glycol *bis*(3-mercaptopropionate) (TEGBMP).

2.2 Results and Discussion

The dynamic mechanical analysis (DMA) results in Figure 2.2 show the relative thermomechanical behavior in tension of cured samples synthesized from TAQA or TATATO and various thiol compounds. This behavior is characteristic of amorphous, covalently crosslinked polymers, which includes a glassy modulus plateau at temperatures below the glass transition, a transition region in which modulus decreases with increasing temperature, and a rubbery plateau region in which the modulus remains constant or slightly increases with increasing temperature. The crosslink density of a thermosetting polymer is proportional to its rubbery modulus plateau in accordance with the relationship for an ideal rubber. Materials incorporating TMPTMP had the highest crosslink density, due to its increased functionality as compared to the other thiol monomers investigated. The relatively low crosslink density of the 2,3-BDT-*co*-TAQA networks, compared to the other materials, can be explained by ineffective crosslinking reactions due to steric hindrance by the bulky secondary thiols of 2,3-BDT. Table 2.1

lists the thermomechanical properties of the poly(thioether-*co*-carbonate) networks containing the various multifunctional thiols investigated. The T_g values, determined by differential scanning calorimetry (DSC), are consistent with the onset of the glass transition region in the storage modulus behavior shown in Figure 2.2. The 1,2-EDT-*co*-TAQA sample contained the greatest weight fraction of the rigid, bicyclic TAQA monomer and the lowest weight fraction of flexible aliphatic spacer atoms and, thus, exhibited the highest T_g value (65 °C), comparable to that of poly(L-lactide) (T_g = 60 - 65 °C). In contrast, the TEGBMP-*co*-TAQA system's longer and more flexible TEGBMP-based spacer resulted in an elastomeric material with a T_g well below room temperature. The 1,2-EDT-*co*-TATATO network expressed a T_g which was 27 degrees lower than that of the 1,2-EDT-*co*-TAQA material. As predicted, the bicyclic TAQA monomer provided the 1,2-EDT-*co*-TAQA network with increased rigidity that could not be achieved with the commercially-available triallyl monomer, TATATO, in the 1,2-EDT-*co*-TATATO network. DMA experiments at multiple frequencies were used to determine the activation energy of the glass transition, E_a, of 1,2-EDT-*co*-TAQA which was 374 ± 14 kJ/mol in accordance with the Arrhenius relationship.[68] In comparison with poly(lactic acid) (E_a = 255 kJ/mol),[69] 1,2-EDT-*co*-TAQA networks require more energy to impart segmental motion. Poly(bisphenol-A carbonate), however, has a considerably higher E_a of 766 kJ/mol, due to its rigidity and ability to dissipate energy effectively.[70]

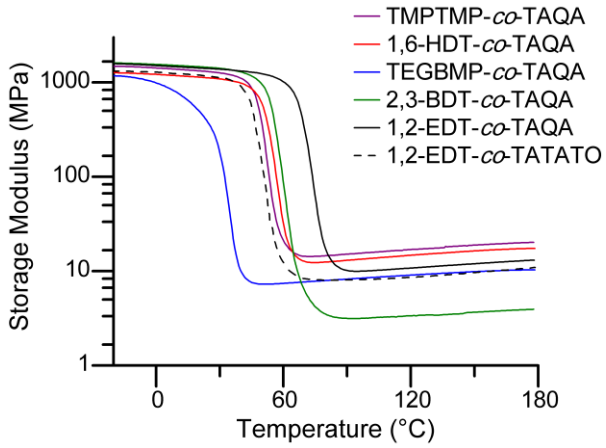

Figure 2.2. Storage modulus measurements by DMA in tension mode of films (post-cured for 24 h) as a function of temperature.

Sample	T_g [°C][a]	T_d [°C][b]	E' [MPa][c]	E_r [MPa][d]
TEGBMP-*co*-TAQA	-18	264	357	7.3
TMPTMP-*co*-TAQA	43	275	1290	14
1,6-HDT-*co*-TAQA	48	261	1110	12
2,3-BDT-*co*-TAQA	51	261	1440	3.1
1,2-EDT-*co*-TAQA	65	262	1400	10
1,2-EDT-*co*-TATATO	38	332	1170	7.2

Table 2.1. Thermal transitions and moduli exhibited by the poly(thioether-*co*-carbonate) networks derived from TAQA in comparison to networks derived from a commercially-available triallyl monomer. [a]Determined by DSC; [b]Onset of thermal decomposition determined by TGA; [c]Storage modulus at 25 °C determined by DMA; [d]Rubbery modulus determined by DMA

The temperature at which the onset of thermal decomposition began, T_d, was determined by thermogravimetric analysis. All of the poly(thioether-*co*-carbonate)s characterized had thermal decomposition temperatures greater than 260 °C (Table 2.2). To determine post-cure time necessary to drive the polymerization to completion, enable vaporization of residual small molecules, and allow for network relaxation, DSC

experiments were run on samples subjected to varying post-cure times at 120 °C. As post-cure time increased from 0 to 4 h, the T_g increased for each sample, and after 4 h, negligible changes in T_g were observed (shown in supporting information). Thermal analysis of the network materials synthesized in this study demonstrates that a significant variation in thermomechanical properties is achievable by varying the thiol monomer chemistry. The diverse array of physiological environments within the body has given rise to the need for biomaterials that conform to a wide range of design criteria.

Each of the poly(thioether-*co*-carbonate) networks that met the requirement of being glassy at 37 °C, 1,2-EDT-*co*-TAQA, TMPTMP-*co*-TAQA, 2,3-BDT-*co*-TAQA, and 1,6-HDT-*co*-TAQA, was subjected to tensile strain-to-failure measurements. The stress/strain behavior of each system at 25 °C is depicted in Figure 2.3 (a). Although all four of the samples performed similarly, the networks with lower T_g values, 1,6-HDT-*co*-TAQA and TMPTMP-*co*-TAQA, failed in a slightly more ductile manner, reaching a yield point at which the material exhibits an increase in strain at a constant or slightly decreasing stress, compared to the networks with higher T_g values, 1,2-EDT-*co*-TAQA and 2,3-BDT-*co*-TAQA. While 1,2-EDT-*co*-TAQA exhibited brittle behavior at 25 °C and fails at 8% strain, it becomes more ductile at elevated temperatures, shown in Figure 2.3 (b). At 63 °C, just below its T_g (65 °C), 1,2-EDT-*co*-TAQA undergoes weak elastomeric failure at a stress of 6 MPa, but at 37 °C, 1,2-EDT-*co*-TAQA exhibits a more ductile behavior and fails at 100% strain while also exhibiting a failure stress greater than 23 MPa. While the average toughness of 1,2-EDT-*co*-TAQA at 25 °C and

63 °C was 1.08 MJ/m^3 and 2.35 MJ/m^3, respectively, the average toughness at 37 °C was 15.56 MJ/m^3. This increase in toughness at physiological temperature is more than an order or magnitude difference from the toughness at room temperature. Along with increased toughness, it is also desirable that a material for orthopedic applications maintains rigidity and is resistant to plasticization upon implantation.

In order to measure solvent plasticization effects, 1,2-EDT-*co*-TAQA films were subjected to *in situ* matrix relaxation DMA experiments in physiologically-relevant conditions, specifically, in phosphate buffered saline (PBS) solution (pH 7.4, 137 mM NaCl, 2.7 mM KCl, 10 mM phosphate buffer) at 37 °C. Figure 2.3 (c) shows the results of the first 17 h of submersion. There was an initial thermal response upon submersion followed by a solvent plasticization response, after which the modulus begins to increase slightly over 15 h. The solvent response, after temperature effects, was a solvent-plasticized material with $\Delta E' = -230$ MPa (−15%) and a saturation lifetime of 31 min (Figure 2.3 (c) inset). Following the solvent plasticization response, a change $\Delta E' = 80$ MPa was observed in which the material stiffens. This may be an indication that, even when fully saturated, the system still requires time, to reach its lowest energy configuration. Therefore, the net response to submersion in a physiologically-relevant environment over 17 h is $\Delta E' = -150$ MPa (−10%). The sample was allowed to recover for 24 h, and was then subjected to the same experimental regimen (shown in supporting information). The storage modulus behaved similarly in response to initial solvent plasticization, but did not increase over the following 15 h. This behavior indicates that

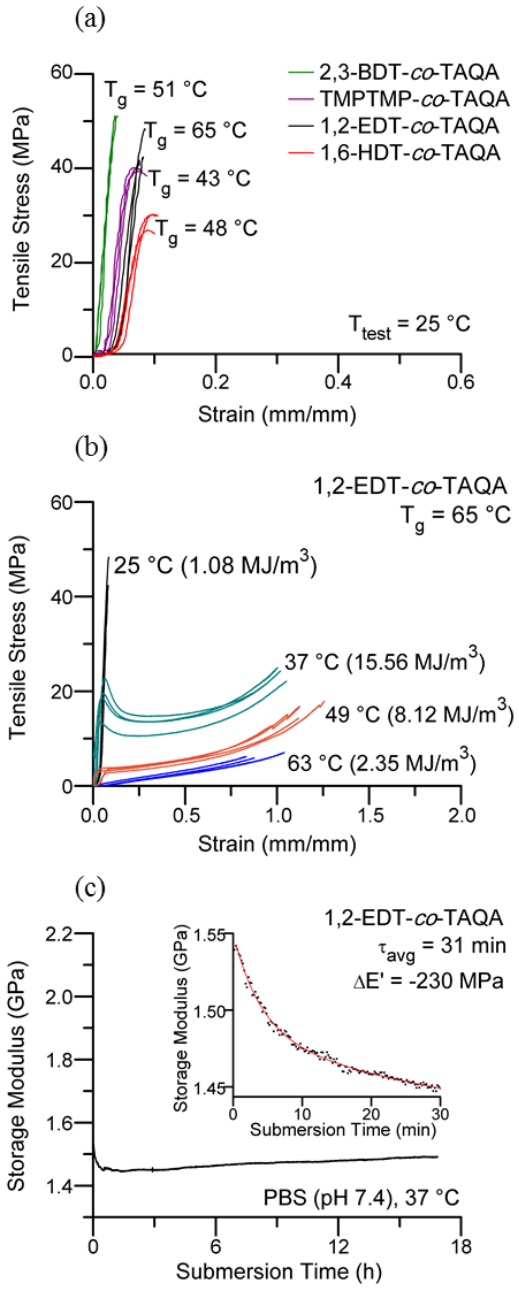

Figure 2.3. (a) Stress/strain behavior of poly(thioether-*co*-carbonate) networks that exhibit T_g values which are greater than physiological temperature, (b) strain-to-failure of 1,2-EDT-*co*-TAQA at various temperatures, and (c) storage modulus as a function of time over 17 h obtained by submersion DMA in PBS at 37 °C. Inset shows *in situ* stress relaxation in response to solvent (first 30 min) fit to a dual exponential decay (R^2 = 0.993).

the lower energy configuration of the matrix was retained for at least 24 h after drying. Beyond 24 h, 1,2-EDT-*co*-TAQA may begin to undergo hydrolytic degradation, at which point there would be a reduction in modulus. No significant differences in surface roughness were observed by atomic force microscopy (AFM), indicating no significant film degradation during 15 h of submersion (shown in supporting information).

2.3 Conclusions

We present a series of photo-crosslinked polymer networks derived from the natural product quinic acid with controlled T_g values from −18 to 65 °C and rubbery modulus values from 3.8 to 20 MPa. The network containing the highest weight percent of rigid bicyclic monomer, 1,2-EDT-*co*-TAQA, exhibited a T_g of 65 °C and a storage modulus of 1.4 GPa, properties comparable to those of common degradable polyesters used in orthopedic applications. At 37 °C 1,2-EDT-*co*-TAQA exhibited an average toughness which was an order of magintude higher than at room temperature and was resistant to plasticization upon submersion in PBS for 17 h. The material maintained its modulus upon submersion in PBS at 37 °C, exhibiting only slight solvent plasticization within the first 30 min. Given the stability of the poly(thioether-*co*-carbonate) networks at 120 °C, for biomedical device applications, it may be possible to sterilize final devices by autoclaving or dry heat, rather than by ethylene oxide or γ-radiation, which each have significant disadvantages.[11] These poly(thioether-*co*-carbonate)s have a wide range of achievable material properties, and potential applications include biomedical applications and expand to non-petroleum-based "green" engineering polymers for commodity plastics applications. We demonstrate the ability to form a polymer with

carbonate linkages without using any harsh conditions or solvents, giving the resulting material a high degree of industrial and environmental relevance. In total, this system represents a thermosetting polycarbonate material that is expected to produce environmentally-friendly and bioresorbable degradation products. Future investigation will focus on the degradation kinetics *in vitro* and *in vivo* of these materials, as well as on strategies for incorporating other chemistries and functional components.

2.4 Materials and Methods

Quinic acid, Amberlyst 15 ion-exchange resin, N,N,N',N'-tetramethylethylenediamine, allyl chloroformate, 2,2-dimethoxy-2-phenylacetophenone, 1,2-ethanedithiol, 2,3-butanedithiol, 1,6-hexanedithiol, trimethylolpropane tris(3-mercaptopropionate), and triallyl-1,3,5-triazine-2,4,6-trione were all used as received from Sigma Aldrich. Tetraethylene glycol bis(3-mercaptopropionate) (Wako Chemical) was also used as received.

^{1}H and ^{13}C NMR spectra were obtained on either a Mercury 300 or an Inova 300 at 300 MHz or 75 MHz, respectively, using the solvent signal as internal reference. Glass transition temperatures (T_g) were measured using differential scanning calorimetry (DSC) by a Mettler-Toledo DSC822 (Mettler-Toledo, Columbus, OH) with a heating rate of 10 °C/min. The T_g was taken as the midpoint of the inflection tangent upon the third heating cycle and averaged over three samples. Thermogravimetric analysis (TGA) was done under an Ar atmosphere using a Mettler-Toledo TGA/DMA1 with a heating rate of 10 °C/min. IR spectra were obtained from a Shimadzu IR Prestige Attenuated Total Reflectance Fourier-transform Infrared Spectrometer (ATR-FTIR).

Dynamic mechanical analysis (DMA) experiments were run in tension to determine thermomechanical profiles for the thermoset poly(thioether-*co*-carbonate) samples. Rectangular DMA specimens (4 mm x 25 mm x 0.4 mm) were machined using a Gravograph LS100 40 W CO_2 laser machining device. All laser machined samples were sanded around the edges using 400, then 600 grit sandpaper. DMA was performed using a TA Instruments Q800 Dynamic Mechanical Analyzer in the DMA Multifrequency/Strain mode in tension using a deformation of 0.1% strain, a frequency of 1 Hz, a force track of 150%, and a preload force of 0.01 N. Each experiment was run from −20 to 180°C using a heating rate of 2°C/min (presented in Figure 1). All other DMA and submersion DMA were performed on a Mettler-Toledo TT-DMA system. DMA data were obtained from Triton Laboratory software and exported to Origin Pro 9.0 for analysis. Kinetic fits were obtained by single or exponential fitting as appropriate, using chi-squared analysis to assign fitting component number. Average lifetimes for multi-exponential kinetics are reported as intensity average lifetimes where $t(avg) = \Sigma(a_i \bullet t_i^2) / \Sigma(a_i \bullet t_i)$. Activation energy data were extracted from frequency tan(δ) maxima as fitted with a single Gaussian distribution in the temperature regime. Variable frequency DMA measurements were done from 0.1 to 100 Hz, and the activation energy was averaged over three samples. To determine toughness values, ultimate tensile strengths, and failure strains, tensile testing experiments were conducted to failure on ASTM type V dog bone samples (n = 5) using a dual-column Instron model 5965 tensile tester with a 500 N load cell, 1000 N high temperature pneumatic grips, and a temerature chamber thermally controlled by forced convection heating. The dog bone

samples were cut with a 40 W Gravograph LS100 CO_2 laser and edges were smoothed with 180 grit sandpaper. Atomic force microscopy was performed using an Asylum 3D-SA instrument operated in tapping mode with a silicon probe (Vista probes T190, k = 48 N/m, f = 190 kHz - nominal). Surface analysis was performed with IGOR 6.0 software.

2.4.1 Functionalization of QA lactone with allyl carbonate groups

QA lactone (4.081 g, 23.43 mmol) was synthesized as previously described[67] and added to a flame-dried 250-mL schlenk flask back-filled with nitrogen. DCM (30 mL) was added and the solution was cooled to −5 °C. TMEDA (14.5 mL, 96.8 mmol) was added and allowed to stir at −5 °C for 20 min. To an addition funnel equipped with a pressure equalizing side arm, allyl choroformate (17.8 mL, 168 mmol) was added and diluted with DCM (10 mL). Dropwise addition (~1 drop/5 s) of the allyl chloroformate and DCM mixture to the flask proceeded for about 4 h. The reaction was maintained between -5 °C and -10 °C, stirring rapidly for 2 h after the addition was complete. The reaction was allowed to warm to room temperature and stirred overnight. The thick white solid that remained was dissolved in DCM and filtered. The filtrate was washed twice with deionized water, once with a 10 wt% $CuSO_4$ solution, dried with $MgSO_4$, filtered and concentrated. The crude product was purified by column chromatography (hexane-ethyl acetate, 3:2) to afford tris(alloc) quinic acid (TAQA) (7.406 g, 74%). T_m = −21 °C. ^{1}H NMR ($CDCl_3$, 300 MHz): δ 5.97-5.88 (m, 3 H, H-10), 5.41 (t, 1 H, J = 5.1, 4.6 Hz, H-4) 5.41-5.27 (m, 6 H, H-11), 5.04 (ddd, 1 H, J = 11.7, 6.9, 4.5 Hz, H-5), 4.96-4.94 (dd, 1 H, J = 6.0, 4.9 Hz, H-3), 4.65-4.62 (m, 6 H, H-9) 3.22-3.18 (ddd, 1 H, J = 11.6, 6.1, 2.8 Hz, H-2), 2.57-2.55 (d, 1 H, J = 11.4 Hz, H-2), 2.46-2.41 (ddd, 1 H, J =

12.1, 6.9, 2.8, H-6), 2.35 (t, 1 H, J = 11.9, H-6); ^{13}C NMR ($CDCl_3$, 125 MHz): δ 170.6 (C7), 153.8 (C8), 153.3 (C8), 152.3 (8), 131.2 (C10), 131.0 (C10), 130.8 (C10), 119.9 (C11), 119.8 (C11), 119.46 (C11), 77.5 (C1), 73.4 (C3), 69.6 (C9), 69.5 (C9), 69.4 (C5), 69.3 (C9), 67.9 (C4), 33.5 (C2), 33.4 (C6); FT-IR (neat, cm^{-1}): 2985, 2956, 1809 (C=O), 1747 (C=O), 1651, 1448, 1425, 1417, 1367, 1274, 1228, 1211, 1161, 1145, 1103, 1083, 1039, 989, 937, 781, 750; HRMS (+ESI) *m/*z calc'd for $C_{19}H_{22}O_{11}$ $[M+K]^+$: 465.08, found 465.0794.

2.4.2 General procedure for fabricating thiol/TAQA films

Mixtures of multifunctional thiol and TAQA were prepared based on equal molar functional groups. The amount of photoinitiator, DMPA, was 1 wt% for each mixture. Table 2.1 shows the composition for each film. DMPA was first dissolved in the multifunctional thiol and then TAQA was added and blended thoroughly. Each mixture was cast between two glass slides separated by a 0.5 mm spacer, and exposed to UV light (365 nm) on a Fusion curing line system (1 m/min, 15 min). The glass slide molds were removed, and the free-standing films were post-cured at 120 °C for 4 h or as otherwise noted.

Formulation	Triallyl Monomer (g)[a]	Thiol (g)	DMPA (g)
TEGBMP-*co*-TAQA	0.3060	0.3986	0.0070
TMPTMP-*co*-TAQA	0.3140	0.2946	0.0059
1,6-HDT-*co*-TAQA	0.3904	0.2056	0.0064
2,3-BDT-*co*-TAQA	0.4174	0.1791	0.0060
1,2-EDT-*co*-TAQA	0.4540	0.1484	0.0058
1,2-EDT-*co*-TATATO	0.7683	0.4313	0.0121

Table 2.2. Thiol-ene network formulations. [a]Triallyl monomer was either TAQA or TATATO.

2.5 Supporting Information

Additional characterization data, including ^{1}H, ^{13}C, COSY, and HSQC NMR spectroscopies of TAQA are depicted below in Figure 2.4, 2.5, 2.6, and 2.7, respectively.

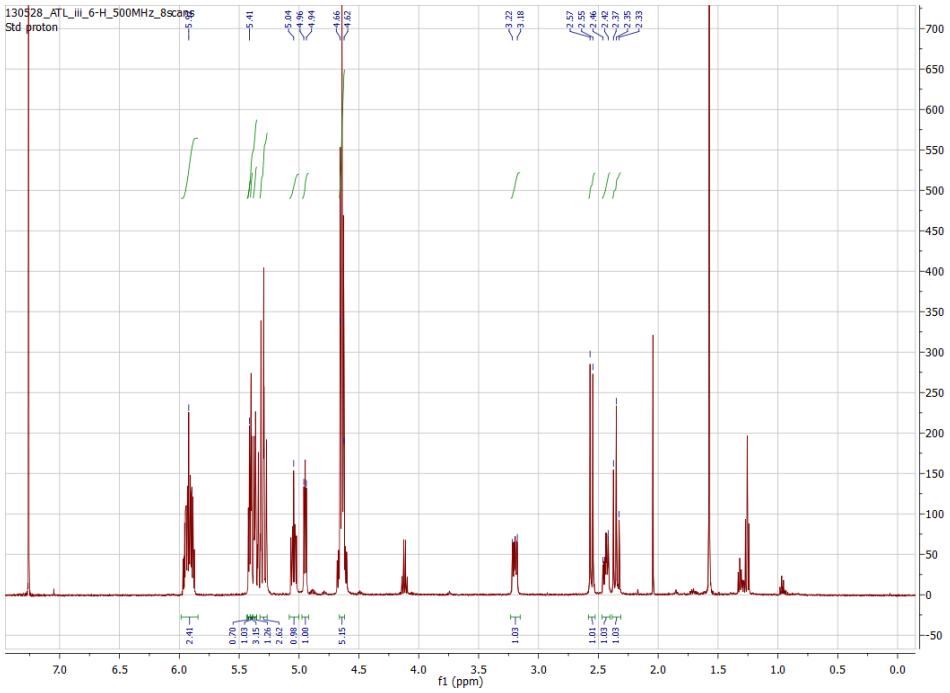

Figure 2.4. ^{1}H NMR spectrum of TAQA.

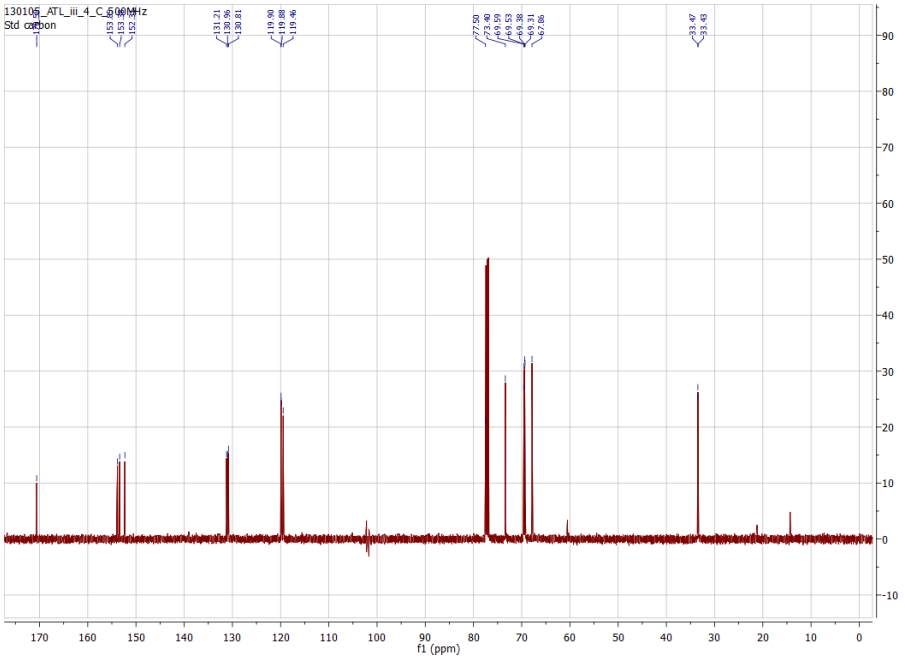

Figure 2.5. ^{13}C NMR spectrum of TAQA.

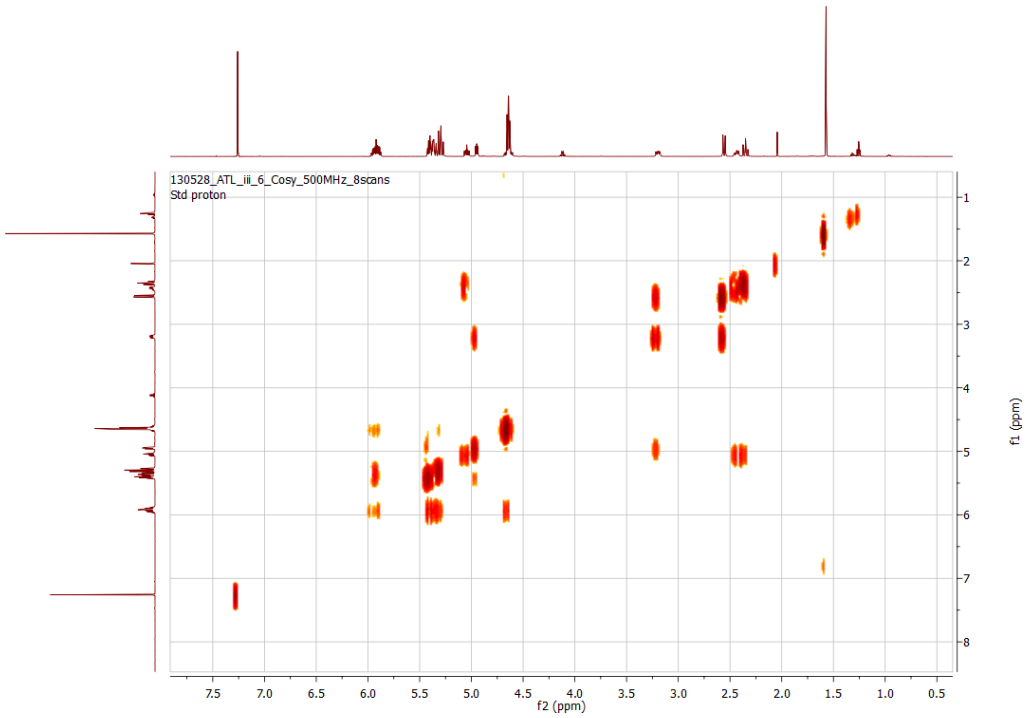

Figure 2.6. COSY NMR spectrum of TAQA.

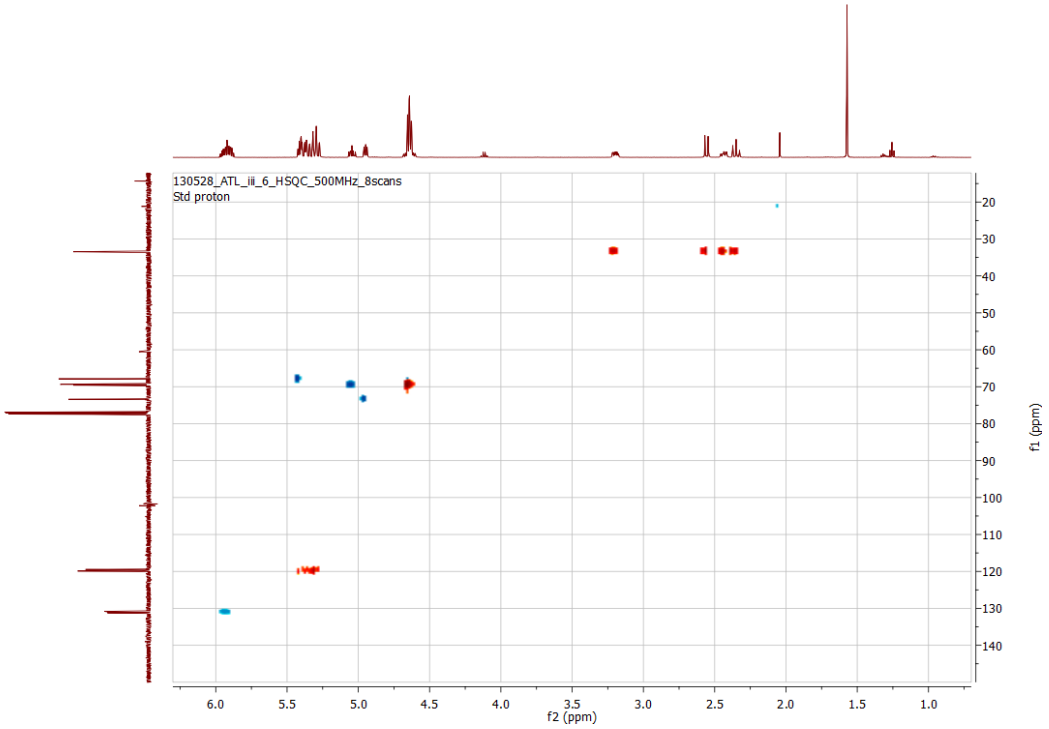

Figure 2.7. HSQC NMR spectrum of TAQA.

The effects of post-cure time on the T_g of the poly(thioether-*co*-carbonate) films was monitored by DSC measurements and shown in Figure 2.8. The repeat of the *in situ* DMA relaxation measurement and the AFM images of the 1,2-EDT-*co*-TAQA film before and after solvent immersion are shown in Figures 2.9 and 2.10.

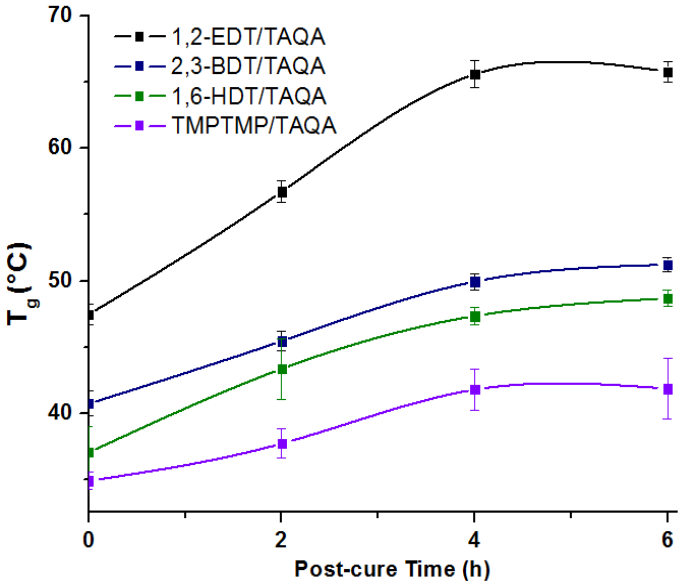

Figure 2.8. Glass transition temperatures of poly(thioether-*co*-carbonate) films as a function of post-cure time at 120 °C, determined by DSC. For each formulation and post-cure time the T_g was averaged from three samples, and the error bars represent the standard deviation.

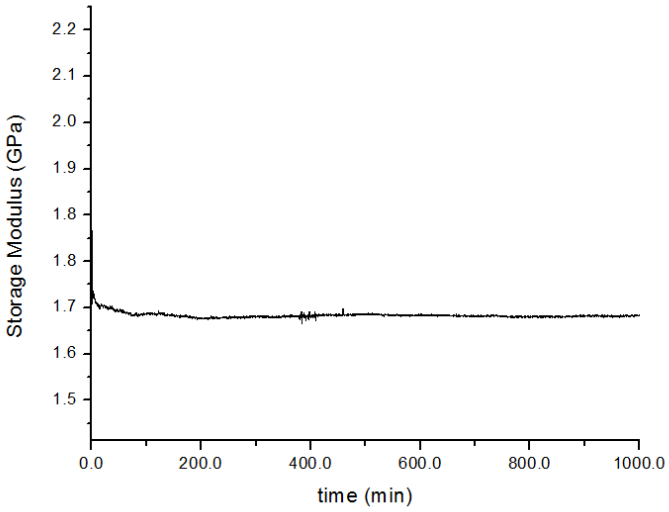

Figure 2.9. Repeat of *in situ* relaxation measurement after 24 h. Storage modulus was measured as a function of time over 15 h obtained by DMA while submerged in PBS at 37 °C.

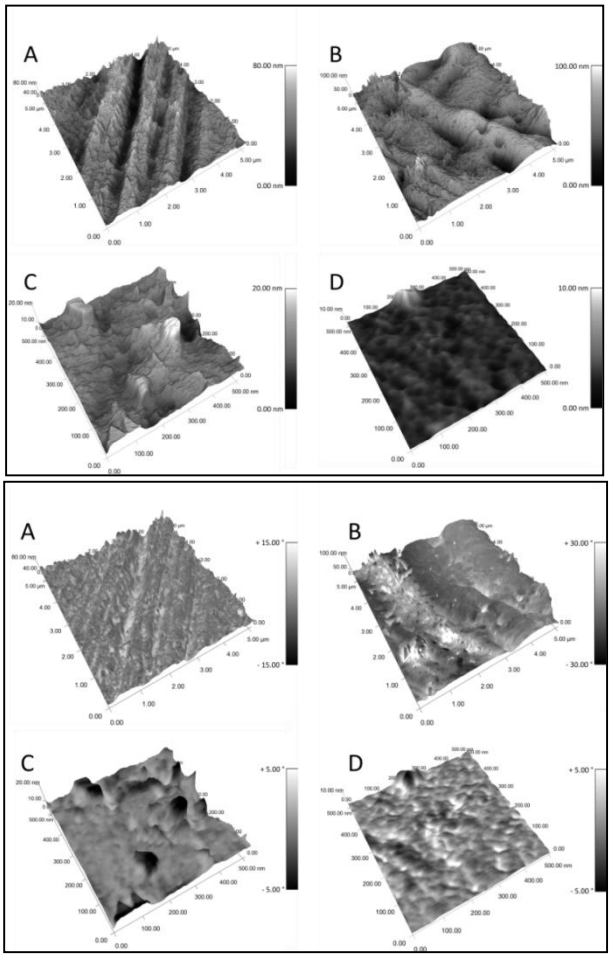

Figure 2.10. Tapping AFM of 1,2-EDT-*co*-TAQA dry and wet after 15 h submersion in PBS. Top: Height profile (A) dry 5 μm^2 (RMS roughness = 12 nm), (B) wet 5 μm^2 (RMS roughness = 16 nm), (C) dry 500 nm^2 (RMS roughness = 2.4 nm), (D) wet 500 nm^2 (RMS roughness = 1.2 nm). Bottom: Phase contrast and height profile overlay (A) dry 5 μm^2 (phase range = ± 15 °) (B) wet 5 μm^2 (phase range = ± 65 °) (C) dry 500 nm^2 (phase range = ± 6.0 °) (D) wet 500 nm^2 (phase range = ± 11 °). The height profiles show an increase in the height of small features at 5 μm^2 and smoothing of features at 500 nm^2 after 15 h of solvent immersion. The drastic increase in phase range indicates a less homogeneous matrix in terms of surface energy at the nanoscale, *e.g.* a greater difference in tip-surface interaction energies.

CHAPTER III

BIOMATERIAL FEASIBILITY STUDIES OF BIO-BASED DEGRADABLE POLYCARBONATE NETWORKS

3.1 Introduction

Bone and cartilage injuries and diseases, including fractures, arthritis, osteoporosis, and osteosarcoma, are among the most physically disabling, chronic, and costly conditions suffered by patients in developed countries.[71] The prevalence of these conditions continues to grow with the aging population and emphasizes the demand for new platform materials that can support and promote the growth of orthopedic tissue. Although the area of orthopedic biomaterials research is vast and extensive, there is still a need for economically tolerable and clinically appropriate devices with material properties that can be customized on a patient-to-patient basis.[72-73] Among the cutting-edge devices developed recently are complex bioresponsive and multifunctional hydrogels, porous 3D-printed scaffolds, and bioceramic composite implants, which utilize degradable polymer crosslinked networks as the base material/matrix of the device.[74-76]

Degradable polymer networks represent versatile materials with attractive properties for biomedical applications. The three-dimensional, crosslinked structure of polymer networks, inspired by the structure of extracellular materials, which provide direction for cell organization, structural integrity, and mechanical support to complex tissues,[42] has the ability to encapsulate biological molecules and cells and helps to

control undesirable swelling. Compared to conventional thermoplastic poly(α-hydroxyacid)s, such as poly(lactic acid), crosslinked polymer networks have a microstructure which more closely matches that of natural tissue, exhibit more favorable material kinetics (swelling, degradation, breakdown of properties) upon tissue integration, and overcome many of the processing limitations possessed by degradable polyesters, including the use of harsh solvents and conditions and the dependence of properties on the physical size of the implant device.[20, 43] Photo-polymerizable networks are especially attractive for their ability to form *in situ* and fill complex geometries.

Hydrolytically labile linkages, such as anhydride, ester, or carbonate moieties, generally make up the degradation sites within the polymer network. While polyester and polyanhydride devices, which primarily degrade by bulk erosion on the order of months (amorphous polyesters) to years (semi-crystalline polyesters) and surface erosion on the order of hours to days, respectively, are the most well known in terms of degradable polymeric biomaterials, aliphatic polycarbonates have very recently started to attract research interest as degradable alternatives to PEG[29-30] and as antimicrobial materials for wound healing applications.[28, 77] Polycarbonates, generally considered tough materials used in engineering applications, have the advantage of forming materials with high modulus, ductility, and toughness, necessary for orthopedic applications, and degrade to produce carbon dioxide and hydroxyl-containing compounds, reducing the risk of adverse side effects as compared to the acidic degradation products of polyesters.[26] By building polycarbonate networks from natural hydroxyl-containing compounds, it's possible to design a polymer that reverts back to its

natural building blocks upon hydrolytic degradation. One such polyhydroxyl-containing natural product is quinic acid. Known for its antioxidant activity, QA is found in many plant-based resources and is one of the dominant acids in roasted coffee. In addition to its interesting biological activity, the structure of QA is attractive for the synthesis of polymeric biomaterials because the multiple hydroxyl groups provide versatile sites for functionalization and the easily-accessible rigid bicyclic structure of QA lactone adds strength and toughness. Previously, the synthesis of poly(thioether-*co*-carbonate)s derived from QA was introduced[78], and herein, an investigation into the feasibility of several poly(thioether-*co*-carbonate) networks for biomedical applications is described. The networks are formed from tris(alloc) quinic acid (TAQA) and commercially-available multifunctional thiols by photo-initiated thiol-ene reactions. Three networks, 1,2-EDT-*co*-TAQA, PETMP-*co*-TAQA, and TEGBMP-*co*-TAQA, were chosen based on the wide range of achievable thermal and mechanical properties they possess, including T_g values from −18 to 65 °C, with the intention of designing a family of biocompatible materials with tunable thermomechanical and degradation properties. The short- and long-term effects of a physiologically-relevant environment on the properties of the networks were studied. To satisfy design requirements of orthopedic biomaterials at molecular level and enable the desired physiological response, chemical properties of the degradation products and interactions at the cellular level with the networks and their degradation products were evaluated.

3.2 Results and Discussion

Three degradable polycarbonate networks, shown in the following figures, were synthesized *via* solvent-free thiol-ene crosslinking of TAQA and multifunctional thiol monomers, 1,2-ethanedithiol (1,2-EDT), petraerythritol *tetrakis*(3-mercaptopropionate) (PETMP), and tetraethylene glycol *bis*(3-mercaptopropionate) (TEGBMP) in the presence of a photo-initiator DMPA (1 wt%). Photo-initiated thiol-ene chemistry is fast and efficient, and results in highly uniform three-dimensional crosslinked networks. Although the networks were chemically similar, they possessed a wide range of properties based on the structure of the multifunctional thiol monomer. Due to the length and flexibility of the TEGBMP-based spacer, the TEGBMP-*co*-TAQA network, shown in Figure 3.1, exhibited elastomeric properties with T_g = −18 °C and is expected to have the lowest crosslink density compared to the other networks (ideally, 33 atoms between crosslinks). In contrast, PETMP-*co*-TAQA, shown in Figure 3.2, is expected to have the highest crosslink density (ideally, 12 atoms between crosslinks) because of the increased functionality of PETMP compared to the other thiol monomers which resulted in a rigid network with T_g = 65 °C. Containing the greatest weight fraction of bicyclic TAQA monomer and the lowest weight fraction of flexible aliphatic spacer atoms, 1,2-EDT-*co*-TAQA, shown in Figure 3.3, also exhibited a T_g of 65 °C and is expected to have a relatively high crosslink density (ideally, 16 atoms between crosslinks). Therefore, at body temperature, 37 °C, both 1,2-EDT-*co*-TAQA and PETMP-*co*-TAQA remain rigid, and TEGBMP-*co*-TAQA behaves as a rubbery solid.

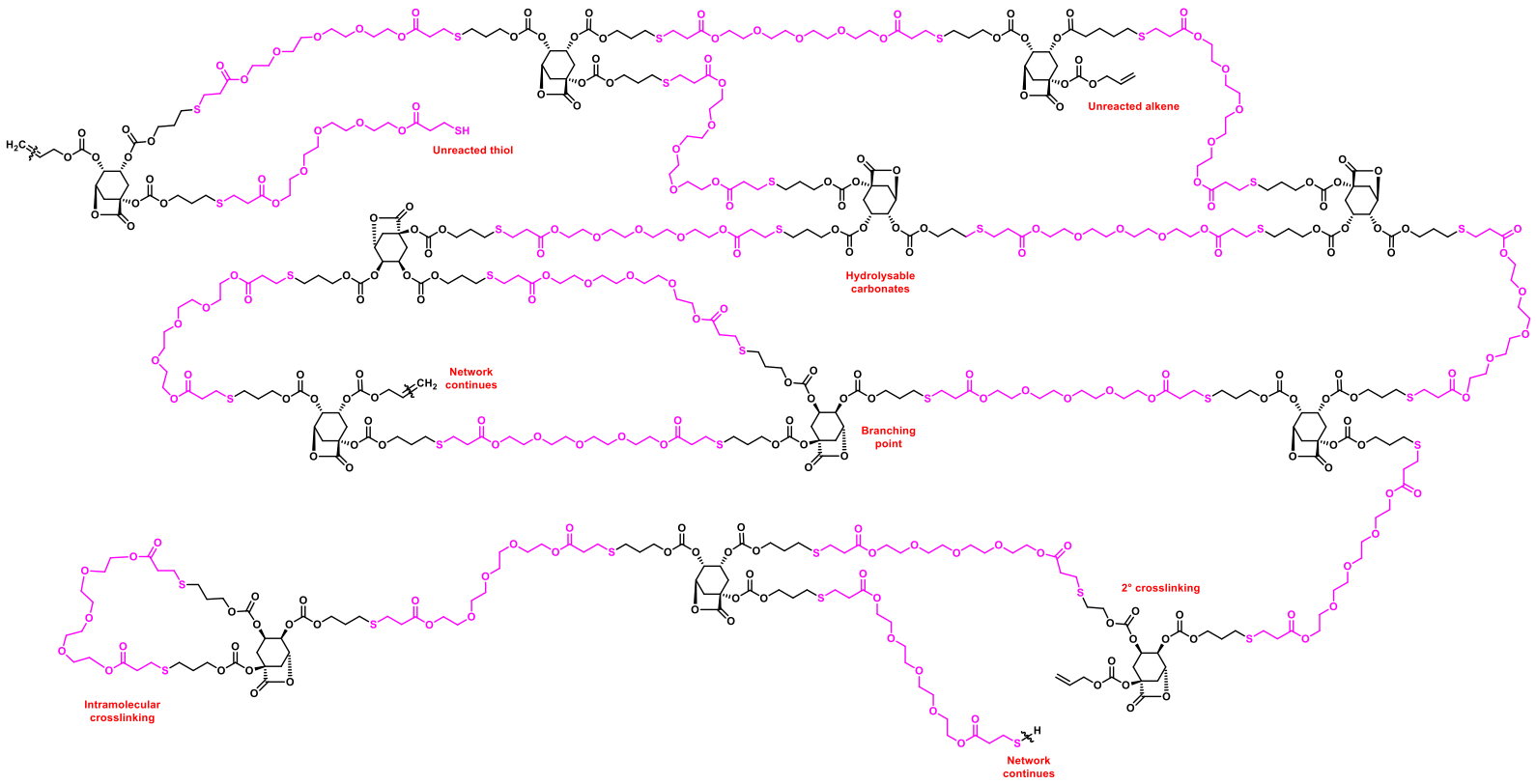

TEGBMP-*co*-TAQA, T_g = -18 °C

Figure 3.1. Structure representing TEGBMP-*co*-TAQA.

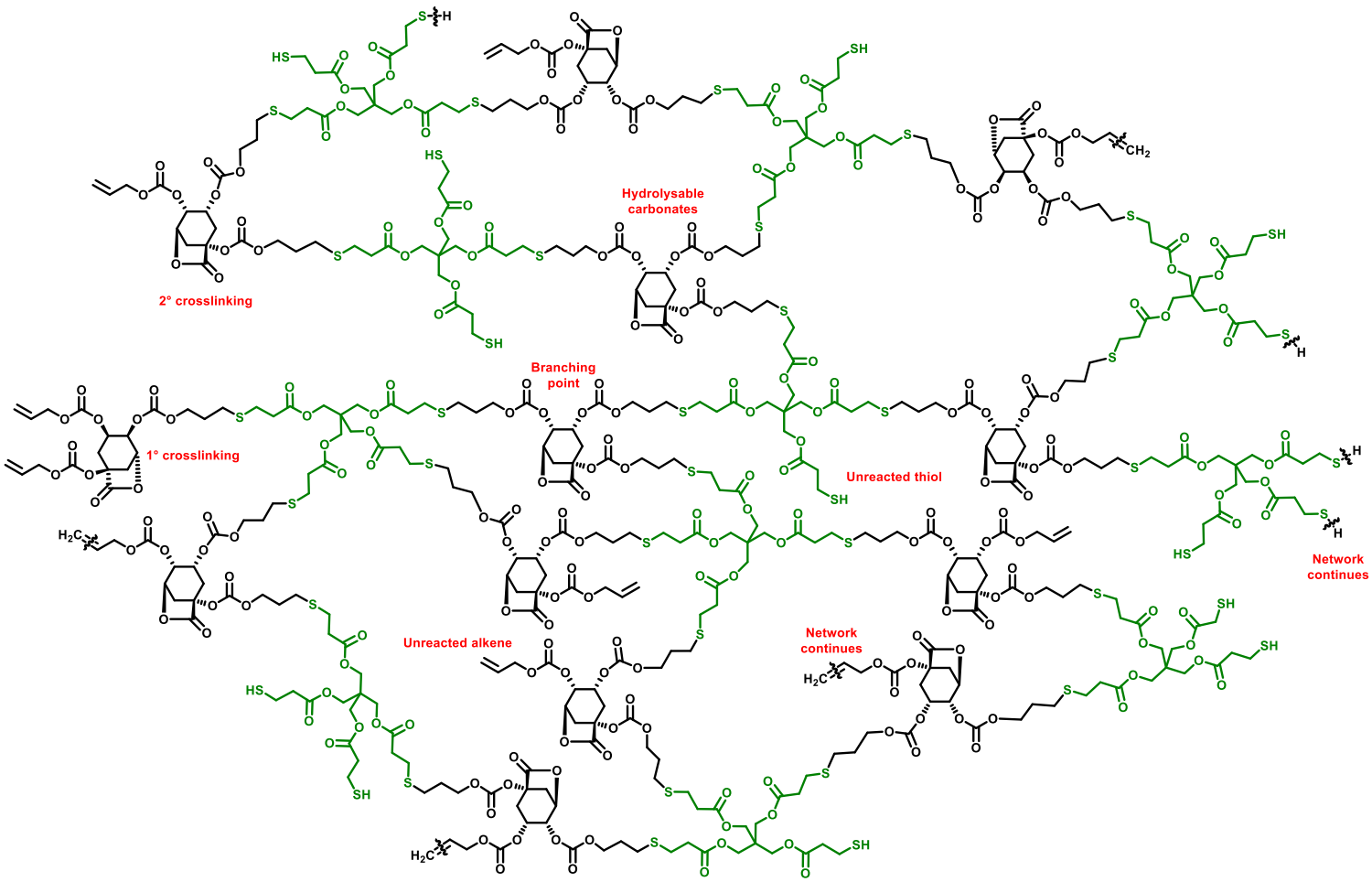

Figure 3.2. Structure representing PETMP-*co*-TAQA

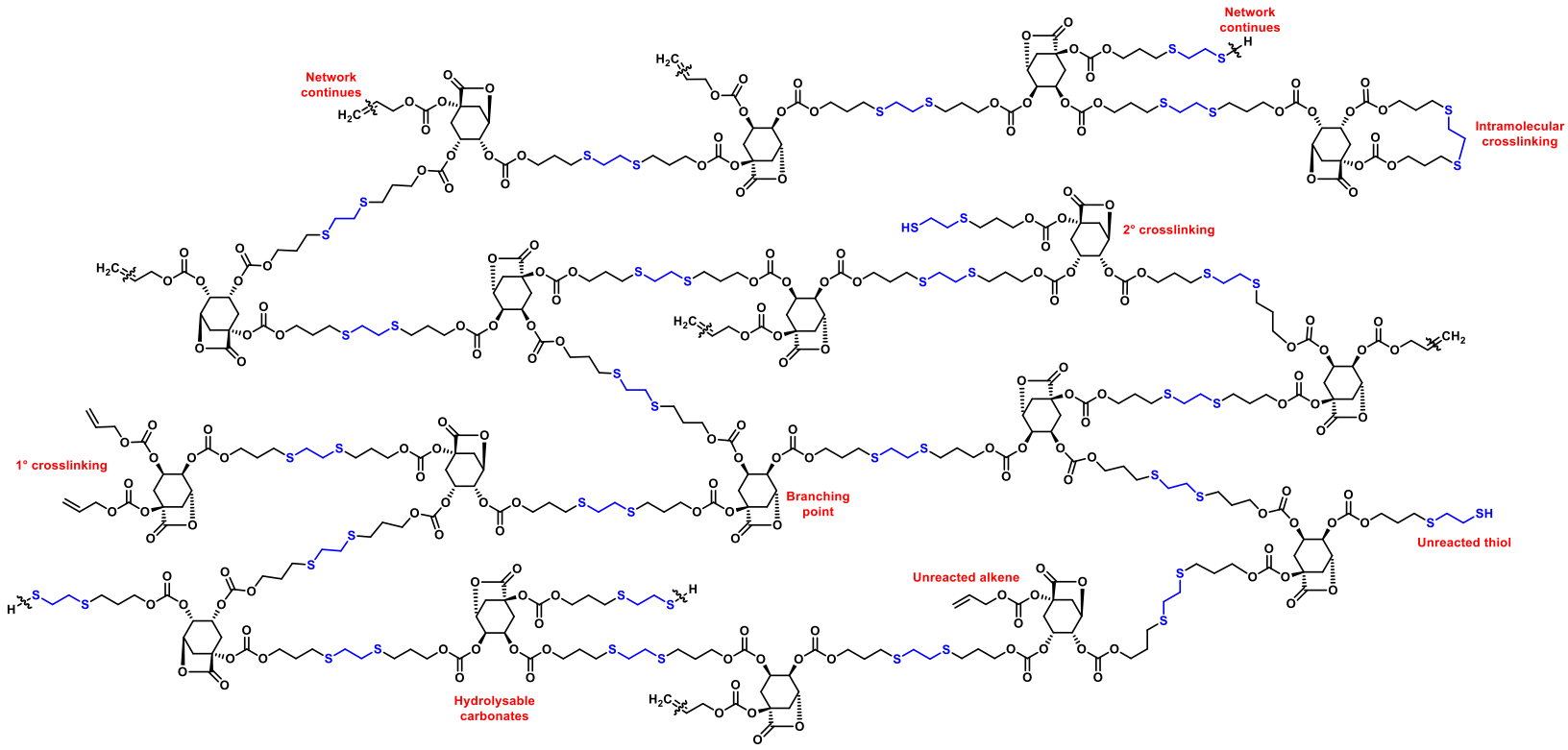

Figure 3.3. Structure representing 1,2-EDT-*co*-TAQA

Because the main goal is to implement these materials in orthopedic applications, for example, as fixation devices where they will act as supportive substrates for tissue (*i.e.* bone, cartilage, tendon, *etc.*) regeneration/growth, it is essential that the polymers are nontoxic and facilitate cell attachment. Cell adhesion plays an important role in the integration of an implant with the surrounding tissue environment. Cytotoxicity and cell attachment studies were performed with MC3T3 preosteoblasts. Cells were seeded into wells containing polymer samples (films, 2 × 2 × 0.6 mm), and viability was determined *via* MTS assay and normalized relative to a PBS control containing no polymer. After 48 h, > 100% cell viability was observed for bone cells exposed to each of the three different networks (see supporting information section for details). Cell were also seeded onto polymer-coated culture dishes, and cell morphology and attachment to the polymer surface was observed by confocal microscopy (Figure 3.4) after staining of actin fibers present in the cytoskeleton (green) and vinculin concentrated in the focal adhesion sites and present in the cytoskeleton (red). The results were compared to a glass-bottom culture dish and a culture dish coated with poly(D,L-lactide) (PDLLA, 10 kDa, T_g = 60 °C). In all cases, cells had some attachment to the substrate as seen by the focal adhesions, represented by bright red spots on the cytoskeleton in which vinculin is very concentrated. Noticeably, there were more focal adhesion sites observed on the 1,2-EDT-*co*-TAQA substrate than any other, including the glass and PDLLA controls, and the sites of attachment were larger, represented by bigger and brighter red spots in the image. On both the 1,2-EDT-*co*-TAQA and PETMP-*co*-TAQA substrates, there are more sites of attachment throughout the entire cell-substrate interface rather than only at

the perimeter of the cell, compared to the glass substrate and the cells appear more spread out (more contact with the substrate) compared to the PDLLA substrate. Cells on the PDLLA substrate had narrower cell width, and during the immunofluorescence process, actin fibers along the perimeter of the cells appeared rounded up. On the TEGBMP-*co*-TAQA substrate, cells also express many attachment sites throughout the cytoskeleton; however, the cells appear more elongated and narrow, resembling cells of softer tissue (the extreme being nerve cells). The difference in cytoskeleton structure between the cells on the rigid substrates, 1,2-EDT-*co*-TAQA and PETMP-*co*-TAQA, and cells on the softer substrate, TEGBMP-*co*-TAQA, may be evidence of mechanosensitive cellular behavior.[79-80] In particular, studies have shown that the stiffness of the matrix is a key regulator in cellular behavior and can ultimately direct stem cell fate; on a matrix with the stiffness of brain, stem cells differentiated into neural cells, and on the matrix with the stiffness of bone, stem cells differentiated into osteoblast-like cells.[81] Therefore, it may be possible to influence the fate of orthopedic tissue (between bone and cartilage, for instance) by tailoring the modulus of the implant material. The material kinetics – how the material properties change as an effect of the tissue environment may also have an effect on the health and function of surrounding tissue.

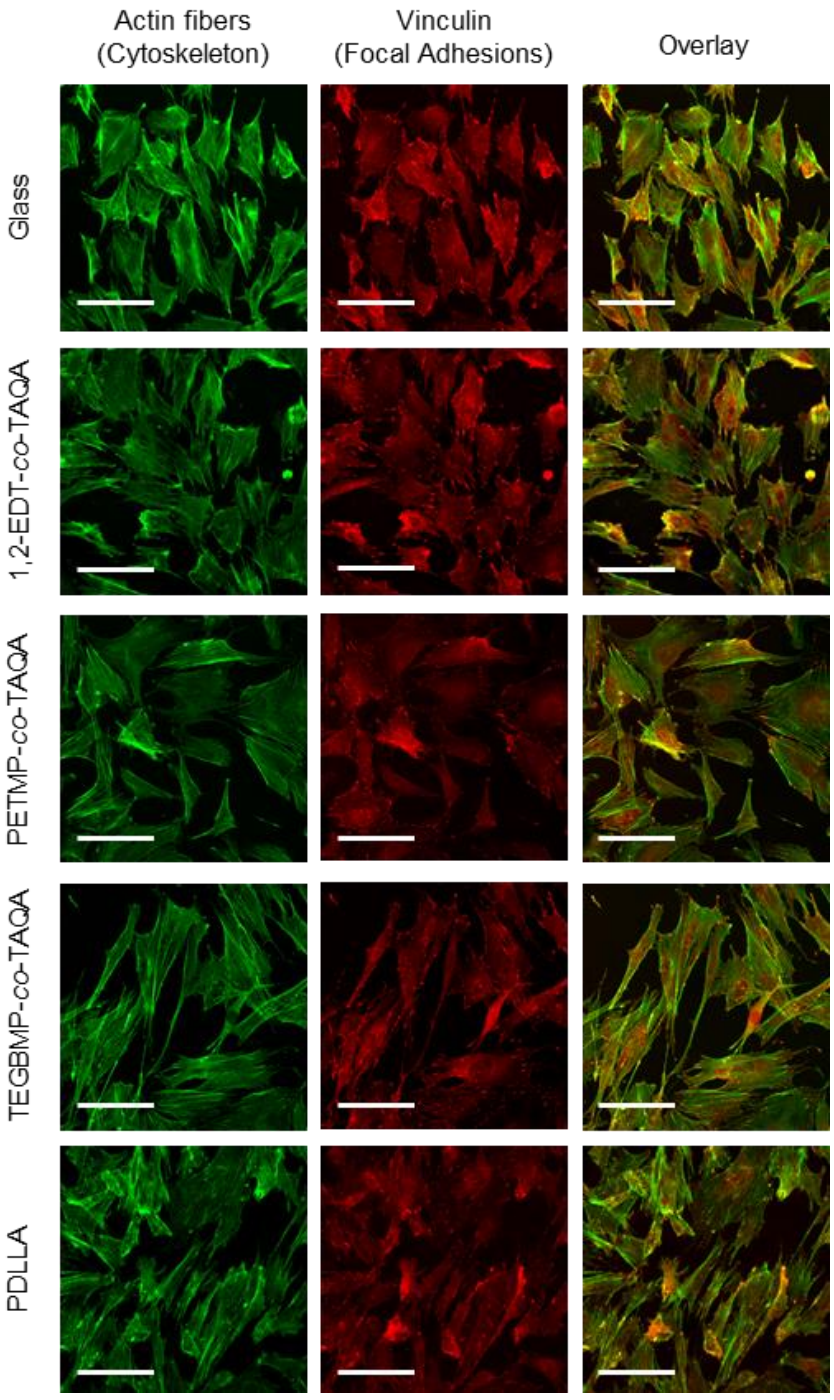

Figure 3.4. Preosteoblast attachment on poly(thioether-*co*-carbonate) substrates. Confocal microscopy images of MC3T3 cells with stained actin fibers (green) present in the cytoskeleton and vinculin (red) present in the focal adhesions to the substrate were taken 24 h after plating. For comparison, cell attachment to a glass substrate and to a PDLLA substrate were observed as well. Scale bar represents 100 μm.

To determine the short-term mechanical response to physiological conditions polymer discs were subjected to *in situ* dynamic mechanical analysis under compression. A constant dynamic compressive stress was applied to the discs while submerged in phosphate buffered saline solution (pH 7.4) heated to body temperature (37 °C). Prior to submersion the compressive modulus was measured for 5 min at ambient conditions (25 °C). The rigid networks, PETMP-*co*-TAQA and 1,2-EDT-*co*-TAQA, exhibited modulus values of 320 and 230 MPa, respectively, prior to submersion. The elastomeric network, TEGBMP-*co*-TAQA expressed a compressive modulus of 1.7 MPa at room temperature. Although all three networks performed similarly overall, the initial thermal response of the materials in their glassy state, PETMP-*co*-TAQA and 1,2-EDT-*co*-TAQA, resulted in a slight decrease in modulus, while the initial thermal response of TEGBMP-*co*-TAQA, in its rubbery state, resulted in a rapid increase in modulus. This change in modulus with increasing temperature is consistent with storage modulus behavior for amorphous crosslinked networks, where in their glassy state ($T < T_g$) the modulus may decrease slightly with increasing temperature, and in their rubbery state ($T > T_g$) the modulus may increase slightly with increasing temperature. Following the initial response, all three networks expressed a gradual increase in compressive modulus over 16 h of submersion. The net response to submersion in a physiologically-relevant environment for over 16 h was an increase in modulus, $\Delta E'$ = 85 MPa (37%), 13 MPa (4%), and 0.29 MPa (17%) for 1,2-EDT-*co*-TAQA, PETMP-*co*-TAQA, and TEGBMP-*co*-TAQA, respectfully. This increase in modulus may be result of decreased free volume within the network caused by the prolonged application of constant dynamic

compressive stress and enhanced by solvent plasticization. Under compressive stress and physiological conditions, the networks experienced an increase in modulus which is expected to plateau until hydrolytic degradation ensues at which point the modulus is expected to decrease.

To measure the long-term effects of physiological conditions and monitor hydrolytic degradation, polymer discs were placed in PBS and kept in an incubator (60 rpm) at 37 °C. Over 25 weeks, the swelling and remaining mass of the discs were measured, shown in Figure 3.4 (A and B). Due to the flexibility and hydrophilicity of the tetra(ethylene glycol) units, the TEGBMP-*co*-TAQA discs swelled and degraded the fastest. After 5 weeks, the discs swelled to double their weight and began a rapid loss of mass over the following 5 weeks by bulk erosion; the discs swelled to a point until they broke open at the surface, exposing a jelly-like interior. The rigid networks,

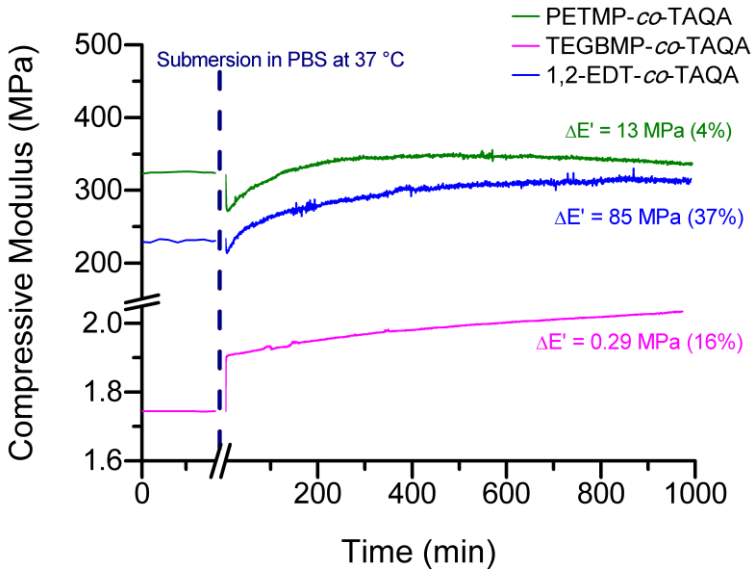

Figure 3.5. Storage modulus response to constant dynamic compression during submersion in a physiologically-relevant environment.

1,2-EDT-*co*-TAQA and PETMP-*co*-TAQA, degraded by surface erosion and took over 20 weeks. The PETMP-*co*-TAQA discs took the longest to degrade and did not swell to the extent of the other networks, most likely due to the increased crosslink density of the network hindering solvent intercalation and contact with hydrolysable moieties. Dry discs that retained their shape and did not contain any noticeable cracks were subjected to compressive DMA to monitor the storage modulus behavior as a function of degradation time, shown in Figure 3.4 (C, D, and E). Prior to degradation the discs performed as amorphous crosslinked networks where at low temperatures the storage modulus is constant or slightly decreasing with increasing temperature until reaching the glass transition temperature at which there is a rapid drop in modulus. Above the glass transition the modulus remained constant or slightly increased with increasing temperature, representing the rubbery modulus plateau distinctive to amorphous crosslinked networks. In all three cases, the storage modulus behavior began to deviate as degradation proceeded, and as expected, the modulus at 37 °C (temperature at which the materials are intended to be used) decreased with increasing degradation time. Interestingly, the 1,2-EDT-*co*-TAQA and PETMP-*co*-TAQA discs tested that had been degrading beyond 4 weeks and 6 weeks, respectively, no longer performed as crosslinked networks even though little to no mass loss occurred in those samples. For biomedical applications, understanding the material kinetics is important for realizing how the tissue environment affects the material, and understanding the chemical properties of the by-products is important for realizing how the material affects the tissue environment.

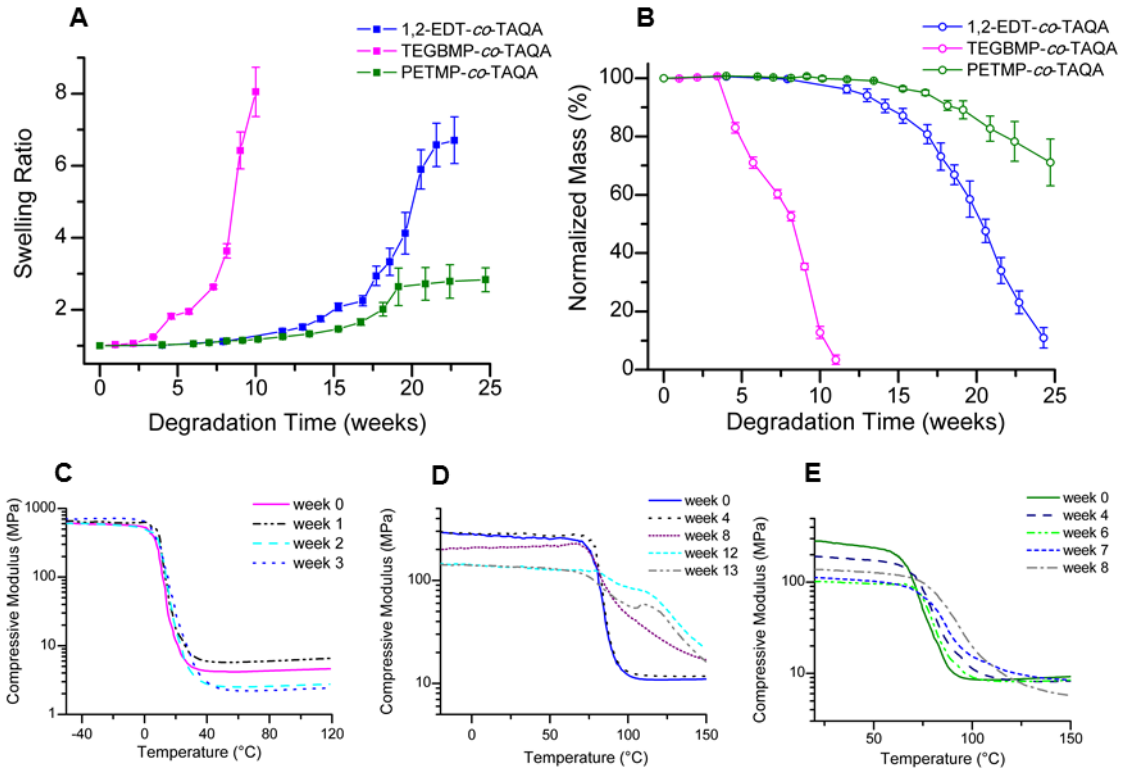

Figure 3.6. Long-term response to physiological conditions. Swelling (A) and remaining mass (B) of polymer discs subjected to hydrolytic degradation in PBS at 37 °C measured for 25 weeks. Changes in viscoelastic behavior as an effect of polymer degradation were determined by compressive DMA for TEGBMP-*co*-TAQA (C), 1,2-EDT-*co*-TAQA (D), and PETMP-*co*-TAQA (E).

The degradation compounds, which remained after full degradation and dissolution of each network, were collected and analyzed. Degradation products were nontoxic to preosteoblasts at concentrations less than 500 µg/mL for all networks determined by cell viability assay (Figure 3.7). Normal cell proliferation was observed in the presence of the degradation compounds for 72 h, and confluency and cell shape were similar to that of the control cells treated with PBS (see supporting information). Shown in Figure 3.8, hydrolysis of the carbonate linkages within the networks is expected to regenerate QA lactone and produce CO_2 and multi-alcohol thioether equivalents of the thiol monomers, and upon hydrolysis of the lactone, QA is expected to be present. In addition to hydrolysis of the carbonates, the ester linkages within the PETMP-*co*-TAQA and TEGBMP-*co*-TAQA are also expected to break down to produce

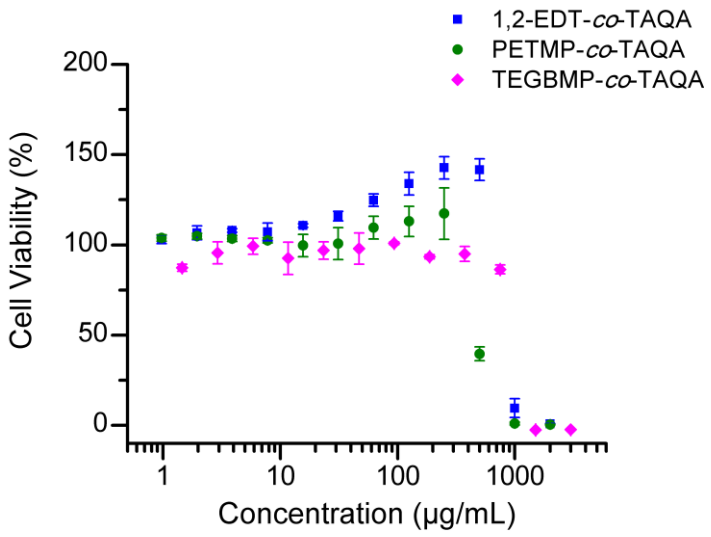

Figure 3.7. Cytotoxicity of degradation products at various concentrations determined by cell viability assay.

carboxylic acids and alcohols. Model degradation products, 1,2-EDT$(OH)_2$, PETMP$(OH)_4$, and TEGBMP$(OH)_2$, were synthesized using similar methods as the polymer networks, photo-initiated thiol-ene reactions with allyl alcohol (see supporting information for more details). The degradation products were analyzed by ESI-MS and ^{1}H NMR and compared to the model degradation products. Figure 3.9 shows the ^{1}H NMR spectra of the degradation products of each network. Under the spectrum of each degradation product is the spectrum of the respective model degradation product, and the spectra of QA and QAL are shown at the bottom of the figure. The presence of the major degradation product expected from network degradation, or compounds very similar, was apparent for all three materials. The spectra of PETMP-*co*-TAQA and TEGBMP-*co*-TAQA contained additional peaks and/or variances in peak intensities and splitting patterns compared to that of the expected degradation product, most likely because degradation of the ester linkages produced additional small molecules. In all cases, the presence of QA or QA lactone was not apparent by NMR, but QA and/or QA lactone were identified *via* ESI-MS analysis (see supporting information for ESI-MS data).

For practical clinical translation, it is important to consider imaging contrast properties of a material, in addition to understanding the material kinetics and biocompatibility. Ideally, an orthopedic implant device should have the imaging contrast properties to enable locating the device, detecting any changes in shape or size, and monitoring the overall degradation *in situ* using non-invasive imaging techniques. The X-ray contrast of the poly(thioether-*co*-carbonate) networks was observed in air and

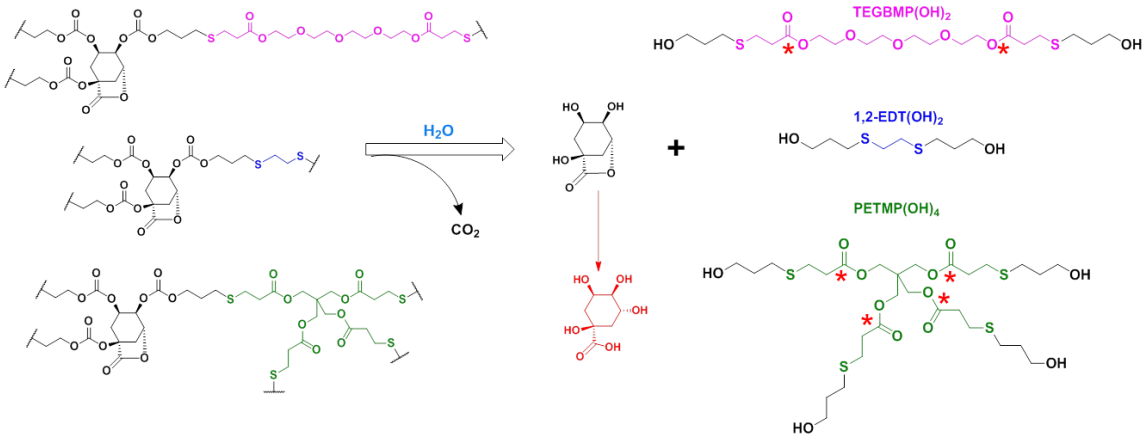

Figure 3.8. Schematic representation of the hydrolysis of the poly(thioether-*co*-carbonate) networks and the expected degradation products

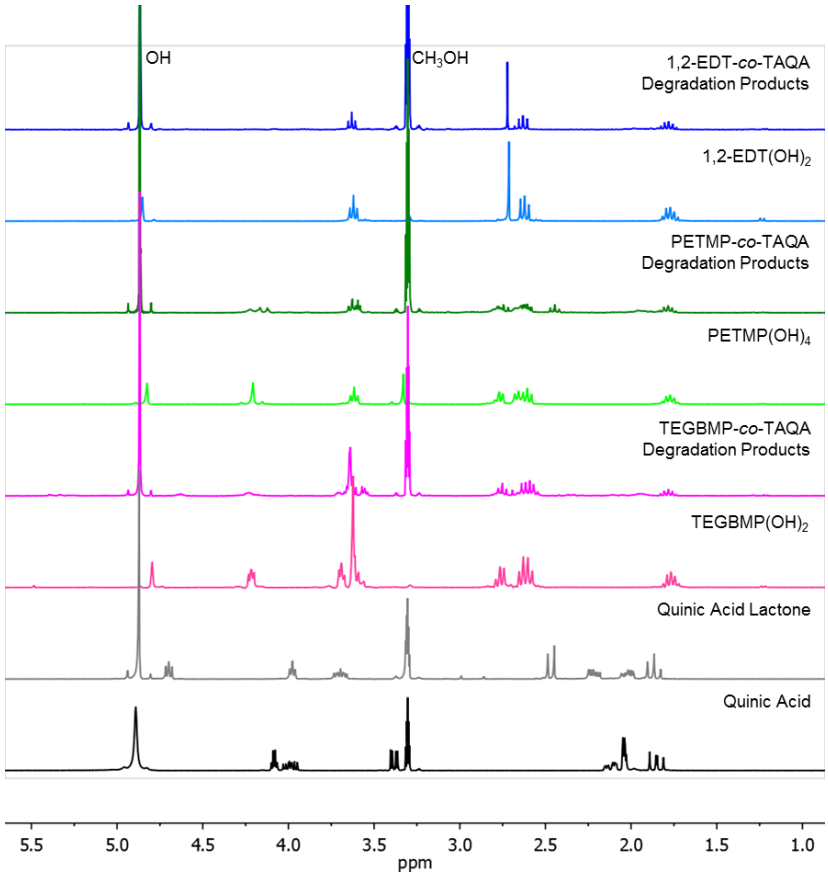

Figure 3.9. ^{1}H NMR spectra of degradation products. The spectrum of the appropriate model degradation product is shown below each measured spectrum, and the spectrum of QA lactone and QA are shown at the bottom.

through two types of tissue, chicken liver and chicken breast. Polymer discs were placed under sliced tissue sections, and differences in imaging intensities were quantified and compared to discs of PDLLA. Intensities were measured for three different discs of each formulation and normalized relative to the background or tissue and an X-ray opaque metal (see supporting information for more details). Shown in Figure 3.10, in air the poly(thioether-*co*-carbonate) discs exhibited slightly higher imaging intensity than PDLLA; quantitatively, the average opacity of the polymer networks was 25%, and the average opacity of the PDLLA discs was 23% relative to the background (0%) and an X-ray opaque metal (100%). Under 6 mm of chicken liver and 2.3 cm of chicken breast the poly(thioether-*co*-carbonate) discs were visibly more opaque than the PDLLA discs, exhibiting an X-ray opacity which was 7% and 9% higher than PDLLA through the liver and breast, respectively. Additional X-ray images can be found in the supporting information.

3.3 Conclusions

This work investigates the biomaterial feasibility of poly(thioether-*co*-carbonate) networks. The three polymers have a wide range of thermomechanical properties which are shown to invoke mechanosensitive cellular behavior in preosteoblasts. Studies were performed to roughly correspond to how the material affects the tissue and how the tissue affects the material and to analyze the ability of these materials to act as supportive substrates for tissue regeneration and growth. In the presence of a physiologically relevant environment, all three networks stiffened over the first 16 h. The elastomeric polymer, TEGBMP-*co*-TAQA began lose mass due to hydrolytic

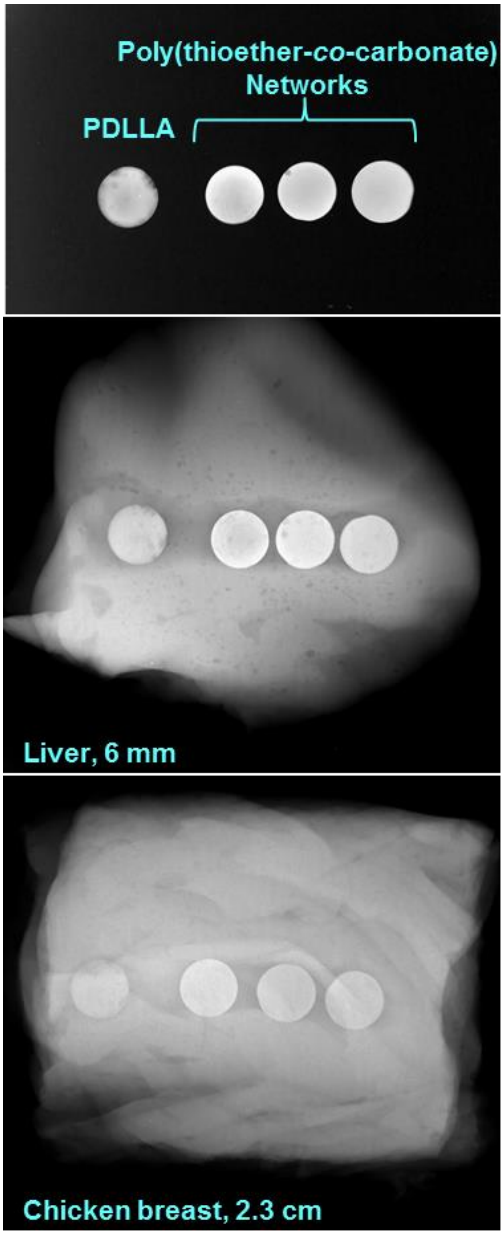

Figure 3.10. X-ray images of the poly(thioether-*co*-carbonate) networks through tissue at various depths. Discs were ~6 mm in diameter and ~2mm thick. In all three images the disc on the far left was PDLLA and the discs on the right (from left to right) were PETMP-*co*-TAQA, 1,2-EDT-*co*-TAQA, and TEGBMP-*co*-TAQA.

degradation at 3 weeks under physiological conditions and fully degraded over 10 weeks. The rigid materials, 1,2-EDT-*co*-TAQA and PETMP-*co*-TAQA, exhibited mass loss beginning at 8 and 13 weeks, respectively and took over 25 weeks to degrade fully. The degradation products were as expected based on the hydrolysis of the carbonate and ester linkages within the networks and in concentrations less than 500 μg/mL showed no cytotoxicity. Ultimately this family of nontoxic polymers may provide solutions to the limitations of conventional poly(α-hydroxyacid)-based devices, in terms of better biocompatibility, controlled degradation kinetics, and X-ray imaging properties. Furthermore, the facile synthesis and rapid curing by UV irradiation is attractive for three-dimensional processing/patterning of devices *via* stereolithography and other 3D printing methods, and future work will focus on the ability of these polymers to serve as customizable platform materials for advanced biomedical applications.

3.4 Materials and Methods

Pentaerythritol tetrakis(3-mercaptopropionate) (PETMP), 1,2-ethanedithiol (1,2-EDT), and 2,2-dimethoxy-2-phenylacetophenone (DMPA) were purchased from Sigma-Aldrich. Tetraethylene glycol bis(3-mercaptopropionate) (TEGBMP) was purchased from Wako Chemicals. Phosphate-buffered saline (PBS) solution (pH 7.4, 137 mM NaCl, 2.7 mM KCl, and 10 mM phosphate buffer) was purchased from Fisher Scientific. Allyl alcohol was purchased from Alfa Aesar. All reagents were used as received.

^{1}H and ^{13}C NMR spectra were obtained on a Varian Mercury 300 at 300 MHz using the solvent signal as internal reference. Glass transition temperatures were measured using differential scanning calorimetry (DSC) by a Mettler-Toledo DSC822

(Mettler-Toledo, Columbus, OH) with a heating rate of 10 °C/min. The T_g was taken as the midpoint of the inflection tangent upon the third heating cycle. Thermogravimetric analysis (TGA) was done under an Ar atmosphere using a Mettler-Toledo TGA/DMA1 with a heating rate of 10 °C/min. Dynamic mechanical analysis experiments were performed on a Mettler-Toledo TT-DMA system, and data were obtained from Triton Laboratory software. Temperature scans in compression mode were performed from −80 to 180 °C at a ramp rate of 3 °/min, a frequency of 1 Hz, and a sampling interval of 10 s. Isothermal submersion experiments were performed at 37 °C in PBS for 999 min (1 Hz, 30 s sample interval). In all DMA experiments the compressive dynamic strain was 0.02 mm, and the ratio of static to dynamic force was 1.5. X-ray imaging was performed using a Bruker Xtreme In Vivo MP4 with 30 kVp, 343 µA, and a 5 s exposure time.

MC3T3 cells were purchased from the American Type Culture Collection (ATCC) and subcultured based on ATCC protocol. Briefly cells were cultured in with MEM-alpha media supplemented with 10% FBS and 1% antibiotic. To plate cells in glass-bottom cell culture dishes, cells were treated with Trypsin:EDTA and the number of cells was counted with a hemocytometer. Each dish was plated with 25×10^3 cells incubated at 37 °C with 5 % CO_2. Polymer-coated dishes were sterilized under UV in the biosafety cabinet for 1 h and washed with sterile DPBS before plating cells on them. For attachment studies, cells were fixed after 24 h from cell plating with 2% paraformaldehyde and stained with Phalloidin-Alexa488 & anti-vinculin with secondary antibody conjugated with Alexa 647. For viability and proliferation test under incubation

with degradation compounds, cells were plated on glass-bottom dishes and after 24 h degradation compounds were mixed into media. Cells were fixed after 48 h and 72 h from exposure. Laser scanning confocal was used to acquire fluorescence images of the stained cells. Excitation and emission filter settings were adjusted according to fluorophore spectra provided by the manufacturer. Autofluorescence from each polymer was checked by a lambda scan. Overall cell population was identified from large filter view with 10X objective. Details of cell morphology were investigated from fluorescence images acquired with 20X objective with 2X zoom (40X magnification).

3.4.1 Polymer network synthesis

The alkenyl monomer, TAQA was synthesized as previously described.[78] Briefly, the two-step synthesis of TAQA starts with the well-known lactonization of QA under acidic conditions. QA and Amberlyst resin are suspended in benzene and DMF and heated to reflux with azeotropic removal of water to afford the bicyclic triol QA lactone. To install the three alloc functionalities, allyl chloroformate (44.7 mL diluted with 20 mL DCM) was added dropwise to QA lactone (10.3 g) suspended in cold (0°C) *N,N,N',N'*-tetramethylethylenediamine (36.4 mL) and DCM (200 mL) to give TAQA as a clear viscous oil. Each formulation of TAQA and a multifunctional thiol was mixed based on equal molar ratio of alkene to thiol and contained no solvent. The photo-initiator was 1 wt% DMPA and was dissolved in the thiol before TAQA was added. All formulations were vortexed and sonicated until a visually homogeneous mixture without any air bubbles was reached. The resins were drop cast into silicone molds containing circular discs approximately 3 mm thick and 6 mm in diameter (or injected into glass

molds to obtain 0.6 mm-thick films (for accelerated degradation and cytotoxicity studies) or onto a glass bottom cell culture dish (for cell attachment studies)). Crosslinking polymerizations were performed by exposing the molds to UV irradiation (365 nm) in a UVP crosslinking chamber for 15 min. Samples were removed from the mold and exposed to UV for an additional 15 min. Following UV exposure samples were post-cured at 120 °C under reduced pressure for 24 h. All samples were stored in the freezer at −80 °C when not in use.

3.4.2 Hydrolytic degradation in physiological conditions

Fifteen discs form each formulation were selected, their initial mass recorded, submerged in 4 mL of PBS (pH 7.4), and placed in the incubator shaker at 37 °C and 60 rpm to mimic physiological conditions. The PBS was changed once a week. At designated time points all of the samples were removed and rinsed with deionized water. The PBS solution containing any degradation products was kept and saved at −80 °C for further analysis. The swollen masses (w_w) of the pucks were measured before the samples were dried under vacuum until they reached a stable dry mass (w_d). The swelling ratio (q) was calculated according to the following equation:

$$q = \frac{w_w}{w_d}$$

The normalized mass (m) at each time point was calculated using the equation below, where w_i is the initial mass of the sample before degradation.

$$m = \frac{w_d}{w_i} \times 100\%$$

One sample was permanently removed from degradation for further characterization. To the others, fresh PBS was added, and they were returned to the degradation environment. The average normalized mass and swelling ratio were determined at various time points until no visible solids remained. Degradation products were collected by freeze-drying degradation solutions containing PBS then extracting with methanol. However, the degradation products collected each week were difficult to characterize due to very low concentrations and interference of PBS.

3.4.3 Analysis of degradation products

Small samples (2 mm × 2 mm × 0.6 mm, cut from films) of each network formulation were added to 4 mL of Nano-pure water and heated at 60 °C until pieces fully degraded (1 week for network containing TEGBMP, 3 weeks for the other two). Aqueous solutions containing degradation products were analyzed by ESI-MS. Degradation products were concentrated and analyzed by ^{1}H NMR in deuterated methanol. The cytotoxicity and effects on cell attachment of the degradation products was also evaluated. Model degradation compounds were synthesized by thiol-ene reactions between the multifunctional thiols and allyl alcohol using similar methods as the network synthesis (see supporting information).

3.5 Supporting Information

The information below contains details on the synthesis of the model degradation compounds, the confocal microscopy images of preosteoblast cells treated with the polymer degradation products (Figure 3.14), and the ESI-MS data for the degradation products (Figure 3.15-3.20). Additional X-ray images and details are also provided.

3.5.1 Synthesis of model degradation products

To a 50 mL round bottom flask equipped with a stir bar multifunctional thiol, allyl alcohol, and DMPA (~5 wt%) were added in the amounts listed in Table 3.1. In all cases allyl alcohol was added in excess, and in the case of PETMP and TEGBMP, allyl alcohol acted as the solvent to reduce the overall viscosity of the mixture. Once the DMPA was fully dissolved, the flask was placed in a UVP crosslinking chamber (λ = 365 nm) for 4 h with constant stirring. The product was purified by flash column chromatography (5% MeOH:DCM) and condensed to afford PETMP$(OH)_4$ and TEGBMP$(OH)_2$ as viscous oils and 1,2-EDT$(OH)_2$ as a white solid. Products were characterized by ^{1}H and ^{13}C NMR shown in Figure 3.11-3.13. PETMP$(OH)_4$: ^{1}H NMR (300 MHz, Methonal-d_4, ppm): δ 4.21 (s, 8 H, H-2), 3.62 (t, 8 H, *J* = 6.2, H-8), 2.83 – 2.72 (m, 8 H, H-5), 2.68 – 2.58 (m, 16 H, H-4 and H-6), 1.82 - 1.73 (m, 8 H, H-7); ^{13}C NMR (75 MHz, Methanol-d_4, ppm): δ 171.65 (C-3), 62.10 (C-2), 60.08 (C-8), 42.18 (c-1), 34.24 (C-4), 32.05 (C-6), 27.78 (C-5), 26.45 (C-7); HRMS (+ESI) *m/*z calc'd for $C_{29}H_{52}O_{12}S_4$ $[M+Na]^+$: 743.2241, found 743.2147. 1,2-EDT$(OH)_2$: ^{1}H NMR (300 MHz, Methonal-d_4, ppm): δ 3.62 (t, 4 H, *J* = 6.2, H-4), 2.71 (s, 4 H, H-1), 2.65 - 2.60 (m, 4 H, H-2), 1.82 - 1.73 (m, 4 H, H-3); ^{13}C NMR (75 MHz, Methanol-d_4, ppm): δ 60.03 (C-4), 32.19 (C-1), 31.64 (C-2), 27.79 (C-3); HRMS (+ESI) *m/*z calc'd for $C_8H_{18}O_2S_2$ $[M+Na]^+$: 233.0646, found 233.0645. TEGBMP$(OH)_2$: ^{1}H NMR (300 MHz, Methonal-d_4, ppm): δ 4.23 – 4.20 (m, 4 H, H-4), 3.71 – 3.67 (m, 4 H, H-3), 3.62 – 3.56 (m, 12 H, H-1 and H-2 and H-10), 2.79 – 2.74 (m, 4 H, H-7), 2.65 – 2.58 (m, 8 H, H-6 and H-8), 1.81 – 1.72 (m, 4 H, H-9); ^{13}C NMR (75 MHz, Methanol-d_4, ppm): δ

172.22 (C-5), 70.15 (C-1 and C-2), 68.67 (C-3), 63.49 (C-4), 60.06 (C-10), 34.37 (C-6), 32.07 (C-8), 27.77 (C-7), 26.41 (C-9); HRMS (+ESI) *m/z* calc'd for $C_{20}H_{38}O_9S_2$ $[M+Na]^+$: 509.1855, found 509.1834.

	Thiol (g)	Allyl Alcohol (g)	DMPA (g)	Yield (%)
$PETMP(OH)_4$	1.280	0.852	0.124	53
$TEGBMP(OH)_2$	1.091	1.244	0.072	55
$1,2\text{-}EDT(OH)_2$	1.123	3.462	0.238	75

Table 3.1. Model degradation product reaction compositions.

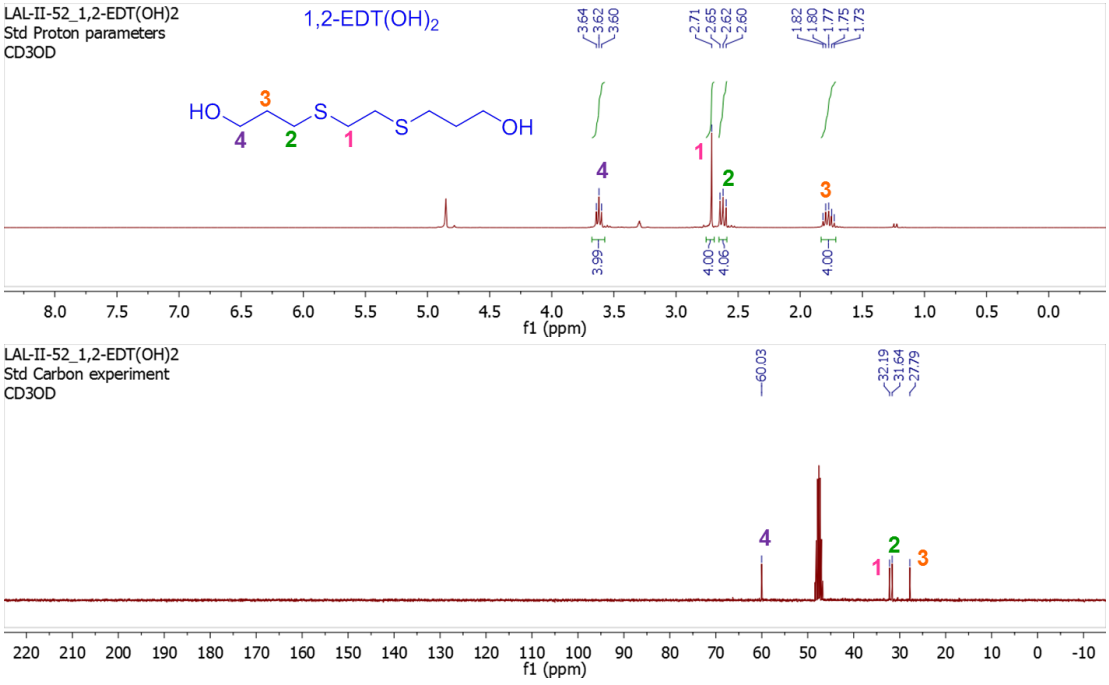

Figure 3.11. ^{1}H NMR (top) and ^{13}C NMR (bottom) spectrum of $1,2\text{-}EDT(OH)_2$.

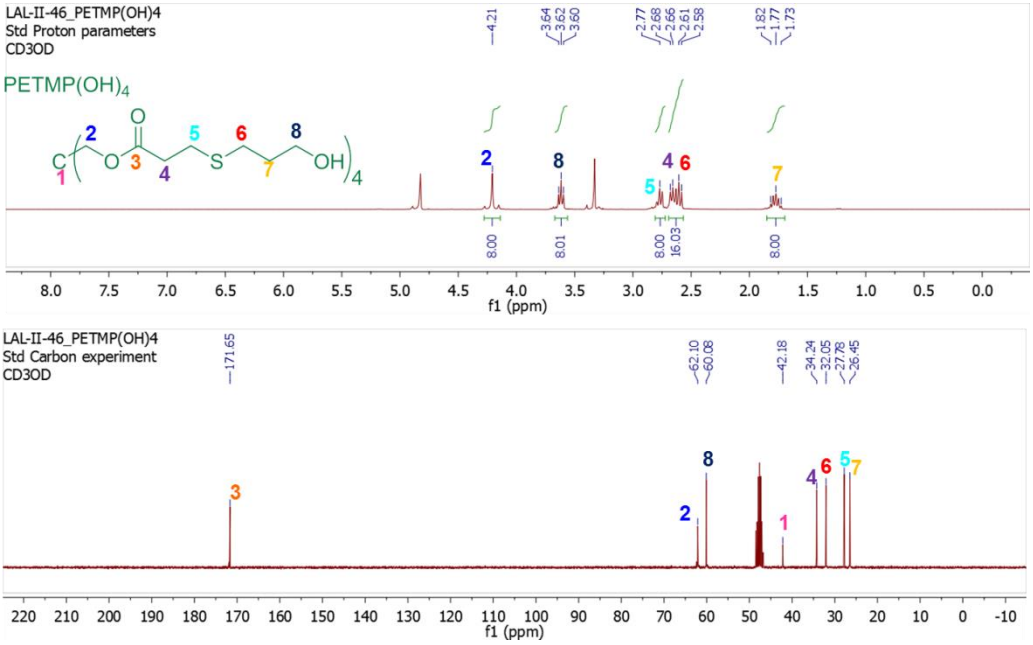

Figure 3.12. ^{1}H NMR (top) and ^{13}C NMR (bottom) spectrum of PETMP(OH)$_4$.

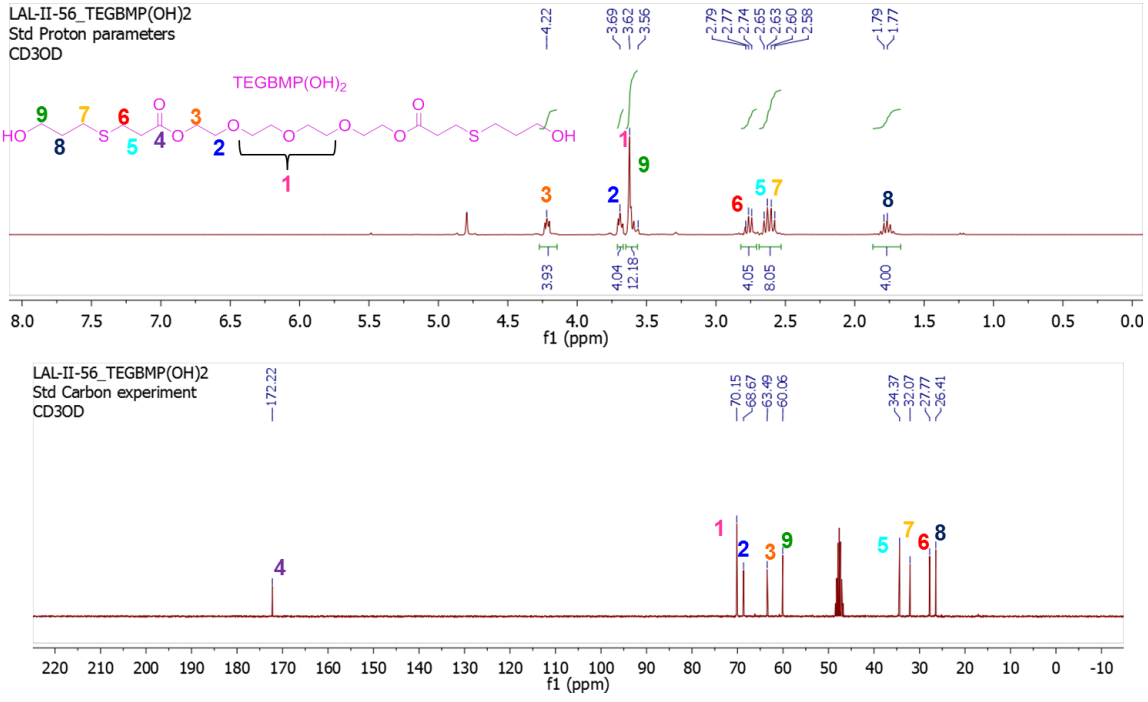

Figure 3.13. ^{1}H NMR (top) and ^{13}C NMR (bottom) spectrum of TEGBMP(OH)$_2$.

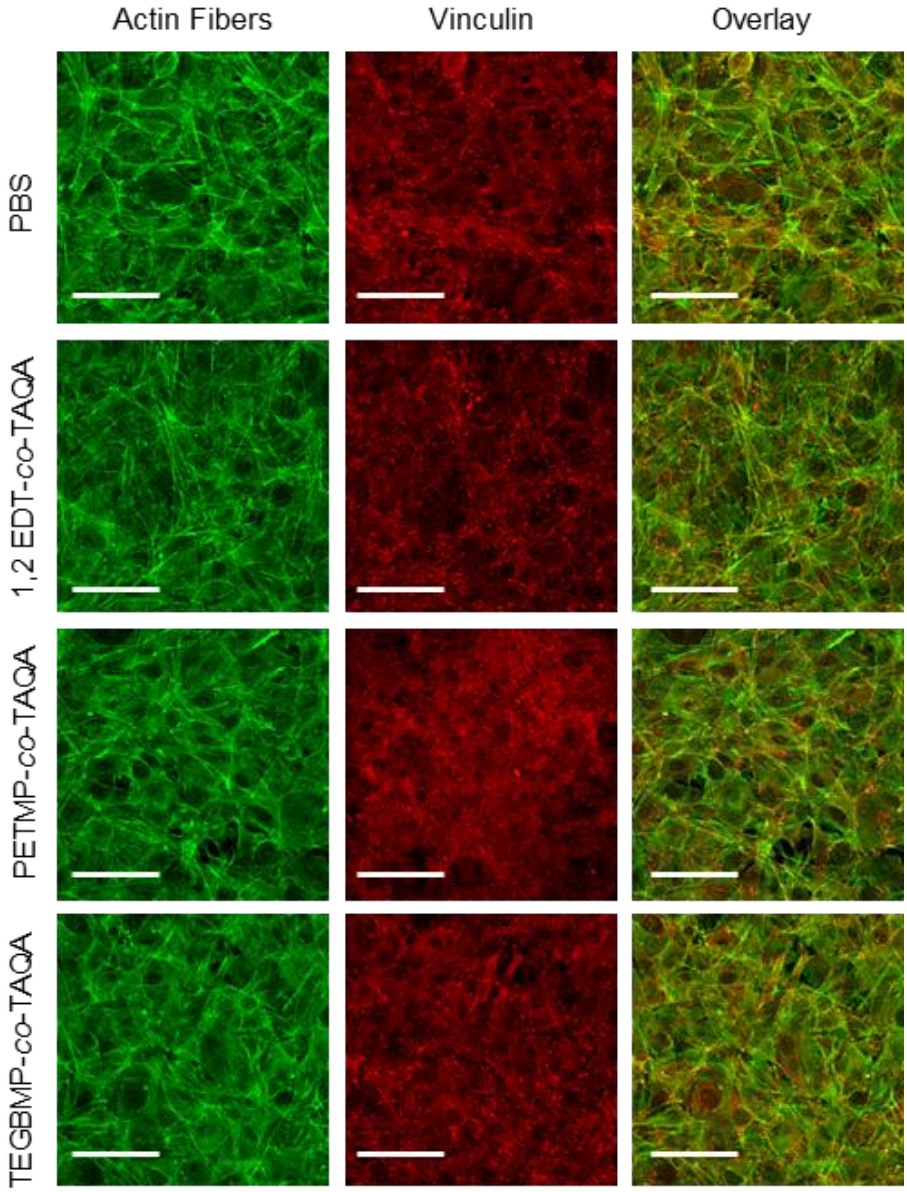

Figure 3.14. Confocal microscopy images of preosteoblasts (MC3T3) 72 h after being treated with the poly(thioether-*co*-carbonate) degradation compounds. The cells were treated with PBS containing 250, 250, and 500 μg/mL of degradation products from 1,2-EDT-*co*-TAQA, PETMP-*co*-TAQA, and TEGBMP-*co*-TAQA, respectively. The scale bar represents 100 μm.

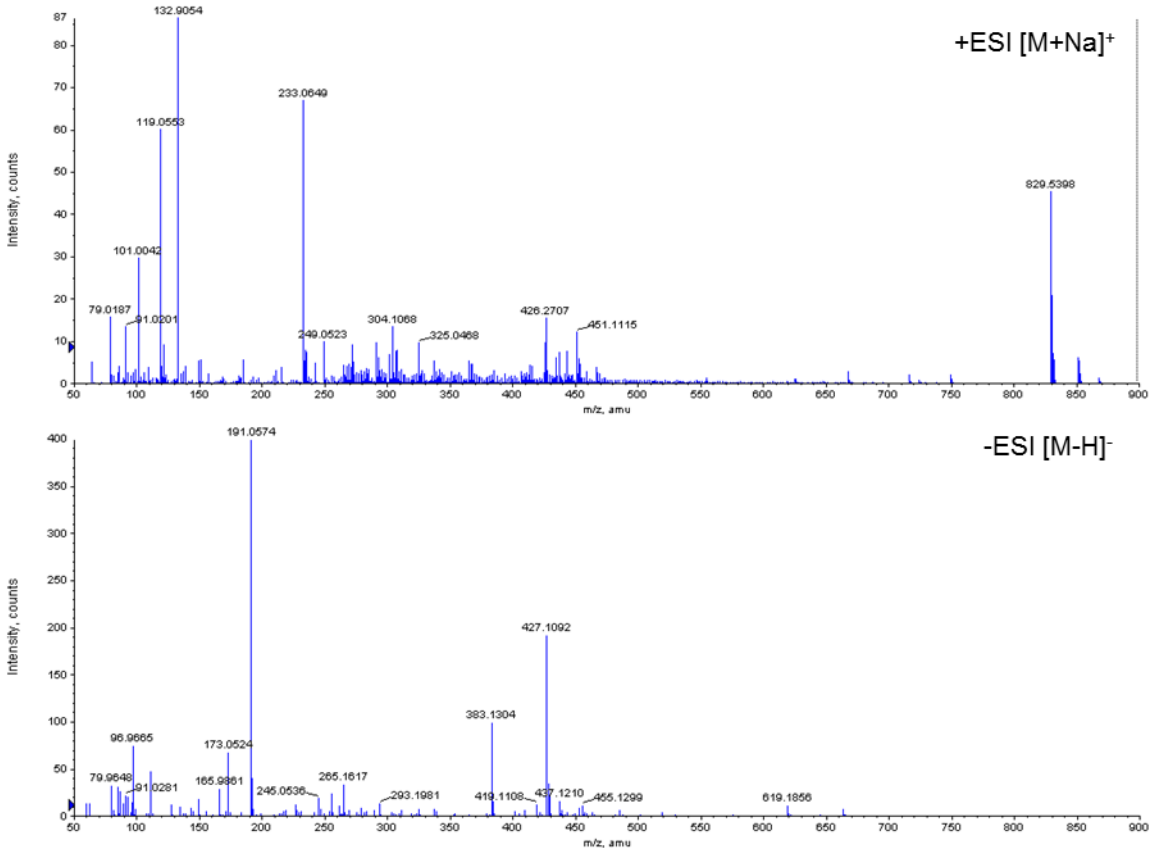

Figure 3.15. ESI-MS spectra of the degradation products of 1,2-EDT-*co*-TAQA.

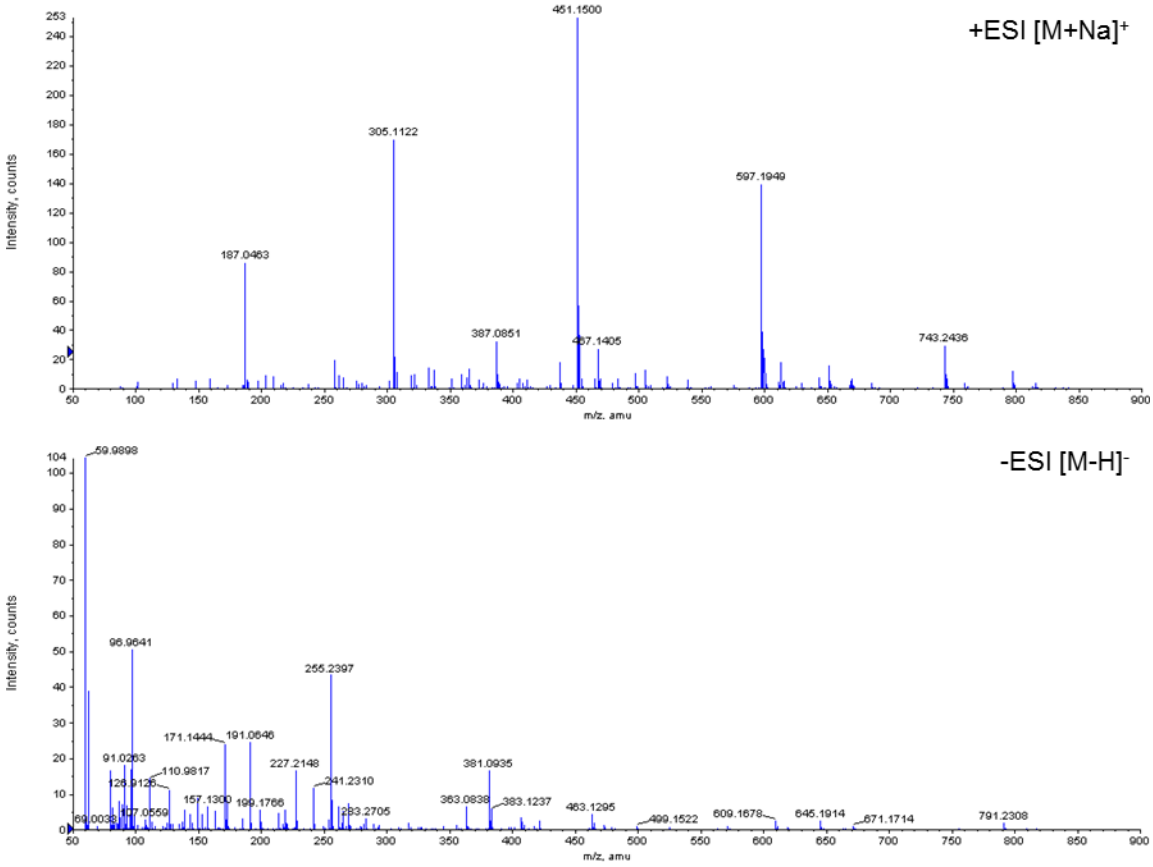

Figure 3.16. ESI-MS spectra of the degradation products of PETMP-*co*-TAQA.

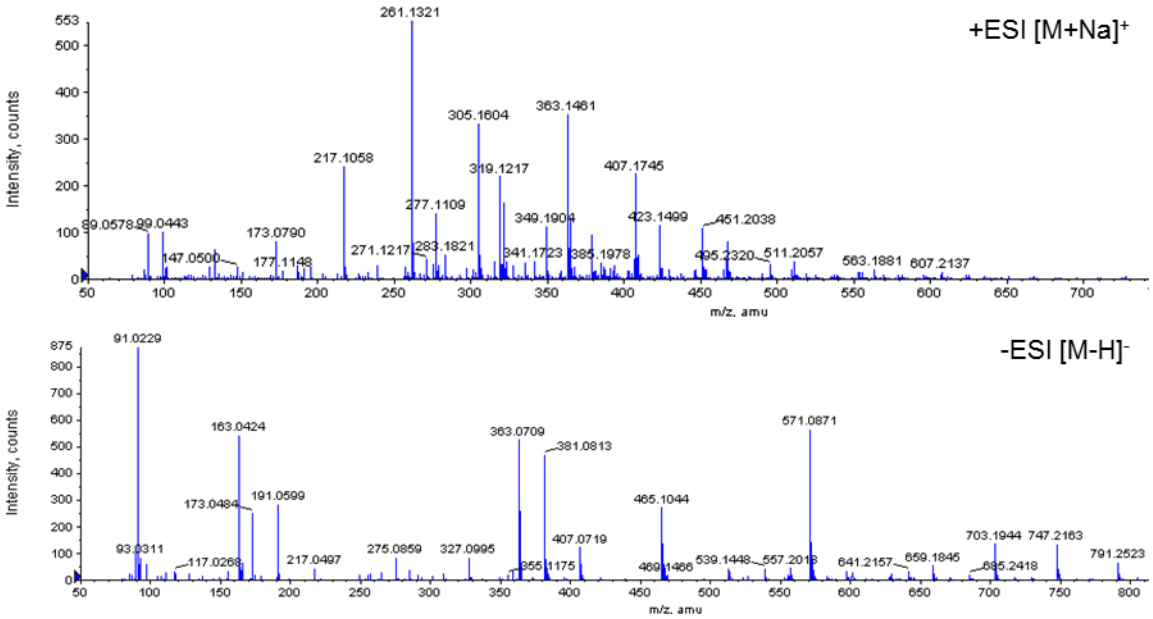

Figure 3.17. ESI-MS spectra of the degradation products of TEGBMP-*co*-TAQA.

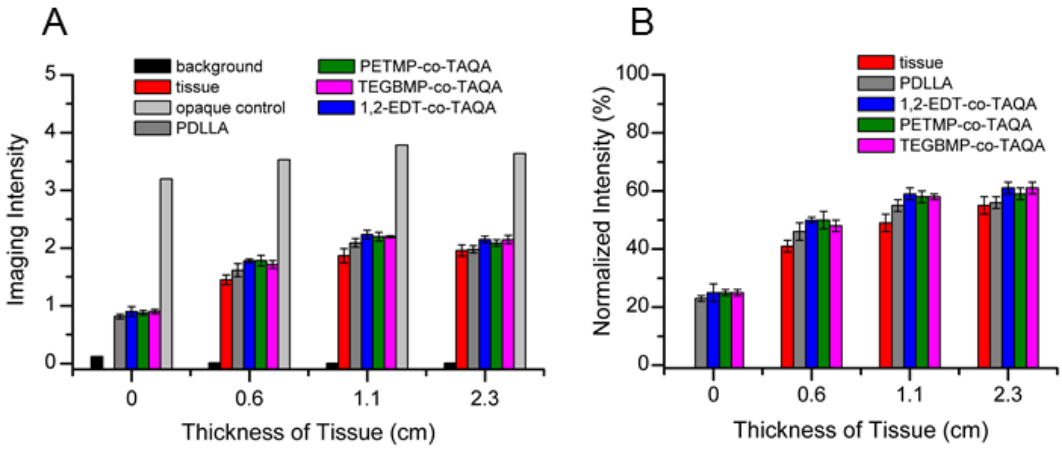

Figure 3.18. Quantification of X-ray image intensities. (A) Intensities corresponding to images depicted in Figure 3.19 (A-D), and the graph represents the average intensity of 3 discs for each sample. The intensity of the tissue was measured in 3 different areas. (B) Intensities are normalized where 0% represents the background and 100% represents the opaque control. The intensities measured at 0 cm were measured in air without any tissue. The 0.6 cm measurement was done through chicken liver, and the 1.1 and 2.3 cm measurements were done through chicken breast. In all cases the poly(thioether-*co*-carbonate) samples exhibited higher intensities than the PDLLA samples.

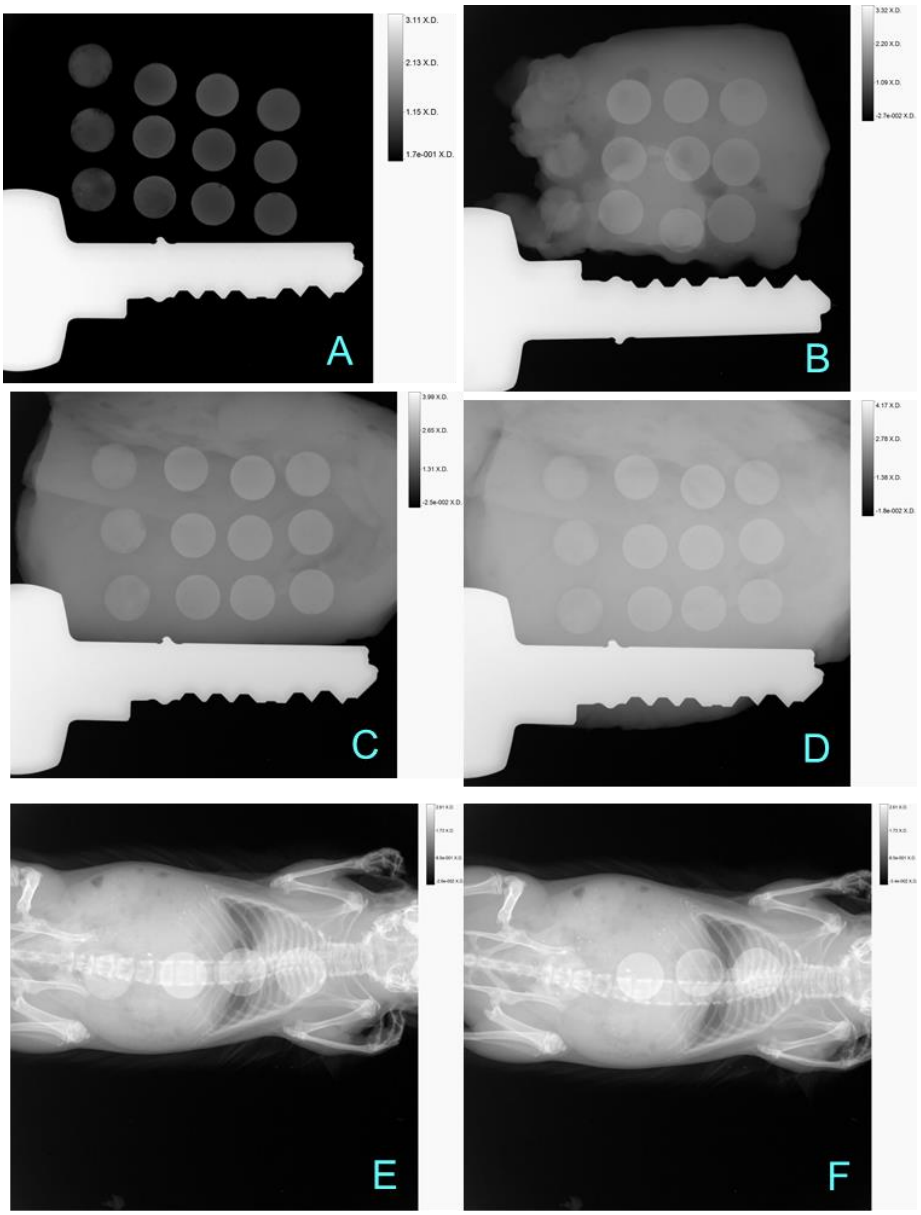

Figure 3.19. Additional X-ray images of poly(thioether-*co*-carbonate) networks through various types and depths of tissue. Discs were ~6 mm in diameter and ~2mm thick. In all images discs were arranged so that the one(s) on the furthest left were PDLLA and the discs on the right (from left to right) were PETMP-*co*-TAQA, 1,2-EDT-*co*-TAQA, and TEGBMP-*co*-TAQA. Images were taken (A) through air (B) through 0.6 cm of chicken liver (C) through 1.1 cm of chicken breast (D) through 2.3 cm of chicken breast (E and F) through a mouse.

CHAPTER IV

MECHANICALLY-ADAPTIVE AND MECHANICAL GRADIENT POLYCARBONATE NETWORKS WITH CONTROLLED PHYSIOLOGICAL RESPONSE

4.1 Introduction

Because many polymers undergo solvent plasticization under aqueous conditions which results in a loss of mechanical integrity, developing tough biomaterials that maintain their properties *in vivo* has been challenging.[65] However, for some biomedical applications, mechanically-dynamic polymeric materials whose mechanical behavior can be switched on demand by exposure to a physiological environment are desirable. For example, implantable softening electronics are being developed that utilize materials that have sufficient stiffness to penetrate tissue and soften under physiological conditions to a stiffness that is similar to surrounding tissue which helps to prevent damage to that tissue.[82] At ambient conditions the material is in its rigid state and upon exposure to physiological environment, a dramatic change in mechanical properties indicative of a glass transition from a glassy state to a rubbery state occurs. The change can be caused by primarily temperature effects if the T_g of the polymer is near physiological temperature or solvent plasticization effects or a combination of both. In polymer networks the solvent plasticization effect has been attributed largely to the disruption of secondary interactions within the network by water molecules in order to form their own secondary interactions (hydrogen bonds) with hydrophilic groups such as hydroxyl,

carbonyl, or amine groups.[83] The water molecules within the network increase the intermolecular distance between polymer chains, increasing chain mobility, and subsequently decreasing polymer rigidity and causing the T_g of the material to decrease.[84]

This work focuses on the design and characterization of poly(thioether-*co*-carbonate) networks *via* thiol-ene crosslinking that are mechanically-adaptive under physiological conditions. The starting materials were the same as previously described, shown in Figure 4.1; TAQA a tri-alkenyl monomer derived from the coffee extract quinic acid and the commercially-available multifunctional thiols, 1,2-ethanedithiol (1,2-EDT), tetraethylene glycol *bis*(3-mercaptopropionate) (TEGBMP), and pentaerythritol *tetrakis*(3-mercaptopropionate) (PETMP) were used. By incorporating mixtures of thiol monomers with different functionalities and hydrophilicities, it may be possible to create a group of materials that exhibit the same T_g in dry conditions, but have relatively different physiological responses and response rates. Furthermore, materials with T_g values near 37 °C were synthesized and their mechanical dynamics were investigated. Temperature and solvent effects were characterized for samples submerged in aqueous solutions under physiologically-relevant conditions, specifically phosphate buffered saline solution at 37 °C, and special attention will was paid to the rate at which mechanical changes occur. Immediate solvent plasticization effects on the modulus of the material will be analyzed by *in situ* DMA. Additionally, several other important parameters will be studied, including the effect of water content on T_g.

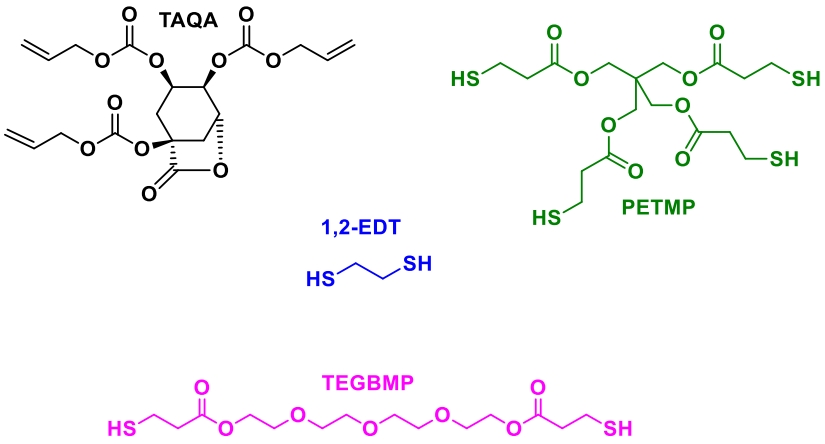

Figure 4.1. Chemical structures of starting materials used to form mechanically-adaptive poly(thioether-*co*-carbonate) networks with T_g = 37 °C.

4.2 Results and Discussion

The tensile dynamic mechanical analysis results shown in Figure 4.1 show the storage modulus behavior as a function of temperature (Figure 4.1A) of the formulations containing only one thiol and the solvent plasticization response of the rigid networks (Figure 4.1B). In the storage modulus behavior, the rubbery modulus plateau (modulus at temperatures above the glass transition) is proportional to the crosslink density of the network. Materials incorporating PETMP exhibited a T_g of 65 °C and had the highest crosslink density because of its increased functionality compared to the other two di-functional thiols. The 1,2-EDT-*co*-TAQA sample contained the greatest weight fraction of the rigid bicyclic TAQA monomer and the lowest weight fraction of flexible aliphatic spacer atoms and thus, also exhibited a T_g of 65 °C but a noticeably lower crosslink density than PETMP-*co*-TAQA. The TEGBMP-*co*-TAQA system's longer and more

flexible tetraethylene glycol-based spacer resulted in an elastomeric material with T_g of −18 °C. Solvent plasticization of rigid networks under physiological conditions (phosphate buffered saline solution at 37 °C) was measured by in situ DMA. Both 1,2-EDT-*co*-TAQA and PETMP-*co*-TAQA exhibited a slight drop in modulus upon submersion from 1.65 and 1.50 GPa to 1.50 and 1.20 GPa, respectively, and saturation lifetimes of 31 and 390 min, respectfully. After solvent plasticization effects, the modulus of the 1,2-EDT-*co*-TAQA network increases slightly, which may be an indication of matrix stiffening as the polymer network interacts with water molecules. Based on these initial results, poly(thioether-*co*-carbonate) networks were synthesized containing mixtures of 1,2-EDT and TEGBMP or PETMP and TEGBMP in order to tune the T_g of the resulting network to 37 °C. Films were fabricated as previously described, where crosslinking of the multifunctional thiols and TAQA was based on

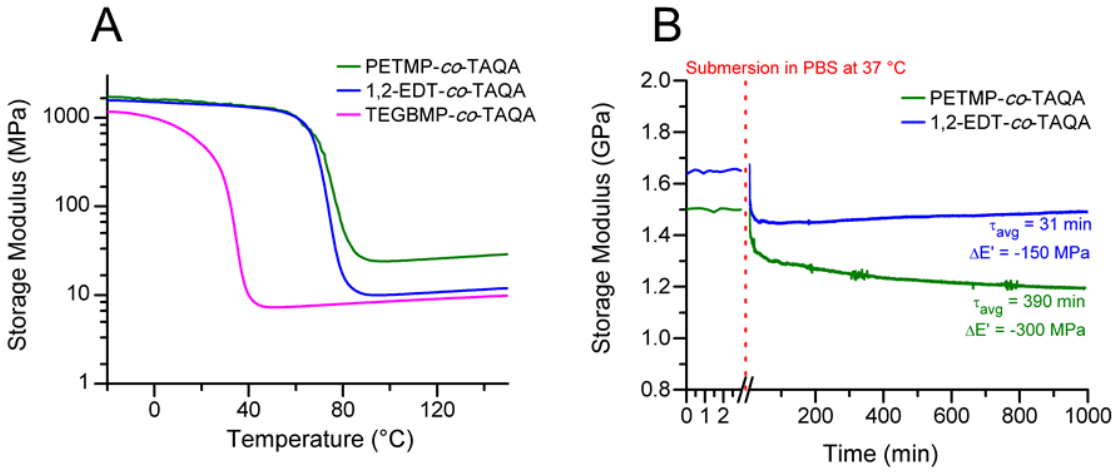

Figure 4.2. DMA results for formulations composed of TAQA and one thiol monomer. (A) Storage modulus as a function of temperature. (B) Solvent plasticization response over 16 h. Modulus was measured for 5 min at 25 °C in air before submerging in PBS at 37 °C

equal molar functional groups. After formulating and analyzing networks with varying ratios of 1,2-EDT to TEGBMP or PETMP to TEGBMP, the compositions which were found to produce films with T_g values of 37 °C were 75%EDT-*co*-TEGBMP-*co*-TAQA (*i.e.* where the total thiol mol fraction was made up of 75% 1,2-EDT and 25% TEGBMP) and 63%PETMP-*co*-TEGBMP-*co*-TAQA. To determine how the films mechanically adapt to physiological conditions, they were subjected to in situ DMA in PBS at 37 °C. The change in modulus was also observed for submersion in PBS at 25 °C to isolate changes due solely to solvent effects, rather than temperature and solvent effects. Figure 5.3 shows the results of the first 16 hours of submersion. Prior to submersion the storage modulus at 25 °C of 75%EDT-*co*-TEGBMP-*co*-TAQA and 63%PETMP-*co*-TEGBMP-*co*-TAQA was ~1.1 GPa and 1.5 GPa, respectively. The solvent response at 25 °C was a plasticized material with $\Delta E' = -900$ MPa (an order-of-magnitude decrease) for both films, and the final storage modulus values were 200 and 570 MPa for 75%EDT-*co*-TEGBMP-*co*-TAQA and 63%PETMP-*co*-TEGBMP-*co*-TAQA, respectively. The tanδ, or dampening factor, of both films steadily increased over the 16 h in PBS at 25 °C, showing no sign of any transition consistent with the glass transition. However, at 37 °C the tanδ reached maximum peak values at 97 and 157 min, for 75%EDT-*co*-TEGBMP-*co*-TAQA and 63%PETMP-*co*-TEGBMP-*co*-TAQA, respectively, then decreases. This is an indication of the time it takes for the films to transition from their glassy to rubbery state under physiological conditions.

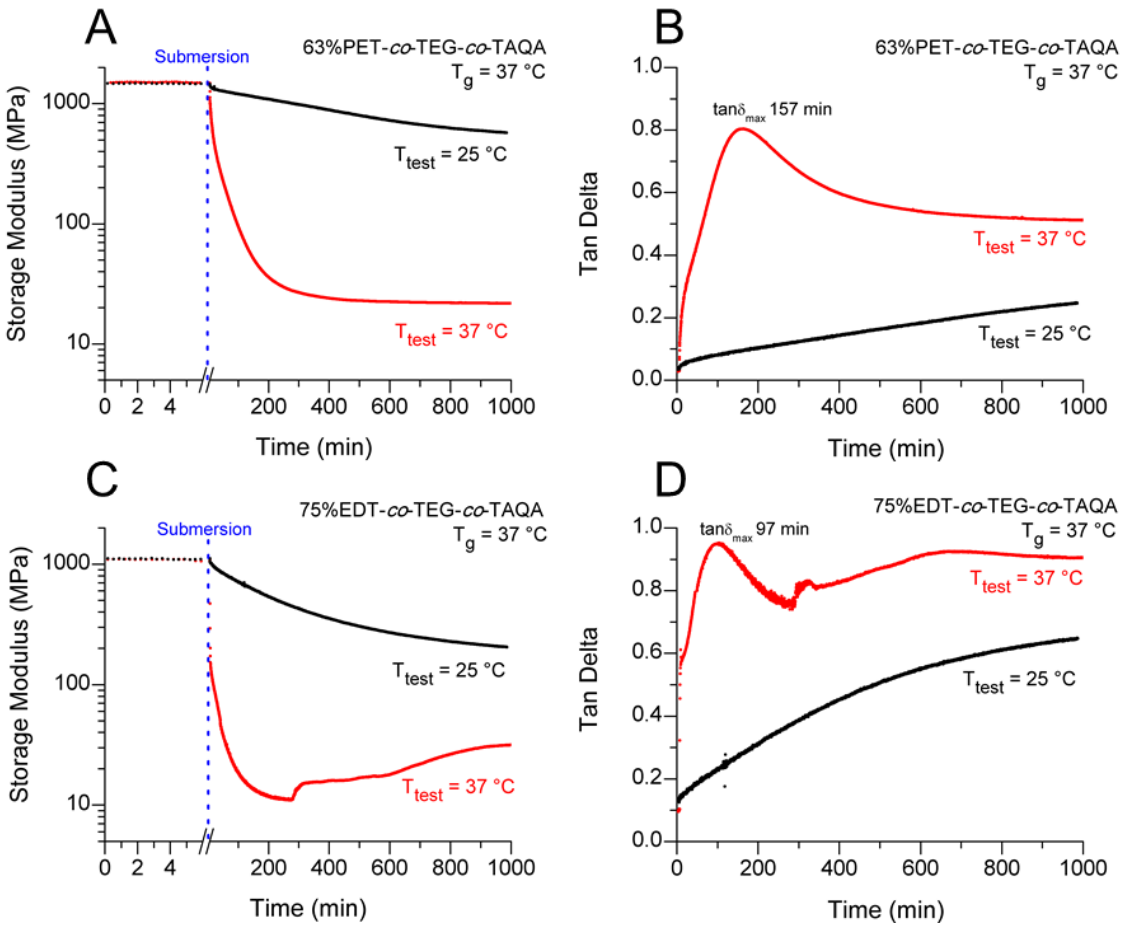

Figure 4.3. Solvent plasticization responses at 25 and 37 °C of films with T_g = 37 °C. (A) Storage modulus and (B) tanδ response of 63% PETMP-*co*-TEGBMP-*co*-TAQA; (C) storage modulus and (D) tanδ response of 75%EDT-*co*-TEGBMP-*co*-TAQA. Analysis was performed in air for 5 min before submersion.

Sample	T_g [°C][a]	T_{test} [°C]	E_{final} [MPa]	$\Delta E'$ [MPa]
1,2-EDT-*co*-TAQA	65	37	1500	-150
75%EDT-*co*-TEG-*co*-TAQA	37	25	200	-900
		37	32	-1100
PETMP-*co*-TAQA	65	37	1200	-300
63%PET-*co*-TEG-*co*-TAQA	37	25	570	-900
		37	22	-1500

Table 4.1. Storage modulus values as an effect of solvent plasticization at various test temperatures. [a]Determined by DSC

The longer time observed for the 63%PETMP-*co*-TEGBMP-*co*-TAQA may be due to the increased crosslink density compared to the other network. Similar to submersion at 25 °C, the solvent plasticization response at 37 °C was a decrease in modulus, in this case, by two orders of magnitude. The final storage modulus values were 32 and 22 MPa for 75%EDT-*co*-TEGBMP-*co*-TAQA and 63%PETMP-*co*-TEGBMP-*co*-TAQA, respectively. Following the solvent plasticization response, an increase in modulus was observed in the 75%EDT-*co*-TEGBMP-*co*-TAQA network. This matrix stiffening was also observed in the 1,2-EDT-*co*-TAQA network, and has been attributed to matrix interactions with water molecules causing an annealing effect, in which the polymer network takes time to reach its lowest-energy configuration.

In order to observe how the materials react to physiological conditions beyond the initial 16 h, films (n = 30, 4 × 4 × 0.6 mm) were submerged in PBS and placed in an incubator shaker at 37 °C and 60 rpm. After 1, 2, and 3 weeks, films (n = 10) were removed, the degree of swelling was measured, and thermal properties of the swollen networks were determined by DSC and TGA. The results are listed in Table 4.2. The initial thermal properties of the networks were T_g = 37 °C, for both, and T_d = 288 and 262 °C for 63%PETMP-*co*-TEGBMP-*co*-TAQA and 75%EDT-*co*-TEGBMP-*co*-TAQA, respectively. Within the 3 weeks of this study the samples did not express any mass loss due to hydrolytic degradation, consistent with what is expected based on previous studies. After 3 weeks the T_g of the swollen networks had dropped to 19 and 11 °C and the T_d had decreased to 257 and 179 °C, for the networks containing PETMP and 1,2-EDT, respectively. This change in properties indicated that even though the networks do

	T_g [°C]	T_d [°C]	Swelling Ratio
63%PET-*co*-TEG-*co*-TAQA			
1 week	25 ± 3	281 ± 1	1.020 ± 0.002
2 weeks	24 ± 2	267 ± 1	1.028 ± 0.003
3 weeks	19 ± 4	257 ± 2	1.050 ± 0.006
75%EDT-*co*-TEG-*co*-TAQA			
1 week	25 ± 1	255 ± 3	1.020 ± 0.001
2 weeks	17 ± 2	234 ± 5	1.121 ± 0.016
3 weeks	11 ± 1	179 ± 1	1.252 ± 0.028

Table 4.2. Thermal properties and swelling of networks after 1-3 weeks under physiological conditions.

not physically lose any polymer mass, hydrolysis of carbonate and/or ester bonds may be decreasing the crosslink densities of the networks resulting in a decrease in thermal properties.

To explore whether network properties can be controlled spatially within a material sample, the fabrication of a film designed to have a one dimensional gradient in thermomechanical properties across the length of the film was performed. Two resin mixtures were formed using the sample formulations for (100%)PETMP-*co*-TAQA and 63%PETMP-*co*-TEGBMP-*co*-TAQA. A small amount of solvent was added to the resins to decrease viscosity and allow for adequate diffusion upon mold casting. The mixtures were injected each at opposite ends of an open-face mold made with a glass slide at the base and coverslips on each side. After evaporation of the solvent, the film was cured by exposing to UV light, removed from the mold, and post-cured at 120 °C for 24 hours. The resulting film is depicted in Figure 4.4, and to the touch had a noticeable difference in mechanical properties across the length of the film. One end was a rigid plastic and the other end felt for malleable and elastomeric. For analysis of

the mechanical gradient, the film was cut into six sections of approximately equal widths. Each section was subjected to DMA to observe storage modulus behavior as a function of temperature (Figure 4.4A) and DSC to measure $T_{g.}$

The resulting T_g values of each section were 48, 44, 38, 34, 28, and 24 °C from left to right for sections 1 to 6, respectively. Based on the rubbery modulus plateaus, the crosslink density of the film also decreases from left to right, as expected. The modulus values at various temperatures were plotted as a function of section on the film to show how the span of the mechanical gradient is expected to change at different temperatures (Figure 4.4B). At 25 °C the difference in modulus across the film is from 1.6 GPa to 700 MPa, and as the temperature increases that gap widens. At 63 °C the modulus across the film is from 1.0 GPa to 10 MPa. Considering the mechanical adaptability of these networks, it can be expected that the span of the mechanical gradient would also change under physiological conditions. At body temperature and dry condition the modulus of the film ranges from 1.6 GPa to 200 MPa. Under physiological conditions the gradient in stiffness is expected be from 1.2 GPa to 32 MPa, spanning two orders of magnitude, based on the submersion DMA studies performed on PETMP-*co*-TAQA and 63%PETMP-*co*-TEGBMP-*co*-TAQA.

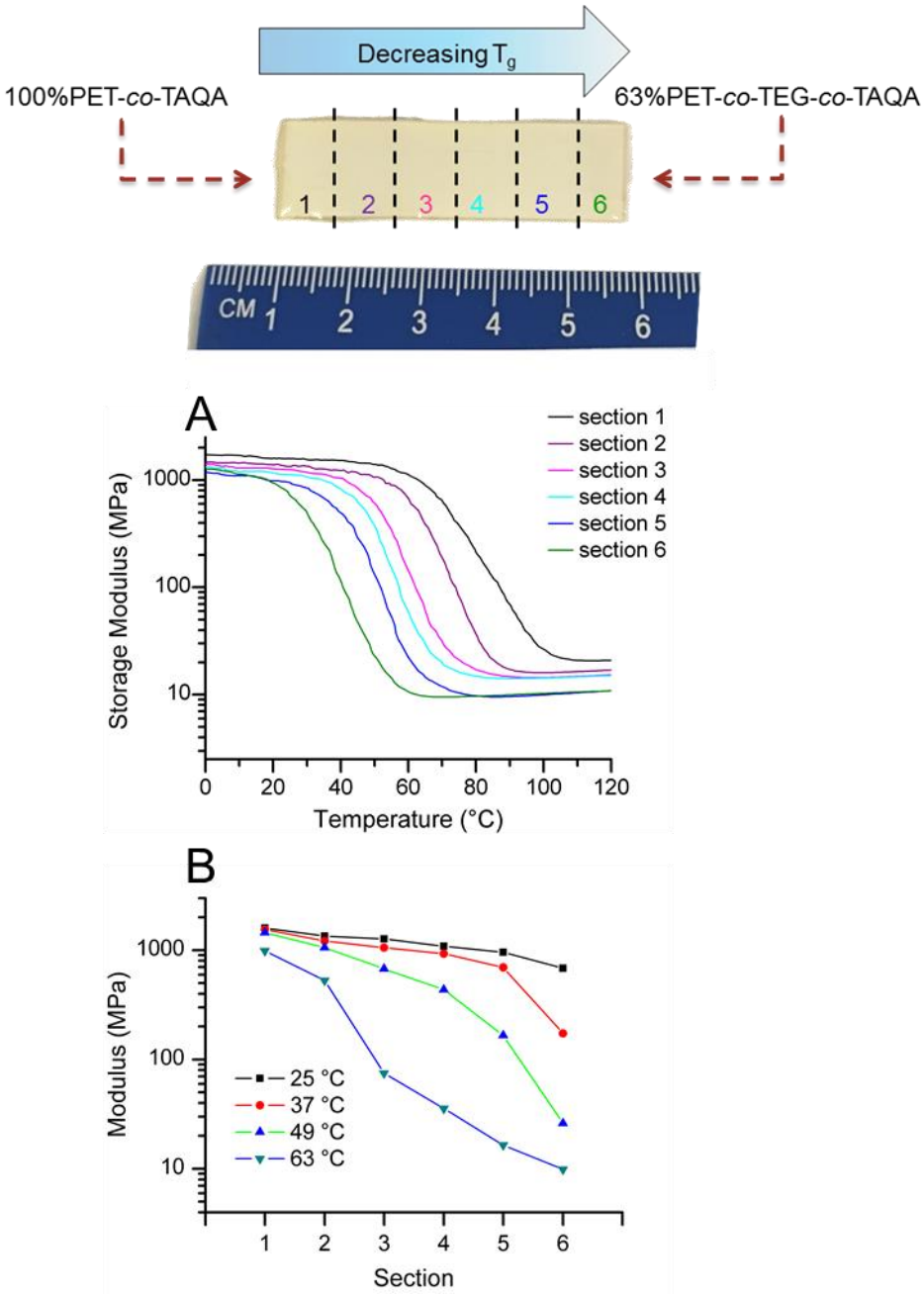

Figure 4.4. Picture and mechanical properties of a poly(thioether-*co*-carbonate) film with 1D mechanical gradient. A photograph of the film is shown at the top; the arrows represent how the resins were injected into the mold and the dashed lines across the film represent how the film was cut into sections for analysis. (A) Storage modulus measurements by DMA of films as a function of temperature. (B) Modulus values determined by DMA plotted for each section at different temperatures; shows the span of the mechanical gradient at various temperatures.

4.3 Conclusions

We present a series of studies which investigate the mechanical-adaptability and spatial controllability of properties in poly(thioether-*co*-carbonate) networks. Mechanical changes from on the order of 1 GPa to 10 MPa were exhibited by networks when exposed to physiological conditions. Designed to be rigid at room temperature and soften upon implantation, these materials may find potential application in softening electrodes for neural interfaces and other dynamic biomedical devices. The spatial control over mechanical properties was also investigated, and a film with a mechanical gradient with a range of moduli from 1.6 GPa to 700 MPa was produced. Under physiological conditions the breadth of the gradient is expected to wide to a range of moduli from 1.2 GPa to 32 MPa, a two-orders-of-magnitude gradient. This material may be used to mimic soft-to-hard transitions in nature and in interfacial tissue engineering applications. For example, the mechanical gradient in the tendon-to-bone transition at the top of the tibia (between tibia and knee) has moduli which range from 1.4 GPa at the surface of the bone to 100 MPa at the tibial cartilage. Future studies will be performed to explore the degradation kinetics of the gradient films and determine how the mechanical gradient affects cell attachment *in vitro*. Strategies for incorporating other functional components which may further enhance the mechanical adaptability of these networks will be explored.

4.4 Materials and Methods

Pentaerythritol tetrakis(3-mercaptopropionate) (PETMP), 1,2-ethanedithiol (1,2-EDT), and 2,2-dimethoxy-2-phenylacetophenone (DMPA) were purchased from Sigma-Aldrich. Tetraethylene glycol bis(3-mercaptopropionate) (TEGBMP) was purchased from Wako Chemicals. Phosphate-buffered saline (PBS) solution (pH 7.4, 137 mM NaCl, 2.7 mM KCl, and 10 mM phosphate buffer) was purchased from Fisher Scientific.

Glass transition temperatures were measured using differential scanning calorimetry (DSC) by a Mettler-Toledo DSC822 (Mettler-Toledo, Columbus, OH) with a heating rate of 10 °C/min. The T_g was taken as the midpoint of the inflection tangent upon the third heating cycle. Thermogravimetric analysis (TGA) was done under an Ar atmosphere using a Mettler-Toledo TGA/DMA1 with a heating rate of 10 °C/min. Dynamic mechanical analysis experiments were performed on a Mettler-Toledo TT-DMA system, and data were obtained from Triton Laboratory software. Temperature scans in were performed in tension mode from −80 to 180 °C at a ramp rate of 3 °/min, a frequency of 1 Hz, and a sampling interval of 10 s. Isothermal submersion experiments were performed in PBS for 999 min (1 Hz, 30 s sample interval). In all DMA experiments the dynamic force was 1 N, and the ratio of static to dynamic force was held constant at 1.5.

4.4.1 Polymer network synthesis

The alkenyl monomer, TAQA was synthesized as previously described.[78] Briefly, the two-step synthesis of TAQA starts with the well-known lactonization of QA

under acidic conditions. QA and Amberlyst resin are suspended in benzene and DMF and heated to reflux with azeotropic removal of water to afford the bicyclic triol QA lactone. To install the three alloc functionalities, allyl chloroformate (44.7 mL diluted with 20 mL DCM) was added dropwise to QA lactone (10.3 g) suspended in cold (0°C) *N,N,N',N'*-tetramethylethylenediamine (36.4 mL) and DCM (200 mL) to give TAQA as a clear viscous oil.

Each formulation of TAQA and multifunctional thiol(s) was mixed based on equal molar ratio of alkene to thiol and contained no solvent. The compositions of the networks containing mixtures of different thiols are listed in Table 4.3. The photo-initiator was 1 wt% DMPA and was dissolved in the thiol before TAQA was added. All formulations were vortexed and sonicated until a visually homogeneous mixture without any air bubbles was reached. Each mixture was cast between two glass slides separated by a 0.6 mm spacer, and exposed to UV light (365 nm) on a Fusion curing line system (1 m/min, 15 min). The glass slide molds were removed, and the free-standing films were post-cured at 120 °C for 24 h.

Formulation	TAQA (g)	TEGBMP (g)	Other thiol (g)	DMPA (g)
63%PETMP-*co*-TEGBMP-*co*-TAQA	0.5102	0.1532	0.3450	0.0101
75%EDT-*co*-TEGBMP-*co*-TAQA	1.2712	0.4107	0.3177	0.0200

Table 4.3. Compositions of formulations containing mixtures of two thiol monomers.

4.4.2 Fabrication of a film with a 1D mechanical gradient

Two resin formulations were mixed as listed in Table 5.4. DCM (0.1 mL) was added to each mixture to decrease their viscosity. The two mixtures were simultaneously injected into opposite ends of an open-faced mold (51 ×13 mm). The filled mold was allowed to sit at room temperature for 12 h under a chemical hood and in the dark before curing. The film was UV-cured (365 nm) on a Fusion curing line system (1m/min, 10 min) and post-cured for 24 h at 120 °C under vacuum. The film was cut into 6 sections, and each section was analyzed to confirm the presence of a mechanical gradient across the length of the film.

Formulation	TAQA (g)	TEGBMP (g)	PETMP (g)	DMPA (g)
63%PETMP-*co*-TEGBMP-*co*-TAQA	0.5249	0.1583	0.3472	0.0103
PETMP-*co*-TAQA	0.5832	0.0000	0.4626	0.0108

Table 4.4. PETMP-*co*-TEGBMP-*co*-TAQA formulations for gradient film

4.5 Supporting Information

Figure 4.5 shows the changes in onset decomposition temperature of the networks after submersion in PBS for 1, 2, and 3 weeks.

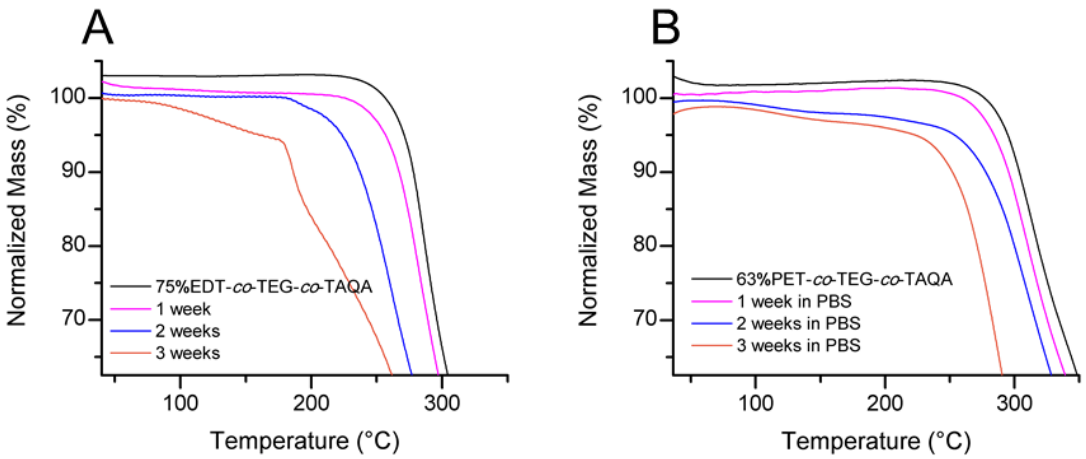

Figure 4.5. Analysis of thermal stability for poly(thioether-*co*-carbonate) networks after time (weeks) under physiological conditions.

CHAPTER V

SUSTAINABLE PHOTO-CROSSLINKED THIOL-ENE NETWORKS FROM QUINIC ACID AND NATURAL DITHIOLANES: TOWARD "ALL NATURAL" DEGRADABLE POLYCARBONATE NETWORKS

5.1 Introduction

The quest for sustainable polymers that are biodegradable and do not require energy from fossil fuels to manufacture is driven by the need to decrease dependence on petroleum feedstocks and address the devastating effects of plastic waste and pollution.[2, 4, 8-9] The design criteria include, but are not limited to, (i) precursor materials which are natural and renewable, (ii) hydrolytically degradable, *i.e.* ester, carbonate, anhydride, *etc.*, linkages, (iii) non-toxic degradation products, preferably the natural building-blocks from which the polymer was constructed, (iv) synthetic strategies which mild, minimizing the use of harsh conditions or reagents. To address processing concerns, one polymerization technique that has been widely adapted to a multitude of different applications is photo-initiated thiol-ene chemistry.[46, 53] The step-growth, free radical polymerization of thiols with alkenes is highly efficient, proceeds under mild conditions to high conversions, is tolerant of many functional groups, water, and oxygen, and produces crosslinked networks, which are significantly more uniform and contain less residual stresses post cure compared to acrylate networks.[51-52] For these reasons, thiol-ene chemistry has proven to be a powerful tool in biomedical applications, where in many cases it has been combined with hydrolytically labile moieties to achieve

degradable thiol-ene networks. Recently, thiol-ene chemistry has been utilized in the development of degradable polyanhydride[88] and poly(ethylene glycol)[89] hydrogels, degradable poly(silyl ether) substrates for neural interfaces,[90] and processable polyurethane shape memory devices.[91] Additionally, to increase the inherent biocompatibility and the sustainability, naturally-derived alkenes have been exposed to thiol-ene chemistry to produce bio-based degradable polymers from plant-based resources, including phenolic acids,[92] isosorbide,[93] and D-limonene.[58]

Many of the naturally-derived thiol-ene networks use commercially-available non-natural multifunctional thiol monomers, such as trimethylolpropanyl *tris*(3-mercaptopropionate) or pentaerythritol *tetrakis*(3-mercaptopropionate), resulting in a network which may actually only 50% or less directly derived from natural products. Additionally, although the polymer may degrade to regenerate its natural building blocks it may also generate other by-products with unknown biological and environmental properties. Herein, we describe a system which not only uses a naturally-derived alkenyl monomer but also natural multifunctional thiol monomers derived from lipoic acid. Present in both plants and animals, α-lipoic acid (LAc) and its reduced form, dihydrolipoic acid (DHLAc) are metabolic antioxidants with the capability to quench free radicals without being destroyed in the process.[94] The most abundant plant-based sources of LAc are spinach, broccoli, and tomatoes, and it is available as a nutritional supplement and as a drug to treat diabetic neuropathy. An essential cofactor in α-ketoacid dehydrogenase complexes and the glycine cleavage system, LAc is often covalently attached to a lysine residue by an amide linkage, in the form of lipoamide

(LAm). Previously, DHLAc and the reduced form of LAm, dihydrolipoamide (DHLAm) were used in the surface functionalization of gold nanoparticles and nanorods with polymers as the ligand-to-metal binding sites.[95-98] However, to our knowledge, they have never been used for the formation of thiol-ene networks. By utilizing natural multifunctional thiols derived from LAc and therefore, increasing the overall bio-based content of the resulting polymer material, it may be possible to increase the sustainability and the inherent biocompatibility of the polymer and its degradation products. The naturally-based alkenyl monomer, *tris*(alloc) quinic acid (TAQA), is derived from quinic acid, a polyhydroxyl compound abundant in roasted coffee and known for its beneficial biological properties, including promoting antioxidant activity and growth. As described previously, the bicyclic structure of TAQA provides rigidity to the network which increases the modulus, and the carbonate linkages are purposefully placed in order to provide sites for degradation and the ultimate regeneration of quinic acid.[78] The result of copolymerization of TAQA and DHLAm or DHLAc *via* photo-initiated thiol-ene reaction is crosslinked degradable polycarbonate networks, DHLAm-*co*-TAQA and DHLAc-*co*-TAQA, shown in Figure 5.1. Polycarbonates, known for their toughness and solvent resistance in engineering plastics, were chosen as the hydrolysable linkages because they breakdown into alcohols and carbon dioxide, making it possible to reproduce quinic acid in its initial polyhydroxyl form upon degradation. The thermomechanical properties and degradation kinetics of the two networks were compared, and the cytotoxicity was analyzed.

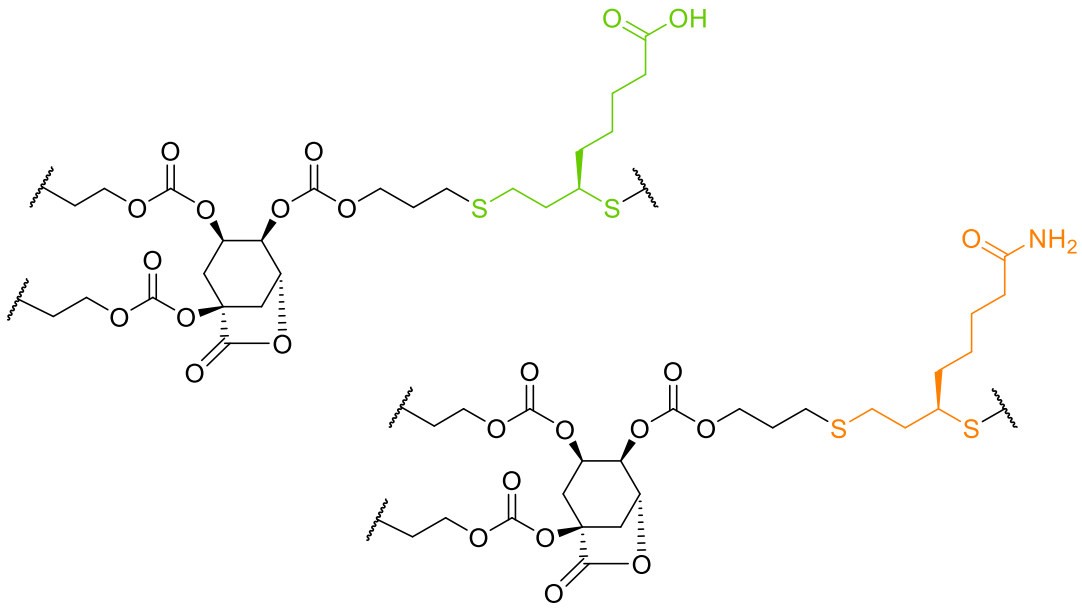

Figure 5.1. Chemical structures representing DHLAm-*co*-TAQA (bottom) and DHLAc-*co*-TAQA (top).

5.2 Results and Discussion

The synthesis of the QA-based alkenyl monomer, TAQA, occurred in two steps, as previously described.[78] First, QA lactone was formed by well-established methods.[67] A suspension of QA and Amberlyst H^+ resin in benzene and DMF was heated to reflux with azeotropic removal of water to afford the bicyclic triol QA lactone in 96% yield. The second step was the installation of the three allyl carbonate (alloc) groups. Allyl chloroformate was added dropwise to QA lactone in cold *N*,*N*,*N'*,*N'*-tetramethylethylenediamine and dichloromethane to produce TAQA in 74% yield as a clear viscous oil. The thiol monomers were synthesized by reducing the disulfides of lipoic acid and lipoamide to thiols. Aqueous sodium borohydride was added and mixed

at 0 °C with either lipoic acid in an aqueous 0.25 M sodium bicarbonate solution or lipoamide in tetrahydrofuran to afford DHLAc in 85% yield or DHLAm in 94% yield, respectively. Interestingly, DHLAc was a clear oil and DHLAm was a white solid. Both were kept at −80 °C when not being used. Conversion of the disulfides to thiols was confirmed by ^{1}H and ^{13}C NMR spectroscopies, FTIR and electrospray ionization mass spectrometry. Solvent-free crosslinking copolymerization by thiol-ene radical addition in the presence of 1 wt% 2,2-dimethoxy-2-phenylacetophenone photoinitiator was performed by mixing TAQA and either DHLAc or DHLAm based on equal molar functional groups, mold casting, and exposing to UV light (λ = 365 nm). The DHLAm and TAQA mixture was mixed at 60 °C to melt the DHLAm prior to mold-casting. Following UV-cure, the samples, either films (0.6 mm thick) or discs (6 mm in diameter and 3 mm thick), were post-cured at 120 °C for 24 h to help drive crosslinking to completion.

The dynamic mechanical analysis (DMA) results in Figure 5.2 (A and B) show the relative thermomechanical behavior of DHLAc-*co*-TAQA and DHLAm-*co*-TAQA. The storage modulus behavior depicted in Figure 5.2 (A) is characteristic of amorphous thermoset polymers, where a glassy modulus plateau is expressed at temperatures below the glass transition, the glass transition is represented by the drop in modulus by two orders of magnitude, and a rubbery modulus plateau is expressed at temperatures above the glass transition. The rubbery modulus is proportional to the crosslink density of the network. Because the only chemical difference between the two networks is the acid or amide functionalized side-chain-end, it makes sense that the crosslink densities of the

two networks were very similar. However, the chemical variation did have a significant effect on the T_g of the network. Table 5.1 lists the thermomechanical properties of the poly(thioether-*co*-carbonate) networks containing the two different thiols investigated. The T_g values determined by differential scanning calorimetry are consistent with the onset of the glass transition region in Figure 5.2 (A) and proportional to the peak of the tanδ behavior in Figure 5.2 (B). The reason the DHLAm-*co*-TAQA network exhibited a much higher T_g (62 °C) compared to DHLAc-*co*-TAQA (T_g = 46 °C) is most likely due the increased ability for secondary interactions, specifically hydrogen bonding, involving the amide groups in DHLAm-*co*-TAQA compared to the acid groups in DHLAc-*co*-TAQA. The onset temperatures of thermal decomposition, T_d, for the two networks were similar and comparable to values reported previously for poly(thioether-*co*-carbonate) networks (*ca*. 260 °C). The modulus values measured at 25 C were also similar (1.5 GPa for DHLAc-*co*-TAQA and 1.4 GPa for DHLAm-*co*-TAQA).

Along with the difference in T_g the networks also exhibited a significant variation in degradation kinetics, shown in Figure 5.2 (C and D). Four discs of each formulation were placed in phosphate buffered saline solution (pH 7.4) and kept in an incubator shaker at 37 °C and 60 rpm for 5 days. Then the discs were removed, swelling was measured, and after drying under vacuum for 24 h mass loss was calculated. Discs were returned to PBS and this protocol was followed approximately every five days until polymers were visually fully degraded and dissolved in solution. Within the first 15 days the discs had taken up at least their weight in water and started to degrade via surface erosion. The DHLAc-*co*-TAQA network took up more water and degraded at a

significantly higher rate than the equivalent amide system, fully degrading over 33 days while the DHLAm-*co*-TAQA samples took 44 days to fully degrade. As the DHLAc-*co*-TAQA samples swelled the acidic side chain moieties may have caused a decrease in the local pH catalyzing carbonate hydrolysis. On the other hand the weakly basic amide groups of the DHLAm-*co*-TAQA network may counter act any decrease in local pH caused by the hydrolysis of the lactone rings of TAQA. Overall, the thermomechanical properties of these two networks are similar to poly(thioether-*co*-carbonate)s formed from TAQA and commercially-available non-natural multifunctional thiols; however, they degrade at a much faster rate. The 1,2-EDT-*co*-TAQA network synthesized from 1,2-ethanedithiol and TAQA has a T_g and rubbery modulus of 65 °C and 7.2 MPa, respectively, values comparable to the DHLAm-*co*-TAQA network, but 1,2-EDT-*co*-TAQA takes over 25 weeks to degrade.

5.3 Conclusions

In conclusion, poly(thioether-*co*-carbonate) networks were designed and synthesized from plant-based derivatives of quinic acid and lipoic acid, and the overall plant-based content of the resulting networks is 80 wt%, which is much greater than any naturally-derived thiol-ene network involving the popular commercially-available tri-and tetra-functional mercaptopropionates. Additionally, the networks presented here exhibit interesting properties compared to previous described poly(thioether-*co*-carbonate)s. The thermal and mechanical properties are very similar, but the degradation times are drastically different. While the DHLAc-*co*-TAQA and DHLAm-*co*-TAQA networks take ~6 weeks to degrade, equivalent networks which use 1,2-ethanedithiol as the thiol

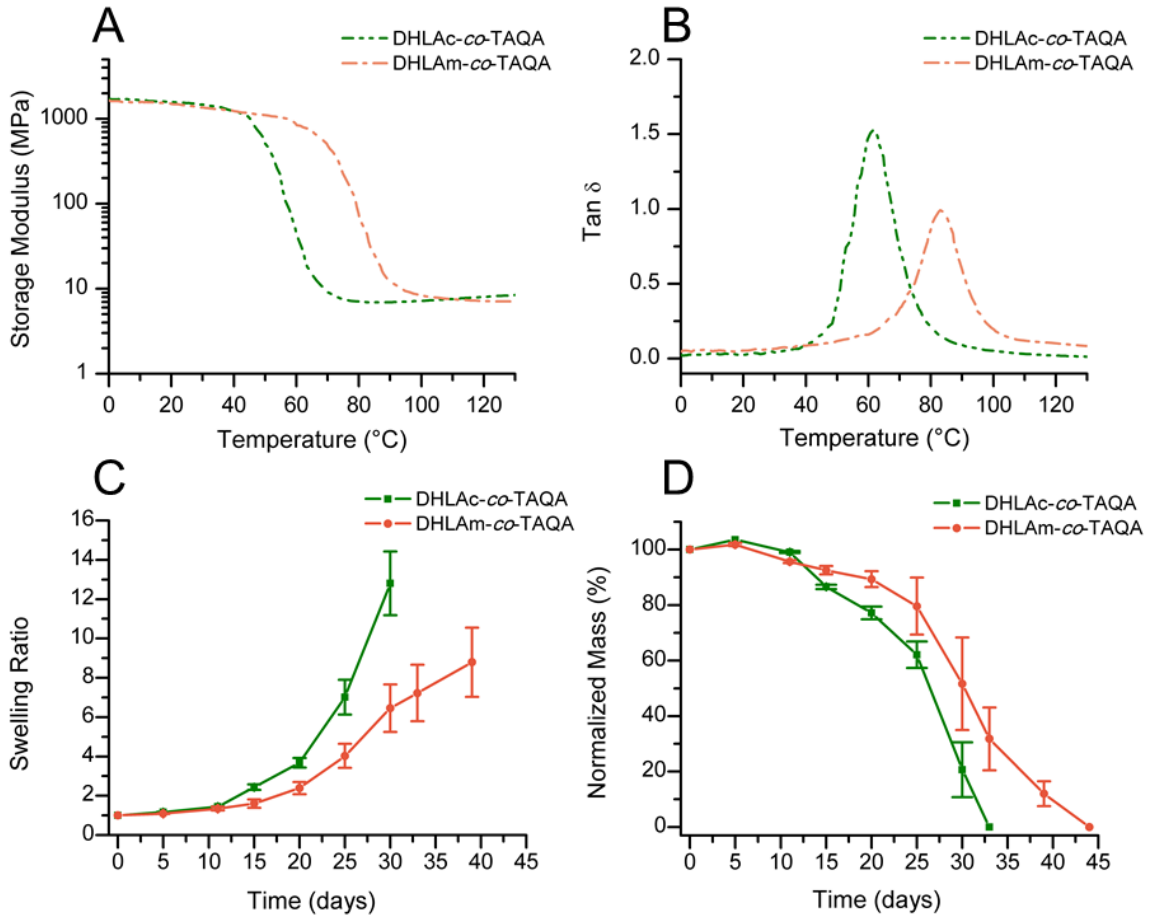

Figure 5.2. Dynamic mechanical behavior and degradation kinetics of DHLAc-*co*-TAQA and DHLAm-*co*-TAQA. (A) Storage modulus and (B) tanδ as a function of temperature determined by DMA in tension mode. (C) Swelling and (D) normalized remaining mass monitoring hydrolytic degradation in physiologically-relevant conditions.

Polymer	T_g [°C][a]	T_d [°C][b]	E' [MPa][c]	E_r [MPa][d]	Tan δ_{max} [°C][e]
DHLAc-*co*-TAQA	46	263	1500	6.9	62
DHLAm-*co*-TAQA	62	252	1400	8.1	84

Table 5.1. Thermal transitions and moduli exhibited by the poly(thioether-*co*-carbonate) networks derived from QA and LAc. [a]Determined by DSC; [b]Onset of thermal decomposition determined by TGA; [c]Storage modulus at 25 °C determined by DMA; [d]Rubbery modulus determined by DMA; [e]Temperature at which the maximum tanδ value occurs.

monomer take over 25 weeks to degrade. Together these networks add to the previously described poly(thioether-*co*-carbonate) networks and make up a family of degradable polymeric thermosets with a wide range of achievable thermomechanical and degradation properties. Future studies will focus on determining the cytotoxicity *in vitro* and investigating the application of other natural thiols in thiol-ene networks.

5.4 Materials and Methods

Quinic acid, Amberlyst 15 ion-exchange resin, N,N,N',N'-tetramethylethylenediamine, allyl chloroformate, 2,2-dimethoxy-2-phenylacetophenone, lipoic acid, lipoamide, and sodium borohydride, were all used as received from Sigma Aldrich. Phosphate-buffered saline (PBS) solution (pH 7.4, 137 mM NaCl, 2.7 mM KCl, and 10 mM phosphate buffer) was purchased from Fisher Scientific.

^{1}H and ^{13}C NMR spectra were obtained on either a Varian Mercury 300 at 300 MHz using the solvent signal as internal reference. Glass transition temperatures were measured using differential scanning calorimetry (DSC) by a Mettler-Toledo DSC822 (Mettler-Toledo, Columbus, OH) with a heating rate of 10 °C/min. The T_g was taken as the midpoint of the inflection tangent upon the third heating cycle. Thermogravimetric analysis (TGA) was done under an Ar atmosphere using a Mettler-Toledo TGA/DMA1 with a heating rate of 10 °C/min. Dynamic mechanical analysis (DMA) experiments were run in tension to determine thermomechanical profiles for the thermoset poly(thioether-*co*-carbonate) samples. Dynamic mechanical analysis experiments were performed on a Mettler-Toledo TT-DMA system, and data were obtained from Triton Laboratory software. Temperature scans were performed on rectangular DMA

specimens (5 mm x 12 mm x 0.6 mm) from −80 to 180 °C at a ramp rate of 3 °/min, a frequency of 1 Hz, and a sampling interval of 10 s. MC3T3 cells were purchased from the American Type Culture Collection (ATCC) and subcultured based on ATCC protocol. Briefly cells were cultured in with MEM-alpha media supplemented with 10% FBS and 1% antibiotic.

5.4.1 Thiol monomer synthesis from lipoic acid and lipoamide

To a 0.250 M solution of $NaHCO_3$ (20 mL), lipoic acid (0.250 g, 1.21 mmol) was added and cooled to 0 °C. Aqueous $NaBH_4$ (0.092 g, 2.42 mmol in 5 mL H_2O) was added and mixed for 24 h. The reaction pH was adjusted to 2 using 6 M HCl before extraction with diethyl ether (3 × 20 mL). The organic layers were combined and dried over Na_2SO_4 and under vacuum to recover dihydrolipoic acid (DHLAc) as a colorless, oil (0.215 g, 85% yield). DHLAc was stored in the freezer at −80 °C when not being used. ^{1}H NMR (300 MHz, $CDCl_3$, ppm): δ 2.97-2.85 (m, 1H), 2.79-2.59 (m, 2H), 2.36 (t, J = 6.0 Hz, 2H), 1.95-1.79 (m, 1H), 1.79-1.40 (m, 8H), 1.37-1.28 (p, J = 9.0 Hz, 2H); ^{13}C NMR (300 MHz, $CDCl_3$, ppm) δ 179.89, 42.64, 39.27, 38.68, 33.89, 26.44, 24.26, 22.28; HRMS (+ESI) *m/z* calc'd. for $C_8H_{16}O_2S_2$ $[M+Na]^+$: 231.0489, found 231.05; (-ESI) $[M-H]^-$: 207.0513, found 207.05.

Lipoamide (0.745 g, 3.63 mmol) was added to 13 mL of THF and cooled to 0 °C. $NaBH_4$ (0.282 g, 7.46 mmol) was dissolved in 6 mL of water and added to the LAm suspension. After 1.5 h of mixing, 5 mL of 1 M HCl was added slowly. The organic content was extracted with ethyl acetate (3 × 20 mL), dried over $MgSO_4$, and condensed

under vacuum to afford DHLAm as a white solid (0.705 g, 94 % yield). DHLAm was kept in the freezer when not being used.

5.4.2 Polymer network synthesis

The alkenyl monomer, TAQA was synthesized as previously described.[78] Briefly, the two-step synthesis of TAQA starts with the well-known lactonization of QA under acidic conditions. QA and Amberlyst resin are suspended in benzene and DMF and heated to reflux with azeotropic removal of water to afford the bicyclic triol QA lactone. To install the three alloc functionalities, allyl chloroformate (44.7 mL diluted with 20 mL DCM) was added dropwise to QA lactone (10.3 g) suspended in cold (0 °C) *N*,*N*,*N'*,*N'*-tetramethylethylenediamine (36.4 mL) and DCM (200 mL) to give TAQA as a clear viscous oil.

Mixtures of thiol and TAQA were prepared based on equal molar functional groups. The amount of photoinitiator, DMPA, was 1 wt% for each mixture. Table 4.1 shows the compositions of each resin. Because DHLAm is a solid at room temperature, TAQA and DHLAm were mixed at 60 °C before the DMPA was added. DHLAc and TAQA, both liquids, were mixed at room temperature. DMPA was added last and blended thoroughly. The resin was cast between two glass slides separated by a 0.6 mm spacer and was used to fill four disc molds (discs, 6 mm in diameter and 3 mm thick). Crosslinking polymerizations were performed by exposing the molds to UV irradiation (365 nm) in a UVP crosslinking chamber for 15 min. Samples were removed from the mold and exposed to UV for an additional 15 min. Following UV exposure samples

were post-cured at 120 °C under reduced pressure for 24 h. All samples were stored in the freezer at −80 °C when not in use.

Formulation	TAQA (g)	Thiol (g)	DMPA (g)
DHLAc-*co*-TAQA	0.2900	0.2157	0.0050
DHLAm-*co*-TAQA	0.0966	0.1340	0.0023

Table 5.2. Thiol-ene network formulations from QA and LAc derivatives.

5.4.3 Hydrolytic degradation in physiological conditions

The initial mass of four discs for each formulation was recorded, and the disc was submerged in 4 mL of PBS (pH 7.4) and placed in the incubator shaker at 37 °C and 60 rpm to mimic physiological conditions. The discs were removed approximately every 5 days rinsed with deionized water. The PBS solution containing any degradation products was kept and saved at −80 °C for further analysis. The swollen masses (w_w) of the pucks were measured before the samples were dried under vacuum until they reached a stable dry mass (w_d). The swelling ratio (q) was calculated according to the following equation:

$$q = \frac{w_w}{w_d}$$

The normalized mass (m) at each time point was calculated using the equation below, where w_i is the initial mass of the sample before degradation.

$$m = \frac{W_d}{W_i} \times 100\%$$

Fresh PBS was added and the discs were returned to the degradation environment. The average normalized mass and swelling ratio were determined at various time points until no visible solids remained.

CHAPTER VI

CONCLUSIONS

In this dissertation synthetic strategies for the preparation of degradable polycarbonates that originate from renewable resources, exhibit novel combinations of properties, and have the ability to undergo hydrolytic breakdown into biologically-beneficial by-products are developed. The polyhydroxyl natural product quinic acid has been selected as the monomeric building block, and carbonates, found in tough engineering materials, have been selected as the degradable linkages. This combination is special because when carbonates hydrolyze they are converted to hydroxyl-containing compounds and carbon dioxide. Therefore, polycarbonates built from polyhydroxyl natural products have the ability to regenerate the natural product as a pure compound, rather than a similar derivative. Additionally, the degradation products of polycarbonates are biocompatible and may reduce the risk of adverse side effects compared to the acidic degradation of FDA-approved polyesters.

In the first project, poly(thioether-*co*-carbonate) networks derived from QA and various multifunctional thiols were introduced and characterized. The relationship between the structure of the thiol monomer and the resulting properties of the network, including crosslink density and T_g, was realized, and initial studies of solvent plasticization were performed. The resulting family of polycarbonates exhibited a glass transition that could be controlled between −18 °C and 65 °C and modulus values similar to other plastics. In Chapter III, those materials were tested in presence of a

physiologically relevant environment, to study their ability to serve as biomaterials. Biological and chemical properties of the polymers and their degradation products revealed that the polymers were nontoxic and degrade to reproduce QA and the hydroxyl-functionalized thioether equivalent of the original thiol monomer, which also exhibited low toxicity. The degradation time ranged from 10 to 35 weeks, presenting another tunable material property. In the third project the tunable thermomechanical properties of the system were exploited and fully utilized to create materials with interesting responsive properties. By tuning the T_g of the material to be close to body temperature using carefully formulated resins with mixtures of thiol monomers, films that behave as rigid thermosets at room temperature and then soften under physiological conditions to their elastomeric state were produced. The modulus values of the materials decrease by two orders-of-magnitude due to a combination of temperature and solvent effects. This ability to mechanically-adapt to physiological conditions was combined with spatially controlling the composition of the material along a 1D gradient, to produce a film with a soft-to-hard transition which was enhanced by heat and water. At physiological conditions the gradient difference along the length of the film was two orders-of magnitude, from 1 GPa to 10 MPa.

Although the goal of synthesizing polymer materials that have modulus values close to those of cortical bone (E' = 17-24 GPa) was not achieved, the materials have modulus values similar to those of cancellous bone (E' = 0.1-4.5 GPa) and may be good candidates for low load-bearing applications in orthopedics. To further increase mechanical properties so that it may be possible to use these polymers in mechanically-

strenuous orthopedic applications, the incorporation of ceramic or organic nanoparticles should be considered. The incorporation of ceramic hydroxyapatite nanoparticles is expected to not only increase the modulus but also increase the structural likeness to bone, which is made up of hydroxyapatite nanoparticles in a collagen matrix. Compared to the conventional degradable polyesters used in orthopedic applications (used in low load-bearing applications), the and PETMP-*co*-TAQA systems have similar mechanical and thermal properties. The degradation kinetics of these materials are different depending on the thiol monomer. For orthopedic applications the large amount of swelling and rapid degradation rate of TEGBMP-*co*-TAQA is concerning. However the low amount of swelling and long degradation times of 1,2-EDT-*co*-TAQA and PETMP-*co*-TAQA may be more suitable for orthopedic applications. Therefore, although these materials are not yet able to serve as replacements to metals and alloys in mechanically-strenuous applications, they may be superior to the conventional degradable orthopedic polymers.

The goal of synthesizing polymer materials from natural products is to not only make advancements toward sustainable, non-petroleum-based plastics, but also to design novel biocompatible materials that exhibit interesting combinations of properties. Overall, the poly(thioether-*co*-carbonate) networks developed in this work have the potential to lead to materials for a wide variety of applications. By using simple fabrication techniques and reliable chemistry, developing degradable polycarbonates for consumer plastics applications that are environmentally and industrially attractive may be possible. Mechanically-dynamic materials have received little attention as stimuli-

responsive materials, but given the rise in the number of potential applications, such as dynamic biomedical devices, adaptive aerospace and automotive materials, adaptive clothing, switchable membranes, smart surface coatings, *etc.*, mechanically-adaptive polymers and composites are sure to receive more attention.[85] The design of materials that mimic the soft-to-hard gradient transitions found in nature can lead to materials for advanced biomedical applications including interfacial tissue engineering of osteochondral tissue[86] and improved tissue-engineered heart valve function.[87]

Looking forward, these UV-curable polymer networks may function as ideal platform materials in advanced material applications including additive manufacturing (*i.e.* 3D printing, electrospinning, stereolithography), naturally-derived composites incorporating cellulose or other natural fillers, and (hydro- and organo-) gel applications, all of which are applications which interest many different industries from medical to sporting goods/toys to consumer plastics. In stereolithographic (3D-printing with UV-curing) applications the workability of the resin in terms of viscosity and quick curing conditions (limited ability to "lightly crosslink") may provide challenges which can be addressed by altering the formulation, perhaps incorporating solvent to decrease viscosity and prevent premature crosslinking. To further increase mechanical properties, as well as, increase the structural likeness to bone, the incorporation of ceramic or organic nanoparticles should be considered. In the same regard, to expand into soft-biomaterials applications the exploring possible hydrogels may be other interest. However the hydrophobicity of the resin may hinder adequate dispersion of nanoparticles and prevent any mixing with water. One solution may be to introduce

more hydrophilic chemistries into the resin, perhaps incorporating plant-based or biomolecule-based thiol monomers which are naturally found in aqueous environments.

From a sustainability standpoint, the use of natural thiol monomers rather than the non-natural commercially-available ones used in the main body of this work, would substantially amplify the overall natural content of the polymers and lead to "all natural" degradable polycarbonates with nontoxic resorbable degradation products. For example, in an ongoing project multifunctional thiols derived from the natural dithiolane, lipoic acid have been incorporated into poly(thioether-*co*-carbonate) networks, described in Appendix A. The project represents the first steps in the quest to develop and study the structure-property relationships of poly(thioether-*co*-carbonate) networks derived from quinic acid and natural dithiolanes/disulfides. Furthermore, as the described polymers are extensively studied and other chemical and materials capabilities are explored, advances in the fundamental understanding of structure-property relationships and how these relationships change as a result of different environments may be made.

REFERENCES

1. Advancing Sustainable Materials Management: Facts and Figures 2013. U. S. Environmental Protection Agency, Office of Resource Conservation and Recovery: 2015; Vol. EPA530-R-15-002.
2. Cózar, A.; Echevarría, F.; González-Gordillo, J. I.; Irigoien, X.; Úbeda, B.; Hernández-León, S.; Palma, Á. T.; Navarro, S.; García-de-Lomas, J.; Ruiz, A.; Fernández-de-Puelles, M. L.; Duarte, C. M., Plastic debris in the open ocean. *Proc. Natl. Acad. Sci. U.S.A.* **2014,** *111* (28), 10239-10244.
3. Azzarello, M. Y.; Van Vleet, E. S., Marine birds and plastic pollution. *Mar. Ecol. Prog. Ser.* **1987,** *37*, 295-303.
4. van Franeker, J. A.; Law, K. L., Seabirds, gyres and global trends in plastic pollution. *Environmental Pollution* **2015,** *203*, 89-96.
5. Wright, S. L.; Thompson, R. C.; Galloway, T. S., The physical impacts of microplastics on marine organisms: A review. *Environmental Pollution* **2013,** *178*, 483-492.
6. Rudel, R. A.; Gray, J. M.; Engel, C. L.; Rawsthorne, T. W.; Dodson, R. E.; Ackerman, J. M.; Rizzo, J.; Nudelman, J. L.; Brody, J. G., Food packaging and bisphenol A and bis (2-ethyhexyl) phthalate exposure: findings from a dietary intervention. *Environ. Health Perspect.* **2011,** *119* (7), 914-920.

7. Schug, T. T.; Janesick, A.; Blumberg, B.; Heindel, J. J., Endocrine disrupting chemicals and disease susceptibility. *J. Steroid Biochem. Mol. Biol.* **2011,** *127* (3–5), 204-215.

8. Miller, S. A., Sustainable Polymers: Opportunities for the Next Decade. *ACS Macro Lett.* **2013,** *2* (6), 550-554.

9. Iwata, T., Biodegradable and Bio-Based Polymers: Future Prospects of Eco-Friendly Plastics. *Angew. Chem. Int. Ed.* **2015,** *54* (11), 3210-3215.

10. Nair, L. S.; Laurencin, C. T., Biodegradable polymers as biomaterials. *Prog. Polym. Sci.* **2007,** *32* (8–9), 762-798.

11. Middleton, J. C.; Tipton, A. J., Synthetic Biodegradable Polymers as Orthopedic Devices. *Biomaterials* **2000,** *21* (23), 2335-2346.

12. Malekani, J.; Schmutz, B.; Gu, Y.; Schuetz, M.; Yarlagadda, P. K., Biomaterials in orthopedic bone plates : a review In *Proceedings of the 2nd Annual International Conference on Materials Science, Metal & Manufacturing (M3 2011)*, qutеprints:47910: Bali, Indonesia, 2011; pp 71-77.

13. McMahon, R. E.; Wang, L.; Skoracki, R.; Mathur, A. B., Development of Nanomaterials for Bone Repair and Regeneration. *J. Biomed. Mater. Res. Part B: Appl. Biomater.* **2013,** *101B* (2), 387-397.

14. Yang, J.; Webb, A. R.; Ameer, G. A., Novel Citric Acid-Based Biodegradable Elastomers for Tissue Engineering. *Adv. Mater.* **2004,** *16* (6), 511-516.

15. Gallagher, J. J.; Hillmyer, M. A.; Reineke, T. M., Degradable Thermosets from Sugar-Derived Dilactones. *Macromolecules* **2014,** *47* (2), 498-505.

16. Bechthold, I.; Bretz, K.; Kabasci, S.; Kopitzky, R.; Springer, A., Succinic Acid: A New Platform Chemical for Biobased Polymers from Renewable Resources. *Chem. Eng. Technol.* **2008,** *31* (5), 647-654.

17. Stakleff, K. S.; Lin, F.; Smith Callahan, L. A.; Wade, M. B.; Esterle, A.; Miller, J.; Graham, M.; Becker, M. L., Resorbable, amino acid-based poly(ester urea)s crosslinked with osteogenic growth peptide with enhanced mechanical properties and bioactivity. *Acta Biomater.* **2013,** *9* (2), 5132-5142.

18. Burg, K., Chapter 6 - Poly(α-ester)s. In *Natural and Synthetic Biomedical Polymers*, Deng, S. G. K. T. L., Ed. Elsevier: Oxford, 2014; pp 115-121.

19. Lopes, M. S.; Jardini, A. L.; Filho, R. M., Poly (Lactic Acid) Production for Tissue Engineering Applications. *Procedia Eng.* **2012,** *42* (0), 1402-1413.

20. Grizzi, I.; Garreau, H.; Li, S.; Vert, M., Hydrolytic degradation of devices based on poly(dl-lactic acid) size-dependence. *Biomaterials* **1995,** *16* (4), 305-311.

21. Kumar, N.; Langer, R. S.; Domb, A. J., Polyanhydrides: an overview. *Adv. Drug Deliver. Rev.* **2002,** *54* (7), 889-910.

22. Noordover, B. A. J., Polyesters, Polycarbonates and Polyamides Based on Renewable Resources. In *Renewable Polymers*, John Wiley & Sons, Inc.: 2011; pp 305-354.

23. Artham, T.; Doble, M., Biodegradation of Aliphatic and Aromatic Polycarbonates. *Macromol. Biosci.* **2008,** *8* (1), 14-24.

24. Zhang, Z.; Kuijer, R.; Bulstra, S. K.; Grijpma, D. W.; Feijen, J., The In Vivo and In Vitro Degradation Behavior of Poly(trimethylene carbonate). *Biomaterials* **2006,** *27* (9), 1741-1748.

25. Albertsson, A.-C.; Eklund, M., Influence of Molecular Structure on the Degradation Mechanism of Degradable Polymers: In Vitro Degradation of Poly(trimethylene carbonate), Poly(trimethylene carbonate-co-caprolactone), and Poly(adipic anhydride). *J. Appl. Polym. Sci.* **1995,** *57* (1), 87-103.

26. Feng, J.; Zhuo, R.-X.; Zhang, X.-Z., Construction of functional aliphatic polycarbonates for biomedical applications. *Prog. Polym. Sci.* **2012,** *37* (2), 211-236.

27. Liu, S. Q.; Yang, C.; Huang, Y.; Ding, X.; Li, Y.; Fan, W. M.; Hedrick, J. L.; Yang, Y.-Y., Antimicrobial and Antifouling Hydrogels Formed In Situ from Polycarbonate and Poly(ethylene glycol) via Michael Addition. *Adv. Mater.* **2012,** *24* (48), 6484-6489.

28. Pascual, A.; Tan, J. P. K.; Yuen, A. Y.; Chan, J. M. W.; Coady, D. J.; Mecerreyes, D.; Hedrick, J. L.; Yang, Y. Y.; Sardón, H., Broad-Spectrum Antimicrobial Polycarbonate Hydrogels with Fast Degradability. *Biomacromolecules* **2015**.

29. Engler, A. C.; Ke, X.; Gao, S.; Chan, J. M. W.; Coady, D. J.; Ono, R. J.; Lubbers, R.; Nelson, A.; Yang, Y. Y.; Hedrick, J. L., Hydrophilic Polycarbonates: Promising Degradable Alternatives to Poly(ethylene glycol)-Based Stealth Materials. *Macromolecules* **2015,** *48* (6), 1673-1678.

30. Stevens, D. M.; Rahalkar, A.; Spears, B.; Gilmore, K.; Douglas, E.; Muthukumar, M.; Harth, E., Semibranched polyglycidols as "fillers" in polycarbonate hydrogels to tune hydrophobic drug release. *Polym. Chem.* **2015,** *6* (7), 1096-1102.

31. Gustafson, T. P.; Lonnecker, A. T.; Heo, G. S.; Zhang, S.; Dove, A. P.; Wooley, K. L., Poly(d-glucose carbonate) Block Copolymers: A Platform for Natural Product-Based Nanomaterials with Solvothermatic Characteristics. *Biomacromolecules* **2013,** *14* (9), 3346-3353.

32. Mikami, K.; Lonnecker, A. T.; Gustafson, T. P.; Zinnel, N. F.; Pai, P.-J.; Russell, D. H.; Wooley, K. L., Polycarbonates Derived from Glucose via an Organocatalytic Approach. *J. Am. Chem. Soc.* **2013,** *135* (18), 6826-6829.

33. Besset, C. l. J.; Lonnecker, A. T.; Streff, J. M.; Wooley, K. L., Polycarbonates from the Polyhydroxy Natural Product Quinic Acid. *Biomacromolecules* **2011,** *12* (7), 2512-2517.

34. Noel, A.; Borguet, Y. P.; Raymond, J. E.; Wooley, K. L., Poly(carbonate–amide)s Derived from Bio-Based Resources: Poly(ferulic acid-co-tyrosine). *Macromolecules* **2014,** *47* (9), 2974-2983.

35. Clifford, M. N., Chlorogenic Acids and other Cinnamates – Nature, Occurrence and Dietary Burden. *J. Sci. Food Agric.* **1999,** *79* (3), 362-372.

36. Scholz-Böttcher, B. M.; Ernst, L.; Maier, H. G., New Stereoisomers of Quinic Acid and Their Lactones. *Liebigs Ann. Chem.* **1991,** *1991* (10), 1029-1036.

37. Draths, K. M.; Knop, D. R.; Frost, J. W., Shikimic Acid and Quinic Acid: Replacing Isolation from Plant Sources with Recombinant Microbial Biocatalysis. *J. Am. Chem. Soc.* **1999,** *121* (7), 1603-1604.

38. Pero, R. W.; Lund, H.; Leanderson, T., Antioxidant Metabolism Induced by Quinic Acid. Increased Urinary Excretion of Tryptophan and Nicotinamide. *Phytother. Res.* **2009,** *23* (3), 335-346.

39. Gordon, M.; Haskins, F. A.; Mitchell, H. K., The Growth-Promoting Properties of Quinic Acid. *Proc. Natl. Acad. Sci. U.S.A.* **1950,** *36* (8), 427-430.

40. Åkesson, C.; Lindgren, H.; Pero, R. W.; Leanderson, T.; Ivars, F., Quinic Acid is a Biologically Active Component of the Uncaria Tomentosa Extract C-Med 100®. *Int. Immunopharmacol.* **2005,** *5* (1), 219-229.

41. Flory, P. J., Molecular Size Distribution in Three Dimensional Polymers. I. Gelation1. *J. Am. Chem. Soc.* **1941,** *63* (11), 3083-3090.

42. Huebsch, N.; Mooney, D. J., Inspiration and application in the evolution of biomaterials. *Nature* **2009,** *462* (7272), 426-432.

43. Bettinger, C. J., Biodegradable Elastomers for Tissue Engineering and Cell–Biomaterial Interactions. *Macromol. Biosci.* **2011,** *11* (4), 467-482.

44. Hoyle, C. E.; Lee, T. Y.; Roper, T., Thiol–enes: Chemistry of the Past with Promise for the Future. *J. Polym. Sci. Part A: Polym. Chem.* **2004,** *42* (21), 5301-5338.

45. Cramer, N. B.; Bowman, C. N., Kinetics of thiol–ene and thiol–acrylate photopolymerizations with real-time fourier transform infrared. *J. Polym. Sci. Part A: Polym. Chem.* **2001,** *39* (19), 3311-3319.

46. Hoyle, C. E.; Bowman, C. N., Thiol–Ene Click Chemistry. *Angew. Chem. Int. Ed.* **2010,** *49* (9), 1540-1573.

47. Hoyle, C. E.; Hensel, R. D.; Grubb, M. B., Temperature dependence of the laser-initiated polymerization of a thiol-ene system. *J. Polym. Sci. Polym. Chem. Ed.* **1984,** *22* (8), 1865-1873.

48. Fairbanks, B. D.; Schwartz, M. P.; Halevi, A. E.; Nuttelman, C. R.; Bowman, C. N.; Anseth, K. S., A Versatile Synthetic Extracellular Matrix Mimic via Thiol-Norbornene Photopolymerization. *Adv. Mater.* **2009,** *21* (48), 5005-5010.

49. Boulden, J. E.; Cramer, N. B.; Schreck, K. M.; Couch, C. L.; Bracho-Troconis, C.; Stansbury, J. W.; Bowman, C. N., Thiol–ene–Methacrylate Composites as Dental Restorative Materials. *Dent. Mater.* **2011,** *27* (3), 267-272.

50. Ware, T.; Simon, D.; Hearon, K.; Kang, T. H.; Maitland, D. J.; Voit, W., Thiol-Click Chemistries for Responsive Neural Interfaces. *Macromol. Biosci.* **2013,** *13* (12), 1640-1647.

51. Wei, H.; Senyurt, A. F.; Jönsson, S.; Hoyle, C. E., Photopolymerization of ternary thiol–ene/acrylate systems: Film and network properties. *J. Polym. Sci. Part A: Polym. Chem.* **2007,** *45* (5), 822-829.

52. Kade, M. J.; Burke, D. J.; Hawker, C. J., The Power of Thiol-ene Chemistry. *J. Polym. Sci. Part A: Polym. Chem.* **2010,** *48* (4), 743-750.

53. Lowe, A. B., Thiol-ene "click" reactions and recent applications in polymer and materials synthesis: a first update. *Polym. Chem.* **2014,** *5* (17), 4820-4870.

54. Williams, C. K.; Hillmyer, M. A., Polymers from Renewable Resources: A Perspective for a Special Issue of Polymer Reviews. *Polym. Rev.* **2008,** *48* (1), 1-10.

55. Fertier, L.; Koleilat, H.; Stemmelen, M.; Giani, O.; Joly-Duhamel, C.; Lapinte, V.; Robin, J. J., The use of Renewable Feedstock in UV-curable Materials - A New Age for Polymers and Green Chemistry. *Prog. Polym. Sci.* **2013,** *38* (6), 932-962.

56. Tschan, M. J. L.; Brule, E.; Haquette, P.; Thomas, C. M., Synthesis of Biodegradable Polymers from Renewable Resources. *Polym. Chem.* **2012,** *3* (4), 836-851.

57. Buerkle, L. E.; von Recum, H. A.; Rowan, S. J., Toward Potential Supramolecular Tissue Engineering Scaffolds Based on Guanosine Derivatives. *Chem. Sci.* **2012,** *3* (2), 564-572.

58. Hearon, K.; Nash, L. D.; Rodriguez, J. N.; Lonnecker, A. T.; Raymond, J. E.; Wilson, T. S.; Wooley, K. L.; Maitland, D. J., Recycling: A High-Performance Recycling Solution for Polystyrene Achieved by the Synthesis of Renewable Poly(thioether) Networks Derived from d-Limonene. *Adv. Mater.* **2014,** *26* (10), 1551-1551.

59. Claudino, M.; Mathevet, J.-M.; Jonsson, M.; Johansson, M., Bringing d-Limonene to the Scene of Bio-based Thermoset Coatings via Free-radical Thiol-

ene Chemistry: Macromonomer Synthesis, UV-curing and Thermo-mechanical Characterization. *Polym. Chem.* **2014,** *5* (9), 3245-3260.

60. Sabir, M.; Xu, X.; Li, L., A Review on Biodegradable Polymeric Materials for Bone Tissue Engineering Applications. *J. Mater. Sci.* **2009,** *44* (21), 5713-5724.

61. Engelberg, I.; Kohn, J., Physico-mechanical Properties of Degradable Polymers used in Medical Applications: A Comparative Study. *Biomaterials* **1991,** *12* (3), 292-304.

62. Vert, M.; Mauduit, J.; Li, S., Biodegradation of PLA/GA Polymers: Increasing Complexity. *Biomaterials* **1994,** *15* (15), 1209-1213.

63. Chiou, B.-S.; English, R. J.; Khan, S. A., Rheology and Photo-Cross-Linking of Thiol−Ene Polymers. *Macromolecules* **1996,** *29* (16), 5368-5374.

64. Ware, T.; Simon, D.; Hearon, K.; Liu, C.; Shah, S.; Reeder, J.; Khodaparast, N.; Kilgard, M. P.; Maitland, D. J.; Rennaker, R. L.; Voit, W. E., Three-Dimensional Flexible Electronics Enabled by Shape Memory Polymer Substrates for Responsive Neural Interfaces. *Macromol. Mater. Eng.* **2012,** *297* (12), 1193-1202.

65. Smith, K. E.; Temenoff, J. S.; Gall, K., On the Toughness of Photopolymerizable (meth)Acrylate Networks for Biomedical Applications. *J. Appl. Polym. Sci.* **2009,** *114* (5), 2711-2722.

66. Hearon, K.; Nash, L. D.; Volk, B. L.; Ware, T.; Lewicki, J. P.; Voit, W. E.; Wilson, T. S.; Maitland, D. J., Electron Beam Crosslinked Polyurethane Shape

Memory Polymers with Tunable Mechanical Properties. *Macromol. Chem. Phys.* **2013,** *214* (11), 1258-1272.

67. Garg, N. K.; Caspi, D. D.; Stoltz, B. M., The Total Synthesis of (+)-Dragmacidin F. *J. Am. Chem. Soc.* **2004,** *126* (31), 9552-9553.

68. Clarke, R. L.; Braden, M., Modified Arrhenius Equation for the Frequency Dependence of the Transition Temperatures of Polymers. *Biomaterials* **1989,** *10* (5), 349-352.

69. Rezgui, F.; Swistek, M.; Hiver, J. M.; G'Sell, C.; Sadoun, T., Deformation and Damage upon Stretching of Degradable Polymers (PLA and PCL). *Polymer* **2005,** *46* (18), 7370-7385.

70. Clarke, R. L., Dynamic Mechanical Thermal Analysis of Dental Polymers: II. Bis-phenol A-related Resins. *Biomaterials* **1989,** *10* (8), 549-552.

71. Weinstein, S. I.; Yelin, E. H.; Watkins-Castillo, S. I. United States Bone and Joint Initiative: The Burden of Musculoskeletal Diseases in the United States (BMUS), Third Edition, 2014. Rosemont, IL. http://www.boneandjointburden.org (accessed July 29, 2015).

72. Oliva, N.; Unterman, S.; Zhang, Y.; Conde, J.; Song, H. S.; Artzi, N., Personalizing Biomaterials for Precision Nanomedicine Considering the Local Tissue Microenvironment. *Adv. Healthcare Mater.* **2015**, *Early view*.

73. Holzapfel, B. M.; Reichert, J. C.; Schantz, J.-T.; Gbureck, U.; Rackwitz, L.; Nöth, U.; Jakob, F.; Rudert, M.; Groll, J.; Hutmacher, D. W., How smart do

biomaterials need to be? A translational science and clinical point of view. *Adv. Drug Deliver. Rev.* **2013,** *65* (4), 581-603.

74. Yu, X.; Tang, X.; Gohil, S. V.; Laurencin, C. T., Biomaterials for Bone Regenerative Engineering. *Adv. Healthcare Mater.* **2015,** *4* (9), 1268-1285.

75. Smith, B. D.; Grande, D. A., The current state of scaffolds for musculoskeletal regenerative applications. *Nat. Rev. Rheumatol.* **2015,** *11* (4), 213-222.

76. Do, A.-V.; Khorsand, B.; Geary, S. M.; Salem, A. K., 3D Printing of Scaffolds for Tissue Regeneration Applications. *Adv. Healthcare Mater.* **2015**, n/a-n/a.

77. Ng, V. W. L.; Chan, J. M. W.; Sardon, H.; Ono, R. J.; García, J. M.; Yang, Y. Y.; Hedrick, J. L., Antimicrobial hydrogels: A new weapon in the arsenal against multidrug-resistant infections. *Adv. Drug Deliver. Rev.* **2014,** *78* (0), 46-62.

78. Link, L. A.; Lonnecker, A. T.; Hearon, K.; Maher, C. A.; Raymond, J. E.; Wooley, K. L., Photo-cross-linked Poly(thioether-co-carbonate) Networks Derived from the Natural Product Quinic Acid. *ACS Appl. Mater. Interfaces* **2014,** *6* (20), 17370-17375.

79. Engler, A. J.; Sen, S.; Sweeney, H. L.; Discher, D. E., Matrix Elasticity Directs Stem Cell Lineage Specification. *Cell* **2006,** *126* (4), 677-689.

80. Discher, D. E.; Mooney, D. J.; Zandstra, P. W., Growth Factors, Matrices, and Forces Combine and Control Stem Cells. *Science* **2009,** *324* (5935), 1673-1677.

81. Guilak, F.; Cohen, D. M.; Estes, B. T.; Gimble, J. M.; Liedtke, W.; Chen, C. S., Control of Stem Cell Fate by Physical Interactions with the Extracellular Matrix. *Cell Stem Cell* **2009,** *5* (1), 17-26.

82. Ware, T.; Simon, D.; Liu, C.; Musa, T.; Vasudevan, S.; Sloan, A.; Keefer, E. W.; Rennaker, R. L.; Voit, W., Thiol-ene/acrylate substrates for softening intracortical electrodes. *J. Biomed. Mater. Res. Part B: Appl. Biomater.* **2013**.

83. Yang, B.; Huang, W. M.; Li, C.; Li, L., Effects of moisture on the thermomechanical properties of a polyurethane shape memory polymer. *Polymer* **2006,** *47* (4), 1348-1356.

84. Corkhill, P. H.; Jolly, A. M.; Ng, C. O.; Tighe, B. J., Synthetic hydrogels: 1. Hydroxyalkyl acrylate and methacrylate copolymers - water binding studies. *Polymer* **1987,** *28* (10), 1758-1766.

85. Hsu, L.; Weder, C.; Rowan, S. J., Stimuli-responsive, mechanically-adaptive polymer nanocomposites. *J. Mater. Chem.* **2011,** *21* (9), 2812-2822.

86. Bailey, B. M.; Nail, L. N.; Grunlan, M. A., Continuous gradient scaffolds for rapid screening of cell–material interactions and interfacial tissue regeneration. *Acta Biomater.* **2013,** *9* (9), 8254-8261.

87. Brugmans, M. M. C. P.; Driessen-Mol, A.; Rubbens, M. P.; Cox, M. A. J.; Baaijens, F. P. T., Poly-ε-caprolactone scaffold and reduced in vitro cell culture: beneficial effect on compaction and improved valvular tissue formation. *J. Tissue Eng. Regen. Med.* **2013**, *Early view*.

88. Poetz, K. L.; Mohammed, H. S.; Shipp, D. A., Surface Eroding, Semicrystalline Polyanhydrides via Thiol–Ene “Click” Photopolymerization. *Biomacromolecules* **2015,** *16* (5), 1650-1659.

89. Olofsson, K.; Malkoch, M.; Hult, A., Soft hydrogels from tetra-functional PEGs using UV-induced thiol-ene coupling chemistry: a structure-to-property study. *RSC Adv.* **2014,** *4* (57), 30118-30128.

90. Ware, T.; Jennings, A. R.; Bassampour, Z. S.; Simon, D.; Son, D. Y.; Voit, W., Degradable, silyl ether thiol-ene networks. *RSC Adv.* **2014,** *4* (75), 39991-40002.

91. Hearon, K.; Wierzbicki, M. A.; Nash, L. D.; Landsman, T. L.; Laramy, C.; Lonnecker, A. T.; Gibbons, M. C.; Ur, S.; Cardinal, K. O.; Wilson, T. S.; Wooley, K. L.; Maitland, D. J., A Processable Shape Memory Polymer System for Biomedical Applications. *Adv. Healthcare Mater.* **2015**, *Early view*.

92. Yang, G.; Kristufek, S. L.; Link, L. A.; Wooley, K. L.; Robertson, M. L., Sythesis and Physical Properties of Thiol-ene Networks Utilizing Plant-derived Phenolic Acids. *Macromolecules* **2015**.

93. Renard, E.; Modjinou, T.; Versace, D.-L.; Abbad-Andaloussi, S.; Bousserrhine, N.; Babinot, J.; Langlois, V., Antibacterial networks based on isosorbide and linalool by photo-initiated process. *ACS Sustainable Chem. Eng.* **2015**.

94. Moini, H.; Packer, L.; Saris, N.-E. L., Antioxidant and Prooxidant Activities of α-Lipoic Acid and Dihydrolipoic Acid. *Toxicol. Appl. Pharmacol.* **2002,** *182* (1), 84-90.

95. Chen, X.; Lawrence, J.; Parelkar, S.; Emrick, T., Novel Zwitterionic Copolymers with Dihydrolipoic Acid: Synthesis and Preparation of Nonfouling Nanorods. *Macromolecules* **2013,** *46* (1), 119-127.

96. Susumu, K.; Oh, E.; Delehanty, J. B.; Blanco-Canosa, J. B.; Johnson, B. J.; Jain, V.; Hervey, W. J.; Algar, W. R.; Boeneman, K.; Dawson, P. E.; Medintz, I. L., Multifunctional Compact Zwitterionic Ligands for Preparing Robust Biocompatible Semiconductor Quantum Dots and Gold Nanoparticles. *J. Am. Chem. Soc.* **2011,** *133* (24), 9480-9496.

97. Sharma, J.; Chhabra, R.; Andersen, C. S.; Gothelf, K. V.; Yan, H.; Liu, Y., Toward Reliable Gold Nanoparticle Patterning On Self-Assembled DNA Nanoscaffold. *J. Am. Chem. Soc.* **2008,** *130* (25), 7820-7821.

98. Dougan, J. A.; Karlsson, C.; Smith, W. E.; Graham, D., Enhanced oligonucleotide–nanoparticle conjugate stability using thioctic acid modified oligonucleotides. *Nucleic Acids Res.* **2007,** *35* (11), 3668-3675.